Calhoun: The NPS Institutional Archive

DSpace Repository

Theses and Dissertations | 1. Thesis and Dissertation Collection, all items

1998-03

Microwave observations of mesoscale convective systems during tropical cyclone genesis in the Western North Pacific

Milot, David

Monterey, California. Naval Postgraduate School

http://hdl.handle.net/10945/8675

Downloaded from NPS Archive: Calhoun

http://www.nps.edu/library

Calhoun is the Naval Postgraduate School's public access digital repository for research materials and institutional publications created by the NPS community. Calhoun is named for Professor of Mathematics Guy K. Calhoun, NPS's first appointed -- and published -- scholarly author.

Dudley Knox Library / Naval Postgraduate School
411 Dyer Road / 1 University Circle
Monterey, California USA 93943

NPS ARCHIVE
1998.03
MILOT, D.

DUDLEY KNOX LIBRARY
NAVAL POSTGRADUATE SCHOOL
MONTEREY CA 93943-5101

NAVAL POSTGRADUATE SCHOOL
Monterey, California

THESIS

MICROWAVE OBSERVATIONS OF MESOSCALE CONVECTIVE SYSTEMS DURING TROPICAL CYCLONE GENESIS IN THE WESTERN NORTH PACIFIC

by

David Milot

March, 1998

Thesis Co-Advisors: Russell L. Elsberry
Patrick A. Harr

Approved for public release; distribution is unlimited.

DUDLEY KNOX LIBRARY
NAVAL POSTGRADUATE SCHOOL
MONTEREY CA 93943-5101

REPORT DOCUMENTATION PAGE

Form Approved OMB No. 0704-0188

Public reporting burden for this collection of information is estimated to average 1 hour per response, including the time for reviewing instruction, searching existing data sources, gathering and maintaining the data needed, and completing and reviewing the collection of information. Send comments regarding this burden estimate or any other aspect of this collection of information, including suggestions for reducing this burden, to Washington Headquarters Services, Directorate for Information Operations and Reports, 1215 Jefferson Davis Highway, Suite 1204, Arlington, VA 22202-4302, and to the Office of Management and Budget, Paperwork Reduction Project (0704-0188) Washington DC 20503.

1. AGENCY USE ONLY *(Leave blank)*	2. REPORT DATE	3. REPORT TYPE AND DATES COVERED
	March, 1998.	Master's Thesis

4. TITLE AND SUBTITLE	5. FUNDING NUMBERS
MICROWAVE OBSERVATIONS OF MESOSCALE CONVECTIVE SYSTEMS DURING TROPICAL CYCLONE GENESIS IN THE WESTERN NORTH PACIFIC	
6. AUTHOR(S) Milot, David	
7. PERFORMING ORGANIZATION NAME(S) AND ADDRESS(ES) Naval Postgraduate School Monterey CA 93943-5000	8. PERFORMING ORGANIZATION REPORT NUMBER
9. SPONSORING/MONITORING AGENCY NAME(S) AND ADDRESS(ES)	10. SPONSORING/MONITORING AGENCY REPORT NUMBER

11. SUPPLEMENTARY NOTES The views expressed in this thesis are those of the author and do not reflect the official policy or position of the Department of Defense or the U.S. Government.

12a. DISTRIBUTION/AVAILABILITY STATEMENT	12b. DISTRIBUTION CODE
Approved for public release; distribution is unlimited.	

13. ABSTRACT *(maximum 200 words)*

A better understanding of the role mesoscale convective systems (MCS) play in the genesis stages of tropical cyclones will increase the ability to predict their formation. This thesis employs polar-orbiter microwave and geostationary infrared satellite imagery to document MCS structure and evolution during tropical cyclone genesis. Microwave imagery at frequencies of 19.35 GHz and 85.5 GHz are used to define convective and stratiform cloud areal amounts, percent coverage, and time-integrated rain rates. Collocations with geostationary infrared images are used to calibrate that imagery so that the hourly values may be calculated until another microwave image is available. Specifically, seven MCSs in two disturbances that eventually developed into tropical cyclones were analyzed. Two MCSs in non-developing storms are also described for contrast.

14. SUBJECT TERMS	15. NUMBER OF PAGES
Mesoscale Convective Systems, Microwave Satellite Imagery, Tropical Cyclone Genesis, Formation	107
	16. PRICE CODE

17. SECURITY CLASSIFICATION OF REPORT	18. SECURITY CLASSIFICATION OF THIS PAGE	19. SECURITY CLASSIFICATION OF ABSTRACT	20. LIMITATION OF ABSTRACT
Unclassified	Unclassified	Unclassified	UL

NSN 7540-01-280-5500

Standard Form 298 (Rev. 2-89)
Prescribed by ANSI Std. 239-18 298-102

Approved for public release; distribution is unlimited.

MICROWAVE OBSERVATIONS OF MESOSCALE CONVECTIVE SYSTEMS DURING TROPICAL CYCLONE GENESIS IN THE WESTERN NORTH PACIFIC

David Milot
Lieutenant, United States Navy
B.S., United States Naval Academy, 1989

Submitted in partial fulfillment
of the requirements for the degree of

MASTER OF SCIENCE IN METEOROLOGY AND PHYSICAL OCEANOGRAPHY

from the

NAVAL POSTGRADUATE SCHOOL
March 1998

DUDLEY KNOX LIBRARY
NAVAL POSTGRADUATE SCHOOL
MONTEREY CA 93943-5101

ABSTRACT

A better understanding of the role mesoscale convective systems (MCS) play in the genesis stages of tropical cyclones will increase the ability to predict their formation. This thesis employs polar-orbiter microwave and geostationary infrared satellite imagery to document MCS structure and evolution during tropical cyclone genesis. Microwave imagery at frequencies of 19.35 GHz and 85.5 GHz are used to define convective and stratiform cloud areal amounts, percent coverage, and time-integrated rain rates. Collocations with geostationary infrared images are used to calibrate that imagery so that the hourly values may be calculated until another microwave image is available. Specifically, seven MCSs in two disturbances that eventually developed into tropical cyclones were analyzed. Two MCSs in non-developing storms are also described for contrast.

TABLE OF CONTENTS

I. INTRODUCTION 1

A. DEFINITION OF A MESOSCALE CONVECTIVE SYSTEM 1

B. LIFE CYCLE OF A MCS 2

C. RECENT STUDIES OF MCS STRUCTURE 4

D. ROLE OF MCS IN TC FORMATION 5

E. PREVIOUS STUDIES CATEGORIZING TC FORMATION TYPES .. 7

F. OBJECTIVES OF THIS THESIS 7

II. METHODOLOGY 9

A. DATA 9

B. ANALYSIS PROCEDURES 10

1. Use of GMS Data 11

2. Use of SSM/I Data 12

C. SATELLITE CLOUD CLASSIFICATION 14

III. CASE STUDIES 19

A. SUPER TYPHOON BING 19

1. Overall Evolution 19

2. MCS Structure 32

B. SUPER TYPHOON IVAN 52

1. Overall Evolution 52

2. MCS Structure 60

C. NON-DEVELOPING MCS 69

1. Overall Evolution 69

2. MCS Structure 74

IV. SUMMARY AND CONCLUSIONS 81

A. SUMMARY 81

B. CONCLUSIONS 87

C. RECOMMENDATIONS 87

LIST OF REFERENCES 91

INITIAL DISTRIBUTION LIST 95

ACKNOWLEDGMENTS

First, I would like to thank my wife and daughter for their love and patience during my time here at NPS. Second, I would like to thank Dr. Russell Elsberry for his guidance in preparing this thesis. Third, I would like to thank Dr. Pat Harr for his guidance and computer expertise which made this thesis possible. I would also like to thank Jeff Hawkins and his team at NRL for collecting all the microwave data for this thesis. Finally, I would like to thank Bob Creasey and Steve Taylor for their computer expertise in helping process the data.

I. INTRODUCTION

Globally, an average of 80 tropical cyclones (TCs) form over the tropical oceans each year, of which nearly two thirds reach severe tropical cyclone strength (McBride 1995). These severe storms are capable of causing mass destruction of life and property and pose a continual threat to military installations and fleet assets worldwide. One of the ways to reduce this threat is to study the genesis stages of the TC. These studies have enabled meteorologists to give the military decision makers advanced warning that a TC is developing and to issue timely warnings, and thus have prevented loss of life and minimized property damage.

There are many ways in which TCs can form. Recent studies suggest that many TCs form from a large cloud system called a mesoscale convective system (MCS). This thesis will use collocated polar-orbiting microwave and geostationary infrared/visible satellite imagery to document the role of MCSs in the genesis of TCs.

A. DEFINITION OF A MESOSCALE CONVECTIVE SYSTEM

The warm tropical oceans are the breeding grounds for TCs. These regions are characterized by large amounts of convective clouds of all sizes. The air masses over the tropical oceans are continuously heated from below and convection acts to mix the air vertically (Houze 1993). These convective clouds form thunderstorms, which can occur independently or in groups. A large group or complex, which is referred to as a MCS, is the largest member of the family of convective clouds (Houze 1993). Houze (1993) defines a MCS *as a cloud system that occurs in connection with an ensemble of thunderstorms and produces a contiguous precipitation area ~100 km^2 or more in*

horizontal scale in at least one direction. Although MCSs can occur in a variety of forms, all MCSs can be divided into two distinct cloud types: convective and stratiform (Houze 1997). Convective regions are characterized by strong updrafts and downdrafts that can range in horizontal scale from a few kilometers to 30 km. These regions are associated with heavy rain and can have updraft velocities up to 10 m/s. Stratiform regions can extend for hundreds of kilometers and will have precipitation that is less intense and more uniformly spread throughout this region. Research radar studies reveal that the stratiform regions of MCSs contribute about 30-60% of the total precipitation of these systems (McGaughey and Zipser 1996). These stratiform regions are characterized by mean ascent above the freezing level and mean descent below the freezing level (McGaughey et al. 1996).

B. LIFE CYCLE OF A MCS

The MCS may live as short as a few hours or as long as 2-3 days (Houze 1993). The precipitation area of a MCS exhibits a characteristic life cycle that is divided by Houze (1993) into four stages that are schematically illustrated in Fig. 1.1 as they would appear on radar.

The formative stage (Fig. 1.1a) consists of a group of isolated convective cells that may be arranged uniformly in the horizontal or in a line. In the intensifying stage (Fig. 1.1b), the cells grow and merge to form a contiguous rain area in which several relatively intense cores of precipitation are interconnected by lighter precipitation. The mature stage (Fig.1.1c) occurs when a large stratiform region develops from older cells blending together as they begin to weaken. Each convective cell goes through a life cycle, and

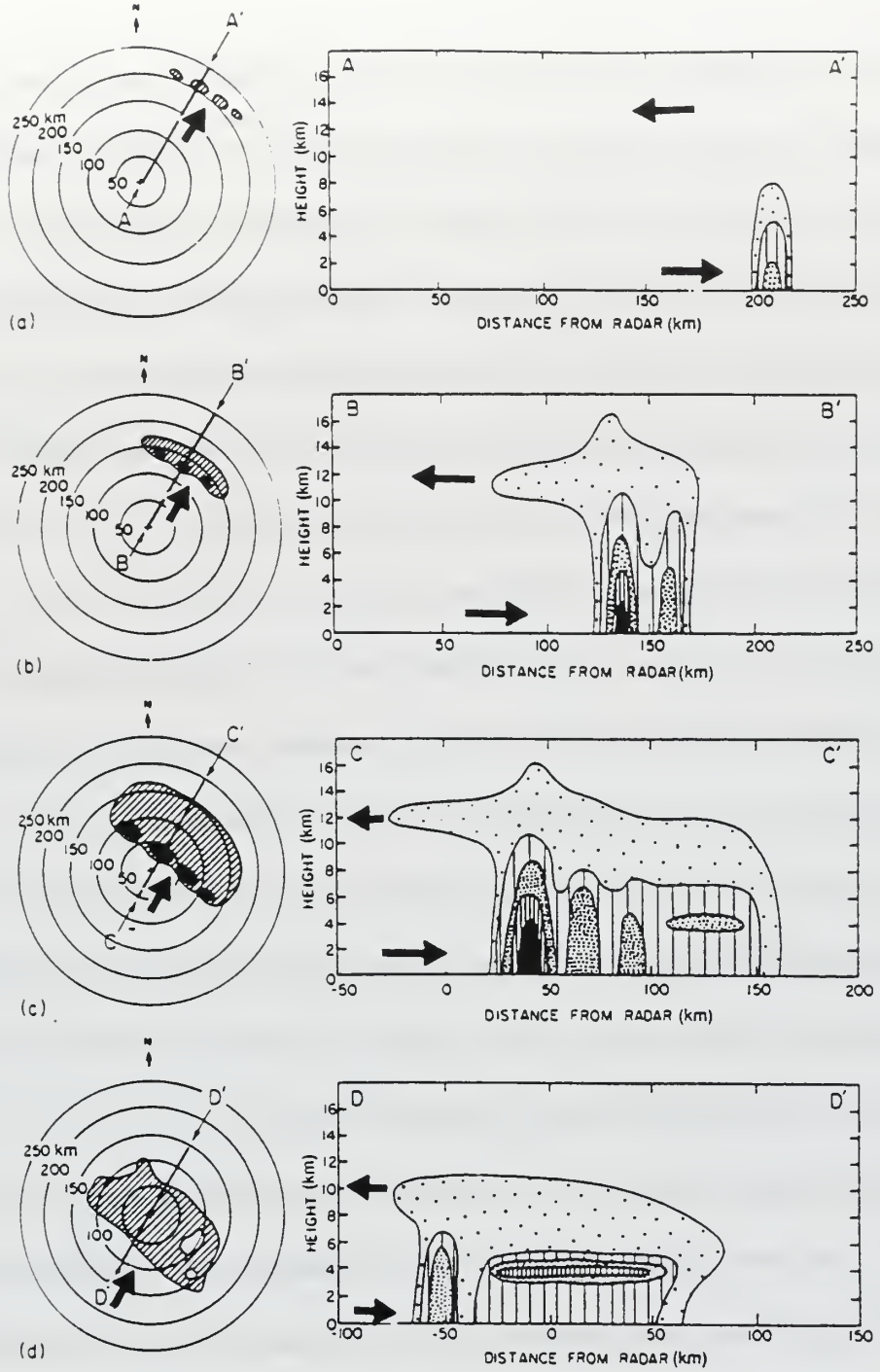

Figure 1.1. Schematic of the life cycle of the precipitation area of a mesoscale convective system as it would appear on radar in horizontal and vertical cross sections during (a) formative, (b) intensifying, (c) mature, and (d) dissipating stages. The outside contour of radar reflectivity represents the weakest detectable echo. The inner contours are for successively higher reflectivity values. Heavy arrows indicate the direction of the wind relative to the system (Houze 1993).

when it weakens becomes a part of the stratiform region. When several neighboring cells reach this stage, they may become indistinguishable and form an extensive stratiform region as large as 200 km in horizontal direction (Houze 1993). As clouds and precipitation are detrained from the tops of active cells, the upper-level winds carry the condensate away from the rain area and an overhang of radar echo can form as shown in Figure 1.1c. In the dissipation stage (Fig 1.1d), the formation of new convective cells diminishes, and the stratiform area begins to weaken and dissipate.

C. RECENT STUDIES OF MCS STRUCTURE

Over the past two decades, several studies have been conducted on the structure of the MCS. The first such study in 1974 was called the Global Atmospheric Research Programme (GARP) Atlantic Tropical Experiment (GATE) (Houze 1997). This experiment collected radar observations of stratiform regions in the Intertropical Convergence Zone (ITCZ) off the west coast of Africa. These observations indicated that both convective and stratiform radar echoes occurred in a regime in which the clouds are generated entirely by atmospheric convection (Houze 1997).

The GATE radar program gave scientists the first good look at the structure of tropical MCS stratiform regions. Unfortunately, radar does not give a complete depiction of the microphysical structure of the entire MCS. The absence of cloud microphysics observations over the tropical oceanic regions has made this study difficult. The use of high-resolution passive microwave observations is one way to overcome this deficiency. Passive microwave observations are currently measured by two systems: the Special Sensor Microwave Imager (SSM/I) on polar-orbiting satellites and the Advanced

Microwave Precipitation Radiometer (AMPR) deployed on high-flying aircraft.

The first study to use AMPR data was the Tropical Ocean Global Atmosphere Coupled Ocean-Atmosphere Response Experiment (TOGA COARE) (McGaughey and Zipser 1996) during 1 November 1992 to 28 February 1993. This was a large field experiment, which used Doppler radar on ships and the AMPR on aircraft, to study MCSs over the western tropical Pacific. These data, collected in both convective and stratiform precipitation, are by far the most comprehensive such AMPR measurements over the tropical ocean to date (McGaughey and Zipser 1996).

D. ROLE OF MCS IN TC FORMATION

Zehr (1992) has proposed a two-stage TC formation model based on satellite imagery in which MCSs play a critical role in TC genesis. Stage one consists of vigorous convection within a MCS. A mid-level mesoscale convective vortex (MCV) forms in the stratiform region and remains after the MCS dissipates. After the stratiform cloud shield dissipates, the MCV may be seen on satellite imagery as a low-level circulation center (LLCC). A time period of between 12 hours to several days may occur until the next stage begins. Stage two begins with deep convection associated with the LLCC. This is the time that the circulation is designated as a tropical depression.

Two critical components of the Zehr conceptual model are development of the MCV at midlevels and its downward extension to low levels. Without the extension to low levels, the MCV cannot tap surface energy sources, which enable development into stage two. Chen and Frank (1993) propose that a cloud cluster can make the transition from an unorganized system to a tropical depression in less than a day in association with

a MCS in a moist-neutral environment. The concentrated vertical ascent and latent heat release in the stratiform region of a MCS contributes to the formation of a MCV in the mid-levels (Chen and Frank 1993). The mechanism by which the MCV translates downward and taps into the heat and moisture sources of the planetary boundary layer remains unknown.

Ritchie and Holland (1997) suggest that within a MCS stratiform region, mesoscale convergence and stretching near the stratiform cloud base produces a positive potential-vorticity (PV) anomaly that forms the MCV. The MCV can develop vertically by increasing the horizontal size of its PV perturbation or by decreasing its local vertical temperature gradient, which partitions more of the PV into its relative vorticity component (Ritchie and Holland 1997). As the MCV grows horizontally, it stretches and expands upward into the troposphere and downward to the surface.

Bister and Emanuel (1997) suggest that downdraft evaporation associated with rain falling from the stratiform portion of the MCS cools the lower troposphere and contributes to the spinup of a mid-level MCV. After some time during which continuous rain is assumed, the lower levels of the stratiform portion become saturated and unstable to deep convection via surface heat flux, which enables the MCV to expand downward and changes the low-level cold core to warm core. Their model suggests that for the warm core development to occur, the stratiform rain must last long enough to drive the MCV down to the boundary layer (Bister and Emanuel 1997).

Finta (1997) hypothesized that the structure of MCSs during TC formation may determine future aspects of the TC, such as size and intensity. Therefore, the role of

MCSs in TC genesis is very important and has been studied extensively in recent years (Elsberry et al. 1995).

E. PREVIOUS STUDIES CATEGORIZING TC FORMATION TYPES

The Tropical Cyclone Motion (TCM-93) mini-field experiment studied the effects of a MCS in a monsoon trough in the western North Pacific and its relationship to TC genesis. The study suggested that the structure of the MCS provided a mid-level subsynoptic contribution to the vorticity of the monsoon depression and contributed to a shift in the center of the monsoon depression toward the MCS (Harr et al. 1996). As this MCS dissipated, the monsoon depression began to organize around a new MCS. Harr et al. (1996) hypothesized that the subsynoptic processes in both MCSs contributed to the concentration of the monsoon depression center and transformed it into a TC.

Finta (1997) observed 13 developing TCs using high space and time resolution satellite imagery and categorized pathways for TC genesis as mesoscale, synoptic, and combination. The first pathway is more strongly dependent on the activity of the mesoscale components. The second pathway is characterized by large-scale environmental effects. The third is a combination of the two, as indicated above in the TCM-93 case study by Harr et al. (1996).

F. OBJECTIVES OF THIS THESIS

This thesis will use visible and infrared imagery from the geostationary meteorological satellite GMS-5 collocated with passive microwave observations from the SSM/I on polar-orbiting Defense Meteorological Satellite Program (DSMP) satellites. The snapshots of microwave data will be combined with the continuous GMS-5 images

to document the evolution of MCSs during the formative stages of two TCs, and contrast the MCS role in a non-developing TC. The microwave imagery is at frequencies of 19.35 GHz, which is correlated with integrated rain water in an atmospheric column, and 85.5 GHz, which is correlated with the scattering of ice crystals. Signatures of the MCV will be examined using both of these channels separately and in linear combination to deduce a total rain rate. The developing TCs will be categorized by the locations, percent coverage, and rain rates of the associated MCS. Non-developing storms and their associated MCSs will also be compared to determine the cause of non-development.

II. METHODOLOGY

A. DATA

The primary data for this thesis are the high temporal and spatial resolution imagery from the Japanese Geostationary Meteorological Satellite (GMS-5) and the polar-orbiting Defense Meteorological Satellite Program (DMSP F-10, F-11, F-13, F-14). To observe the life-cycle stages of the MCS in a continuous manner, hourly visible and infrared images are animated over a grid from 0° to 30° N and 115° E to 175° E. Instantaneous snapshots from SSM/I images in the frequency bands of 19.35 GHz and 85.5 GHz allow a more detailed analysis of the cloud structure and rain rates in the MCS. The analyzed systems are selected from the western North Pacific during 10 June 1997 through 31 October 1997 after exclusion of cases with extended or multiple gaps in the imagery. Analysis methods include animation of the GMS imagery and use of an objective tracking program created by Dr. P. Harr that follows the movement of each individual MCS. Analyzed wind fields from the Naval Operational Global Atmospheric Prediction System (NOGAPS) are used to determine the low-level and upper-level synoptic-scale environments.

All software packages are run on the IRIS 5.3 UNIX system on Silicon Graphics Indigo workstations. The hourly GMS-5 imagery with a resolution of 1 km in the visible (from 20-07 UTC) and 4 km in the infrared is processed with the Terrascan (TSCAN) software package. The TSCAN program allowed latitude and longitude gridding to be

overlaid on the imagery, as well as zooming, coloring, and pixel enhancement of the infrared images, and forward and backward animation. For animation purposes, remapped GMS imagery has an 8-km resolution. One disadvantage of the SSM/I microwave data is that the 85.5 GHz microwave channel has a footprint at the zenith point of 15 km by 13 km, and the 19.35 GHz channel has a footprint of 69 km by 43 km. The collocated GMS and DMSP imagery are remapped to a 25-km grid Mercator projection for detailed analyses. Thus, the GMS image resolution is considerably degraded, the 85 GHz microwave data is slightly degraded, and the 19.35 GHz data resolution is artificially enhanced.

B. ANALYSIS PROCEDURES

The goal is to analyze the characteristics of MCSs that were present in two developing TCs (developers), and compare these with MCSs in systems that were thought to be developing into TCs but did not (non-developers). The MCSs studied here are a small subset of the MCSs in developing and non-developing TCs, as well as other MCSs separate from the TCs that are part of the population of general convective systems followed during 1997. The MCSs in the developing TCs are defined by following a TC backward in time to identify the MCS(s) that contributed to the overall organization of the total circulation. The set of MCSs that were thought to have a potential to contribute to TC development, but did not, were identified from Tropical Cyclone Formation Alerts (TCFA) that were issued by the Joint Typhoon Warning Center (JTWC) and then canceled due to lack of TC development. The JTWC issues a TCFA whenever synoptic,

satellite, or other germane data indicate development of a significant TC is likely within 24 h.

1. Use of GMS Data

The primary use of the GMS data is to define the overall MCS characteristics, such as size, cloud-top temperatures, and duration. For developers, the infrared (IR) and visible imagery are used to identify individual MCSs that appear to have contributed to the TC development. Animated three-hourly IR imagery is first used to view the life-cycle stages of the MCS(s), and then hourly imagery is cataloged to define specific MCS characteristics. A similar procedure is used to define the characteristics of MCSs for the case in which a TCFA was issued and later canceled.

As mentioned above, an objective tracking program developed by Dr. P. Harr was used to track the movement of each individual MCS in the hourly GMS imagery. The tracking program is able to detect the movement of MCSs from the IR imagery based on two threshold cloud-top temperatures that may be set by the operator. Based on Chen et al. (1996), a cloud-top temperature of 235°K is used to indicate overall MCS coverage, and a cloud-top temperature of 208°K is used to indicate the boundary of the precipitating core of deep convection. A MCS is tracked when at least five contiguous image scan lines contain overlapping pixels (at 25 km resolution) at the appropriate threshold temperature for at least three continuous hours. The program terminates the tracking process when less than five contiguous image scan lines of the threshold temperature exist.

In addition to MCS tracks, the size, shape, and duration of each MCS are calculated. The MCS size and shape characteristics are defined from the irregular pixel edges satisfying the threshold temperature criteria. The distances from the center of the contiguous scan lines to these edges are fit with a bivariate normal distribution to define an ellipse that contains a 95 percentage of the MCS area. Coverage statistics for the MCS sets in developing versus non-developing TCs are obtained by cross referencing the MCSs that were subjectively determined to be in these categories with the parameters defined by the objective tracking system.

2. Use of SSM/I Data

The SSM/I data may be used to define a more detailed MCS cloud structure because the microwave radiance emanates from within the clouds rather than at the cloud top as in the infrared imagery. The passive microwave retrievals of the SSM/I are grouped into two categories. The lower frequency (19.35 GHz) is emission-based, where liquid precipitation in the MCS causes brightness temperature increases over a radiametric cold (ocean) background. The higher frequency (85.5 GHz) is scattering-based, in which precipitation particles, particularly above the freezing level, cause brightness temperature decreases over a radiametrically warm background. Thus, the upwelling brightness temperatures measured by the SSM/I are functions of the total liquid water and ice amounts in clouds (McGaughey et al. 1996).

Although the ocean surface has a low emissivity at 85.5 GHz, the emissivity is a strong function of polarization for the oblique viewing angles of the SSM/I (Spencer et al.

1989). For oceanic systems, the low brightness temperatures caused by low emissions can be confused with low brightness temperatures caused by ice scattering (Mohr and Zipser 1996). To compensate for this background effect, a polarization-corrected temperature (PCT) is required. As defined by Spencer et al. (1989), the PCT is calculated from the 85.5 GHz horizontally (T85h) and vertically (T85v) polarized brightness temperatures by the following formula:

$$PCT = 1.818(T85h) - 0.818(T85v). \quad (1)$$

In the following sections, reference to 85.5 GHz brightness temperatures will be to this PCT.

Different threshold temperatures from the SSM/I data can be used to identify regions with varying rain rates in the MCS. At 19.35 GHz, a 220 °K brightness temperature threshold corresponds to an average rain rate of about 3 mm/h, which was derived from radiative transfer modeling by Wilheit et al. (1977) and Savage (1976). Similarly, a 255 °K threshold at 85.5 GHz is also 3 mm/h (Spencer et al. 1989). By specifying these threshold temperatures, identification of the convective and stratiform regions under the cirrus shield becomes possible.

For this study, a technique defined by Liu and Curry (1992) is used to define a threshold relationship between brightness temperature and rain rate. Precipitation thresholds are based on a 10-day history of the difference between T19h and T85h brightness temperatures. The minimum in this difference relative to the T19h temperature has been shown to be related to the onset of precipitation (Liu and Curry

1992). The threshold temperature (T_{TH}) at 19.35 GHz is defined as the minimum difference between the T19h and T85h temperatures. The Liu and Curry (1992) rain rate algorithm is defined as:

$$R = \propto (\Delta T_B - \Delta T_{bo})^{\gamma}, \qquad (2)$$

where ΔT_B = T19h - T85h and $\Delta T_{bo} = T_{TH}$ - T85h. The coefficients $\propto$ and γ are defined to account for non-uniform rainfall within one satellite pixel, which is referred to as the beamfilling problem. Liu and Curry (1992) define $\propto = 5.5 \times 10^{-3}$ and $\gamma = 1.6$. The primary advantages of this algorithm are that it accounts for both emission and scattering signals and the precipitation threshold is defined from SSM/I data that are current to the period rather than a climatological reference state.

C. SATELLITE CLOUD CLASSIFICATION

In this study, the cloud classification scheme uses both satellite infrared and microwave data similar to the method used by Liu et al. (1995). The GMS infrared data are used to determine the cloud-top temperature, and the SSM/I microwave data are used to determine an index that includes both microwave scattering and emission.

The GMS infrared data are used to separate cloudy from clear-sky pixels and to determine cloud-top temperature. After determining the distribution of cloud-top temperatures, a high brightness temperature (T_{max}) is defined as the median temperature over the warmest portion of the distribution. If a pixel has a brightness temperature lower than T_{max} - 3°K, it is then categorized as a cloudy pixel, and all pixels with higher temperatures than this threshold are defined as cloud-free. The 3°K threshold is similar

to the value (2.5°K) used by Rossow and Schiffer (1991). It is found that T_{max} ranges from 292°K to 297°K in the tropical regions (Liu et al. 1995).

A "microwave index" f is defined by Liu et al. (1995) to represent the strength of the microwave signal from a cloudy pixel:

$$f = (1-D/D_o) + 2(1-PCT/PCT_o), \quad (3)$$

where D = T19v - T19h represents the polarization at 19 GHz, T19v and T19h are the vertically and horizontally polarized brightness temperatures respectively, and D_o is the D value at the threshold for precipitation. Similarly, PCT_o is the PCT value at the threshold for the onset of precipitation. The precipitation threshold is determined according to Liu and Curry (1992) as defined above with reference to the rain rate algorithm. The first term on the right side of (3) represents the microwave emission signal, and the second is the microwave scattering signal, so that the index f accounts for both emissions and scattering.

The relationship between the microwave index (f) and the rain rate derived from SSM/I data of a single MCS on 24 August 1997 is shown in Figure 2.1. The rain rate increases with f, is zero when f equals zero, and about 9 mm/h when f is about 1.6.

As mentioned above, the microwave index f is a good indicator of rainfall rate, which can then be used to identify convective and stratiform regions of the MCS. Following Liu et al. (1995), a satellite pixel is classified into one of eight categories (Figure 2.2) based on the microwave index f and the GMS cloud-top temperature: (1) warm, nonprecipitating cloud; (2) warm, precipitating cloud; (3) mid-level,

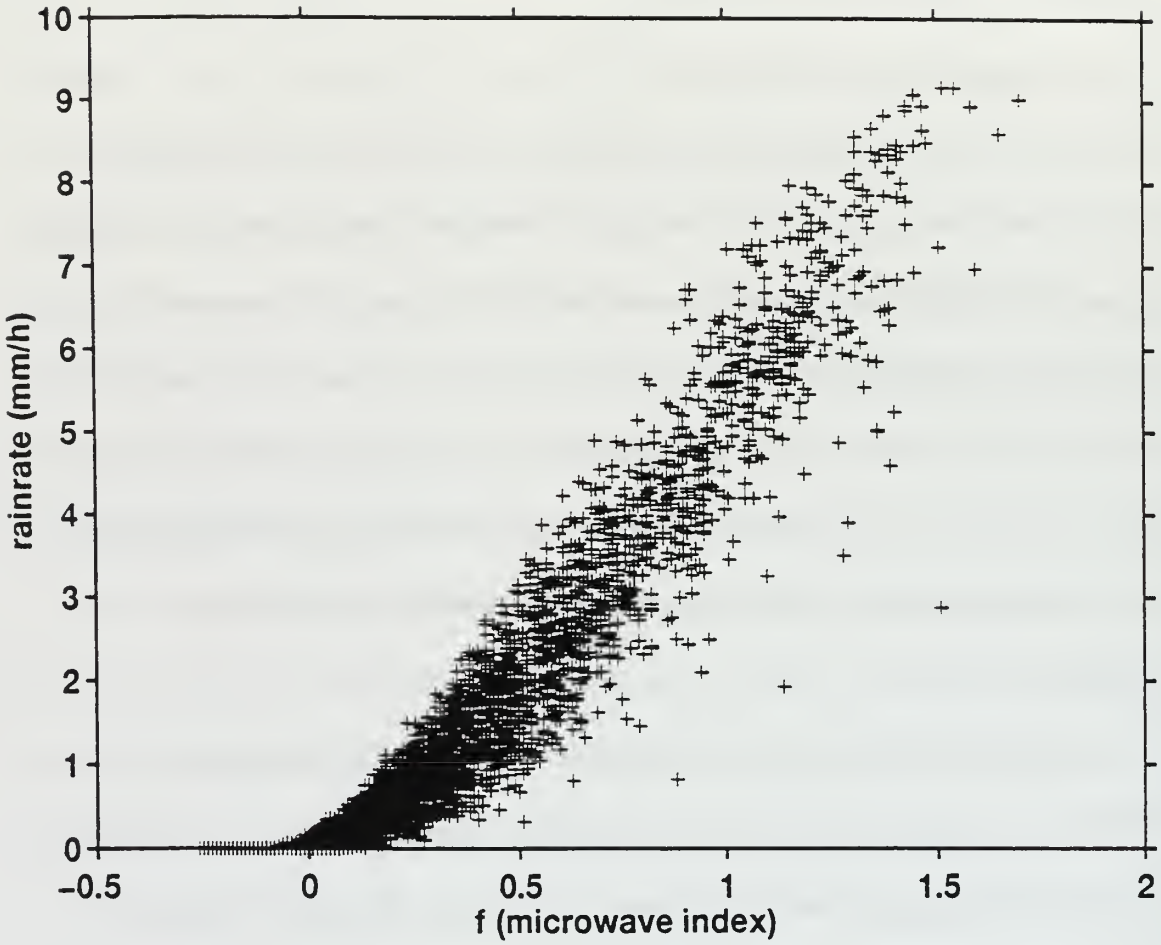

Figure 2.1. Relationship between microwave index f derived from SSM/I data and rain rate for life cycle of MCS A associated with Super Typhoon Bing.

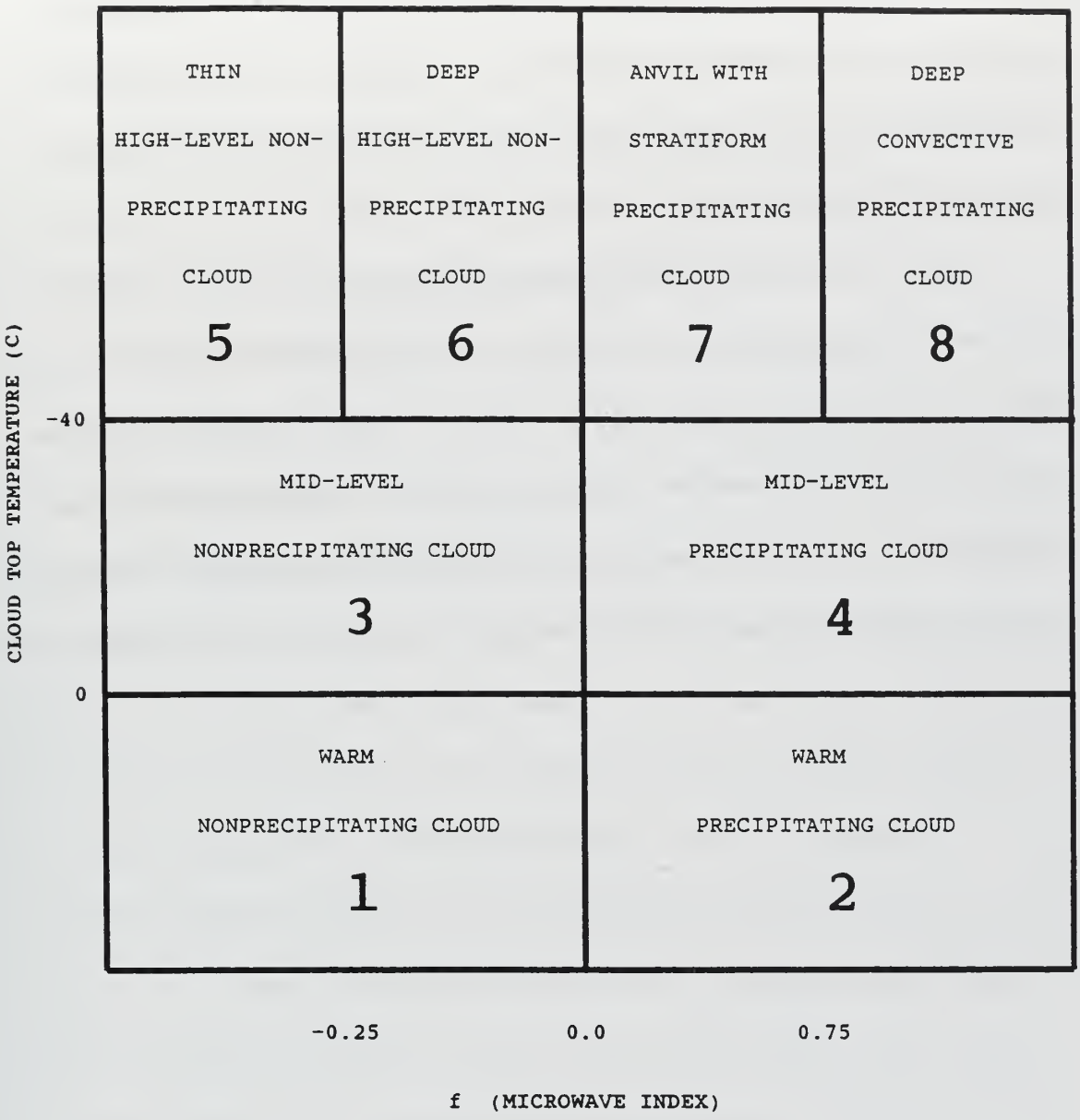

Figure 2.2. Diagram of microwave index f versus cloud-top temperature for cloud classification (after Liu et al. 1995).

nonprecipitating cloud; (4) mid-level, precipitating cloud; (5) thin high-level nonprecipitating cloud; (6) thin high-level precipitating cloud; (7) anvil with stratiform precipitating cloud; and (8) deep convective precipitating cloud. Cloud-top temperatures that are higher than T_{max} - 3, where T_{max} is chosen from the thresholds defined for each image, are classified as cloud-free.

With the above data evaluation methods, instantaneous snapshots of SSM/I data can be used to determine rain rate, which characterizes the intensity of the convective and stratiform regions. The microwave index in conjunction with GMS imagery determines cloud type, which makes identification of the convective and stratiform regions easier. This information can be used in conjunction with a sequence of hourly GMS imagery until the next SSM/I overpass to define the temporal evolution of each type of MCS, and thus its contribution to TC genesis.

III. CASE STUDIES

Tropical systems were categorized by MCS characteristics as discussed in Chapter II.B. and C. This chapter will discuss three case studies in detail using the techniques discussed earlier. The three case studies are Super Typhoon (ST) Bing, ST Ivan, and two MCSs during a TCFA that did not develop into a TC.

A. SUPER TYPHOON BING

1. Overall Evolution

ST Bing was a large TC in the western North Pacific during late August 1997 (Figure 3.1). A pre-Bing tropical disturbance, which is identified as MCS A in Figure 3.2, formed well east of the monsoon trough. The MCS A track begins at 1330 UTC 24 August 1997 as a cloud cluster at approximately 8°N, 170°E and grows rapidly through the nighttime diurnal maximum period (Figure 3.3). The MCS moved westward as it progressed through the life-cycle stages discussed in Chapter I.B. During one development period, the MCS exhibited deep convection with a nearly circular anvil (Figure 3.4). Following this development cycle, the MCS broadened and convection became concentrated in distinct cells, which were embedded within a broad stratiform cloud region (Figure 3.5). Rotation became evident at this time as the curved low-level cloud bands became exposed. Although the area of the circulation expanded (Figure 3.6), convection remained along the periphery with new convection being forced in the confluent southwesterly flow. The deep convection that defined MCS A finally

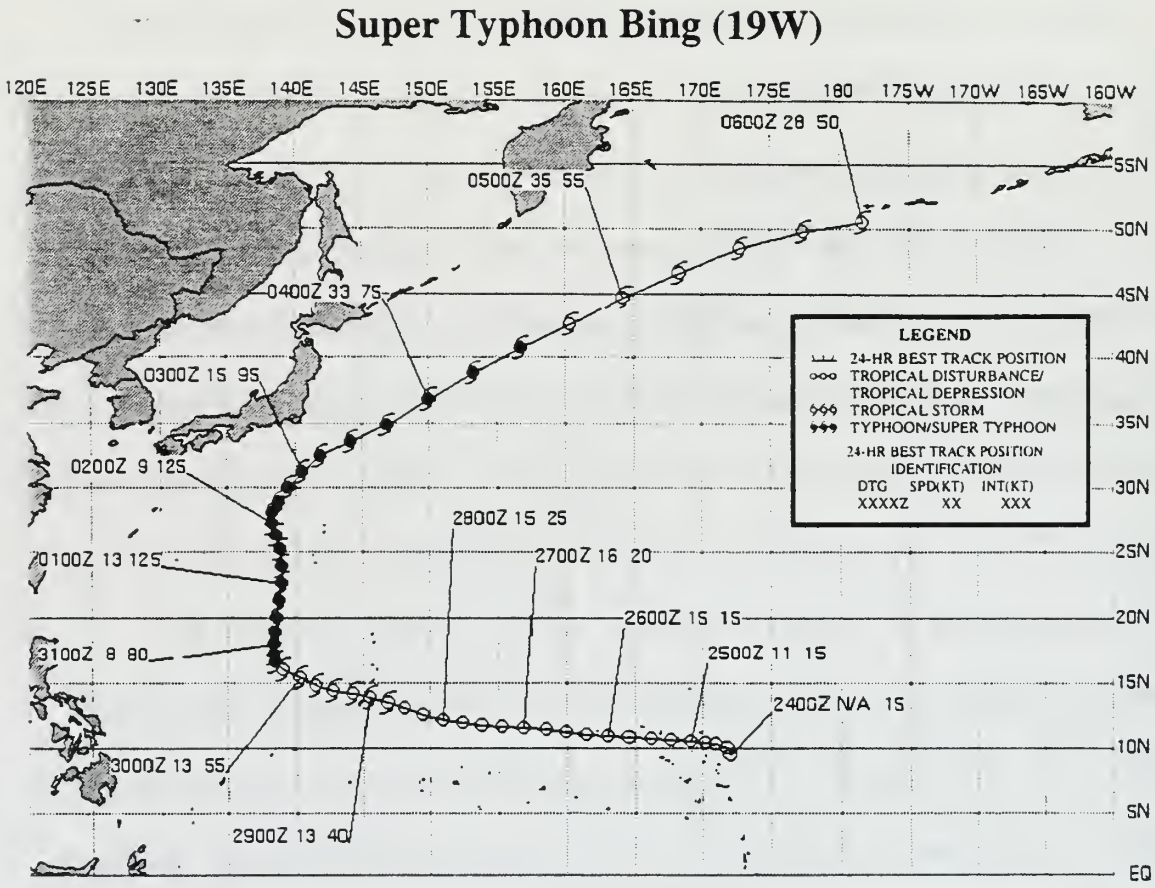

Figure 3.1. Super Typhoon Bing (19W) best track from JTWC each 6 h from 24 August to 6 September 1997. The minimum sea-level pressure (not shown) was 904 mb and the maximum intensity was 135 kt.

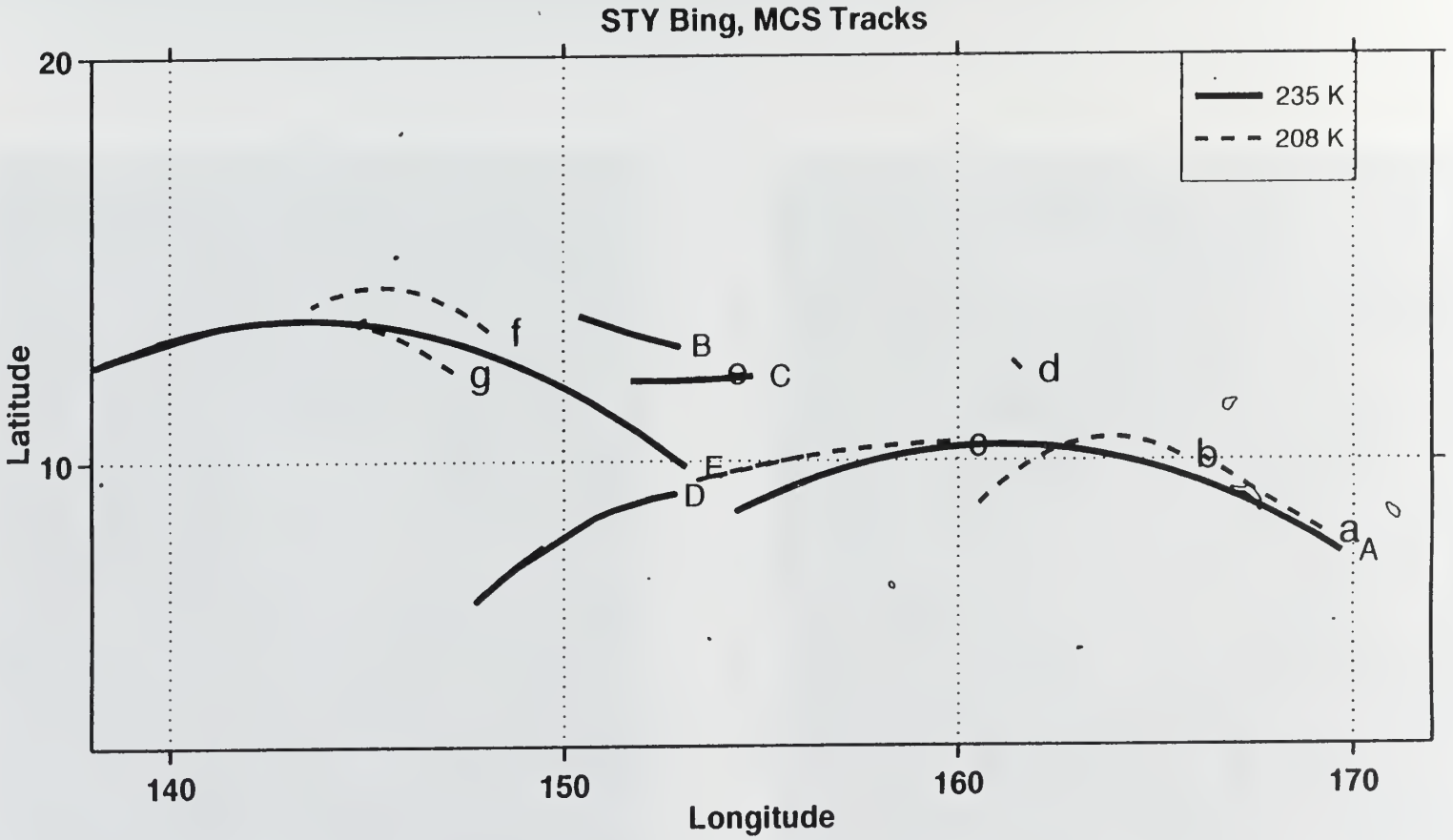

Figure 3.2. Tracks of MCSs associated with the development of Super Typhoon Bing from 1330 UTC 24 August 1997 through 2330 UTC 28 August 1997. The solid lines with upper case letters are the track of the 235°K temperature core of the MCS, and the dashed lines with lower case letters are the track of the 208°K temperature core of the MCS.

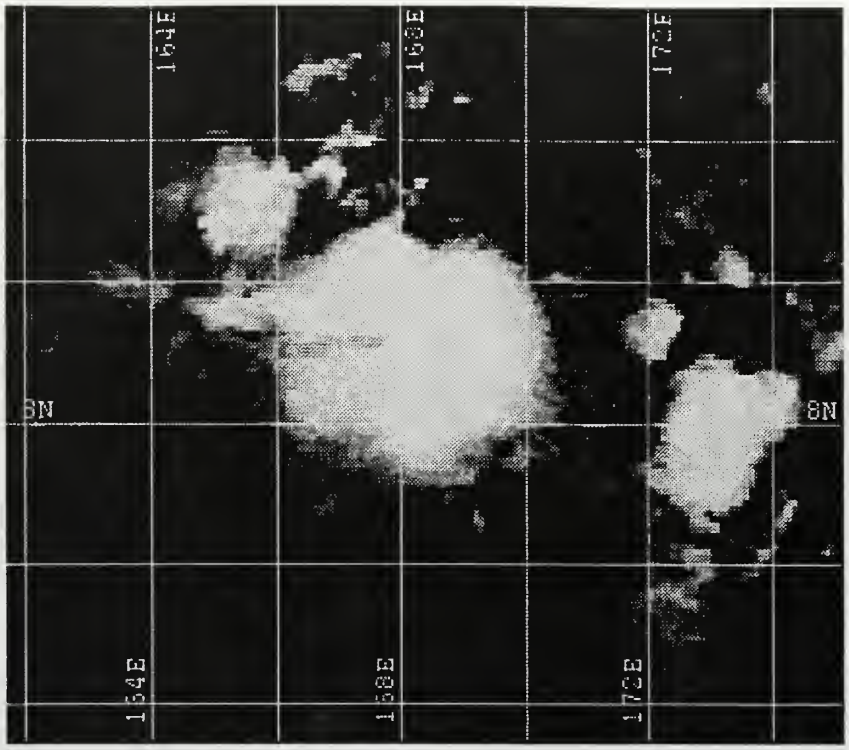

Figure 3.3. GMS IR image of MCS A at 2132 UTC 24 AUG 97.

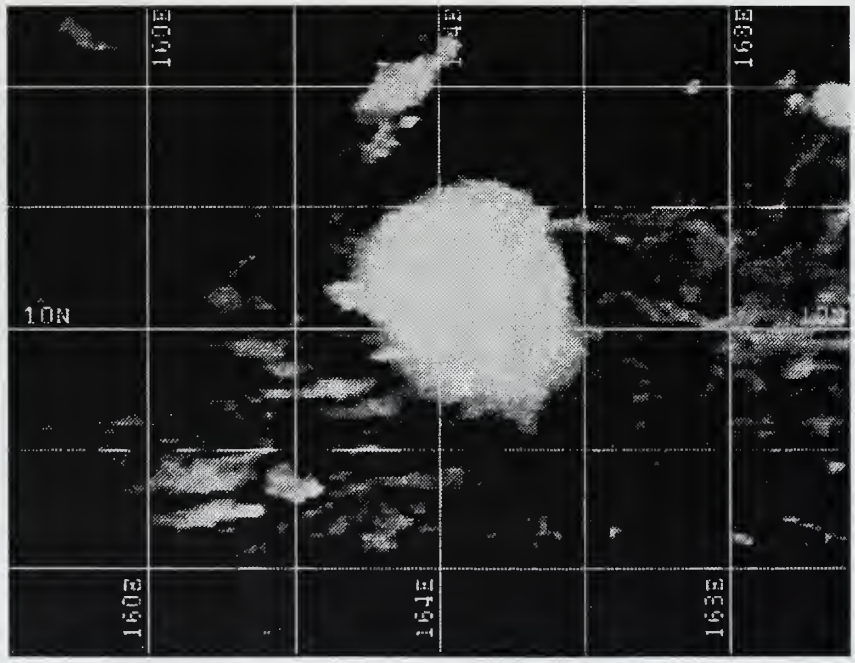

Figure 3.4. GMS IR image of MCS A at 0932 UTC 25 AUG 97.

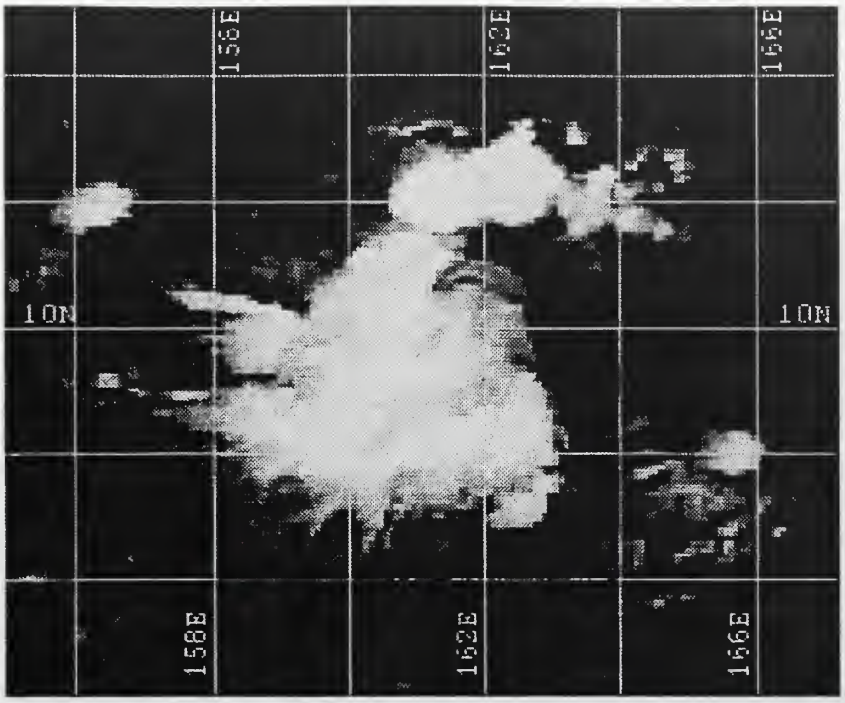

Figure 3.5. GMS IR image of MCS A at 1932 UTC 25 AUG 97.

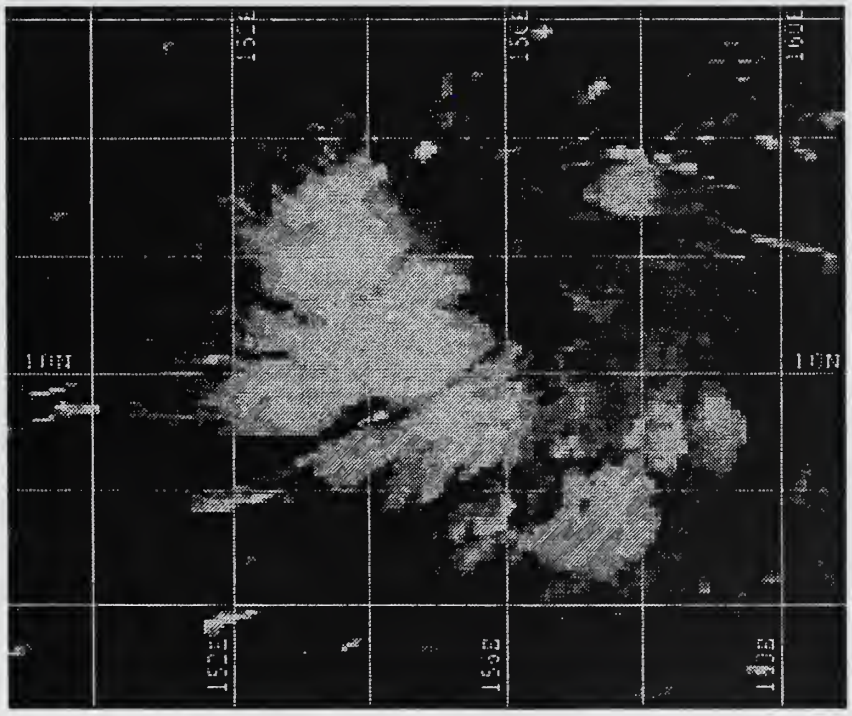

Figure 3.6. GMS IR image of decaying MCS A at 1232 UTC 26 AUG 97.

dissipated at approximately 1700 UTC 26 August 1997 near 9°N, 154°E after having persisted for more than 51 h and traveled westward about 16° longitude (Figure 3.1).

After the cirrus shield thinned at 1930 UTC 26 August 1997 (Figure 3.7), it became evident that the broad circulation was not maintained and a circulation center seemed to be located to the southwest where new convection appeared. A new MCS began to develop in this region at 0030 UTC 27 August 1997 (Figure 3.8), which is labeled MCS B in Figure 3.2. The first TC warning was issued by JTWC as Tropical Depression (TD) 19W at 0600 UTC 27 August 1997 (Figure 3.9), as a weak cyclonic circulation became evident even though MCS B was actually dissipating. Over the next two hours, the deep convection in MCS B moved rapidly westward and began to dissipate (Figure 3.10). New convection formed (MCS C in Figure 3.2) in the low-level confluent flow to the southwest, which coincides with the initial warning position issued by JTWC. MCS C followed a similar track (Figure 3.2) to MCS B and also dissipated once it became separated from the low-level southwesterly flow.

As MCS C decayed, new convection (MCS E) again formed to the east and slightly south (Figure 3.2). Also, there was an increase in overall convective activity in the broad southwesterly flow (Figure 3.11) farther to the south (MCS D in Figure 3.2), which suggests that conditions for further organization were improving. During the life cycle of MCS E, the entire circulation seemed to organize about it (Figure 3.11). Whereas a multitude of individual MCS elements within the overall convective complex had cyclonically curved paths and variable translation speeds from formation to

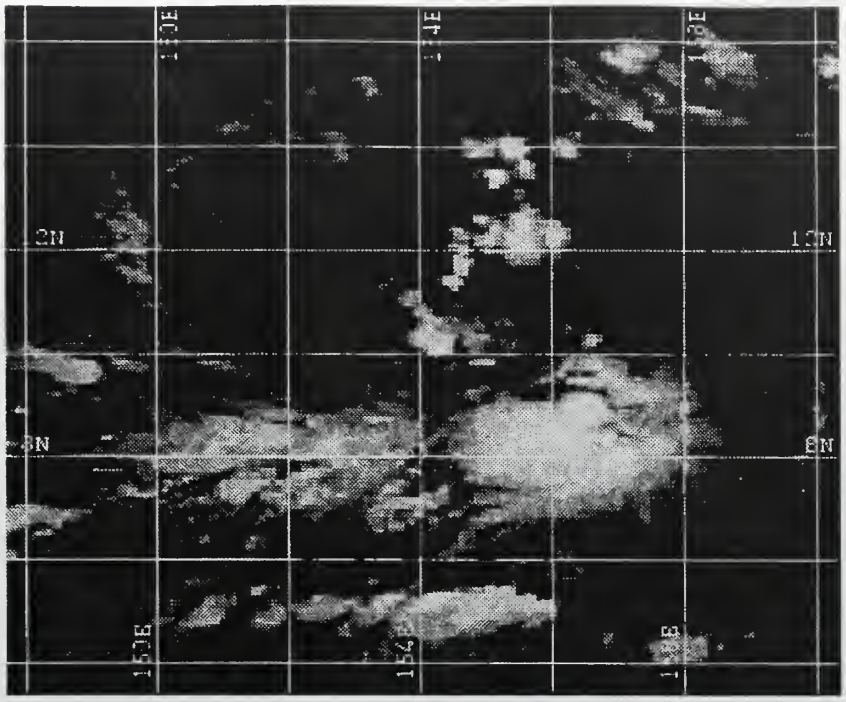

Figure 3.7. GMS IR image at 1932 UTC 26 AUG 97.

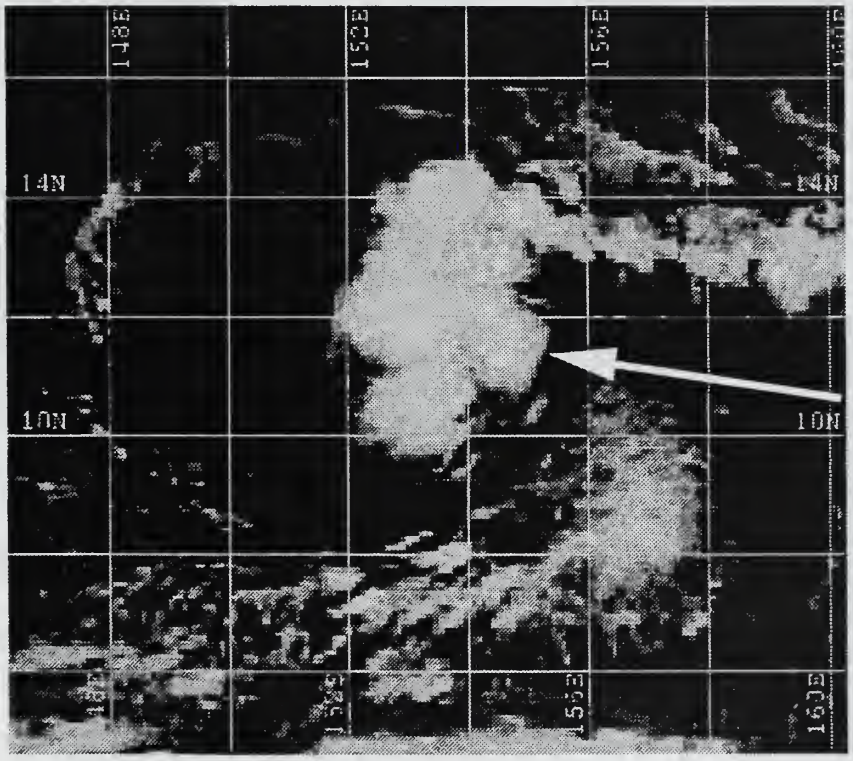

Figure 3.8. GMS IR image of MCS B at 0032 UTC 27 AUG 97.

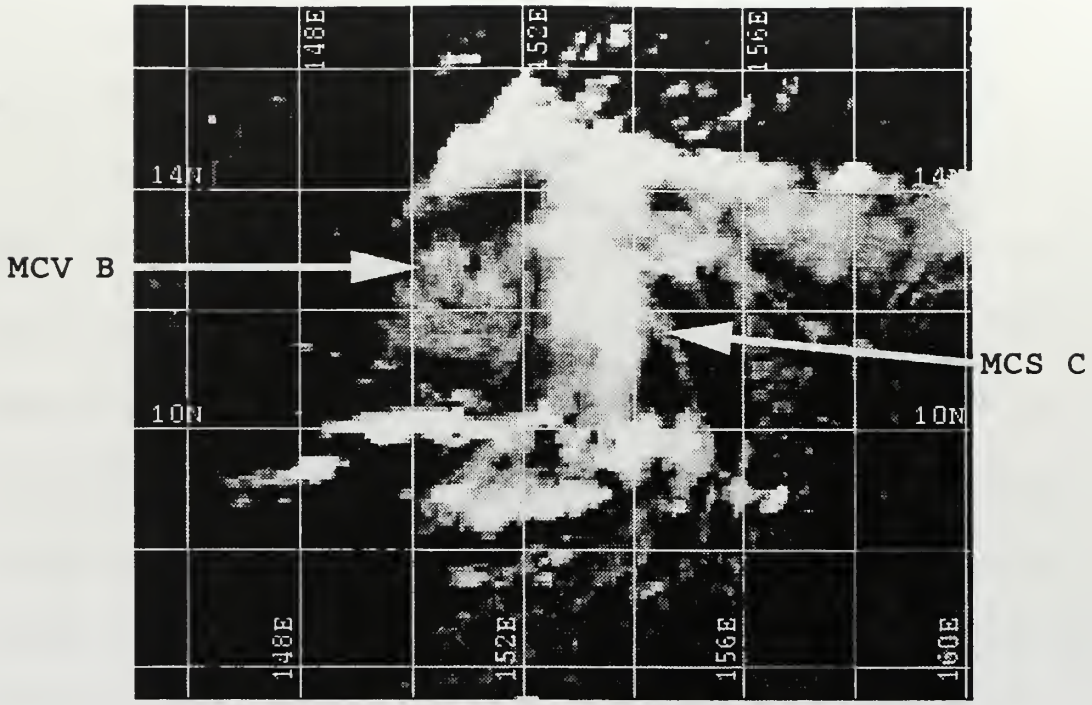

Figure 3.9. GMS IR image at 0632 UTC 27 AUG 97.

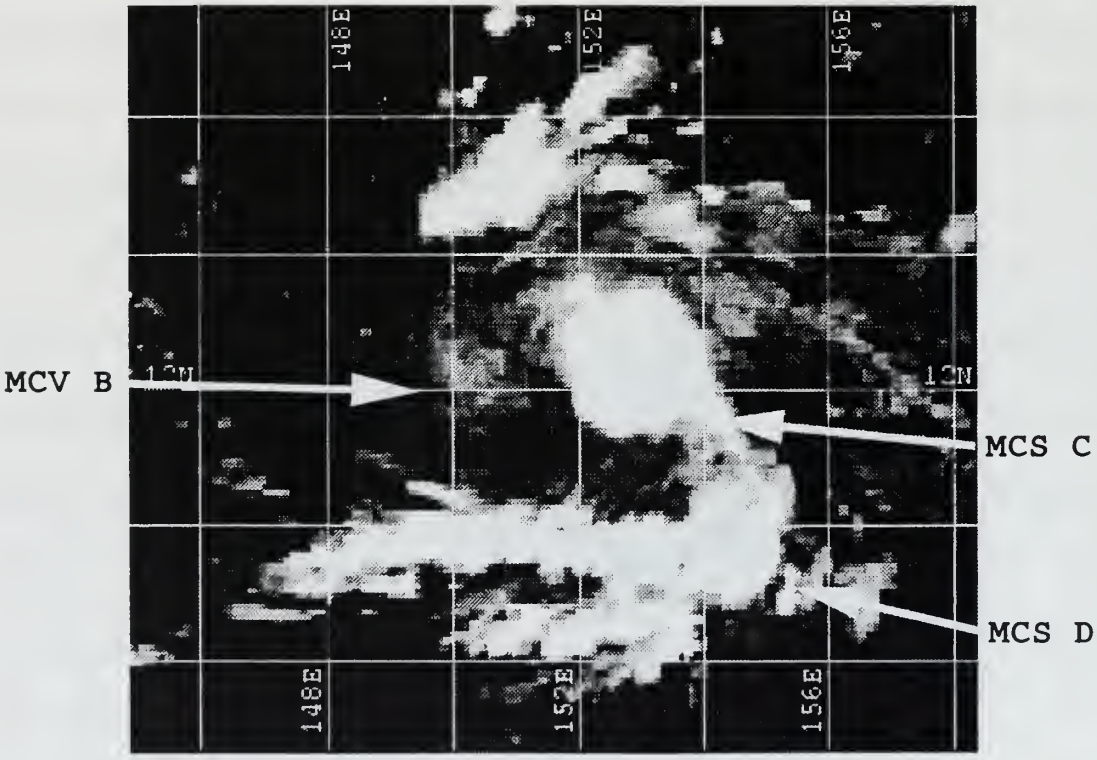

Figure 3.10. GMS IR image at 0832 UTC 27 AUG 97.

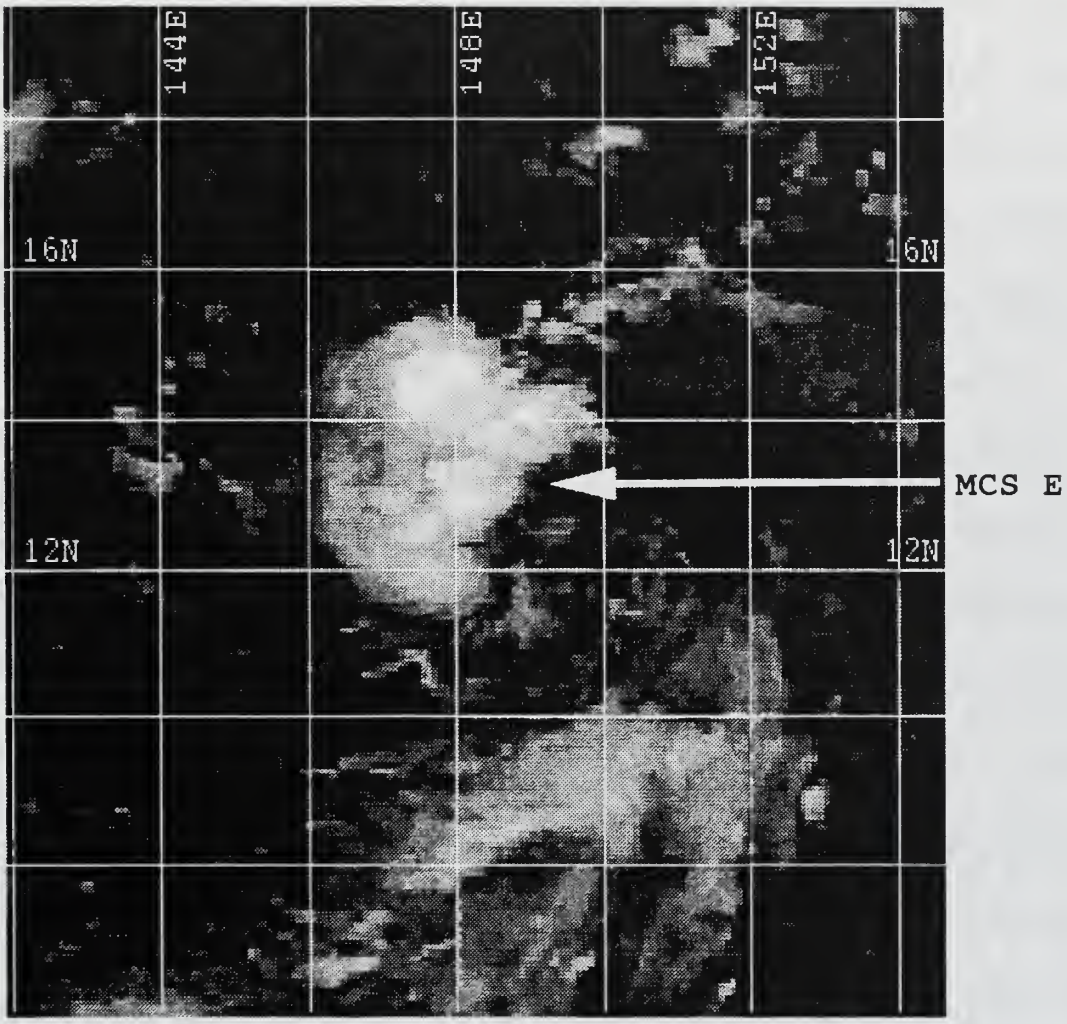

Figure 3.11. GMS IR image of MCS E at 0732 UTC 28 AUG 97.

dissipation (Figure 3.2), the post-storm analysis by JTWC has a straight track and nearly uniform translation speed of 15-16 kt.

The NOGAPS 200-mb analysis field (not shown) suggests that MCS A decayed because of moderate northeasterly upper-level wind shear. The NOGAPS 850-mb analyses at 0000 UTC 24 August 1997 and 0000 UTC 25 August 1997 (Figures 3.12a,b) depict a small stationary cyclonic circulation near 9°N, 171°E that initially seems to be associated with the formation of MCS A midway between these two analyses. This small circulation moves into the eastern edge of the monsoon trough, which results in a broad eastward extension of the trough by 0000 UTC 26 August 1997 (Figure 3.12c).

Even though MCS B formed three hours later in the eastern portion of the monsoon trough, the circular nature of the cirrus in Figure 3.8 suggests MCS B was considerably less influenced by upper-level wind shear (not shown) than MCS A. The track of MCS B (Figure 3.2) indicates that it moved westward into the monsoon trough by 0000 UTC 27 August 1997 (Figure 3.12e), where there was an environment of cyclonic vorticity. However, after MCS B moved away from the influence of the southwesterly flow, it dissipated and its associated low-level curved cloud lines also dissipated a short time later. In the interval between Figures 3.12e and f, MCS C then formed near 12°N, 153°E in westerly flow equatorward of the broad trough, and seemed to follow a similar life cycle to MCS B. MCS E formed near 10°N, 154°E in the confluent southwesterly flow as the entire circulation finally began to organize (Figure 3.12e,f).

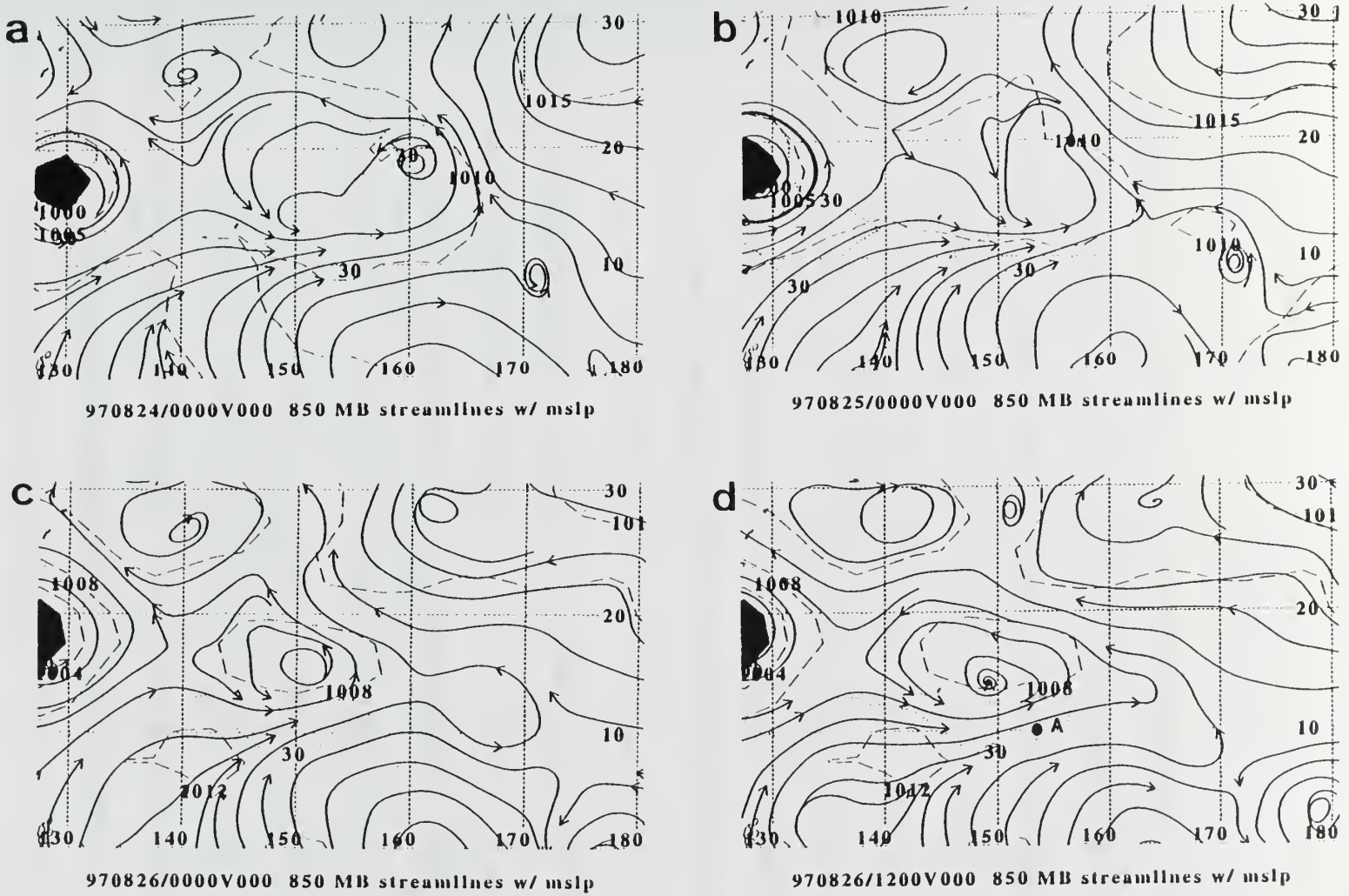

Figure 3.12. NOGAPS 850-mb streamline (solid with arrows), 850-mb 30 kt isotach (dotted), and mean sea-level pressure analyses (dashed, interval 4 mb) for 0000 UTC on (a) 24, (b) 25, and (c) 26 August, (d) 1200 UTC 26 August, (e) 0000 UTC and (f) 1200 UTC 27 August 1997. Locations of the MCSs in Figure 3.2 at the times of these analyses are shown by dots.

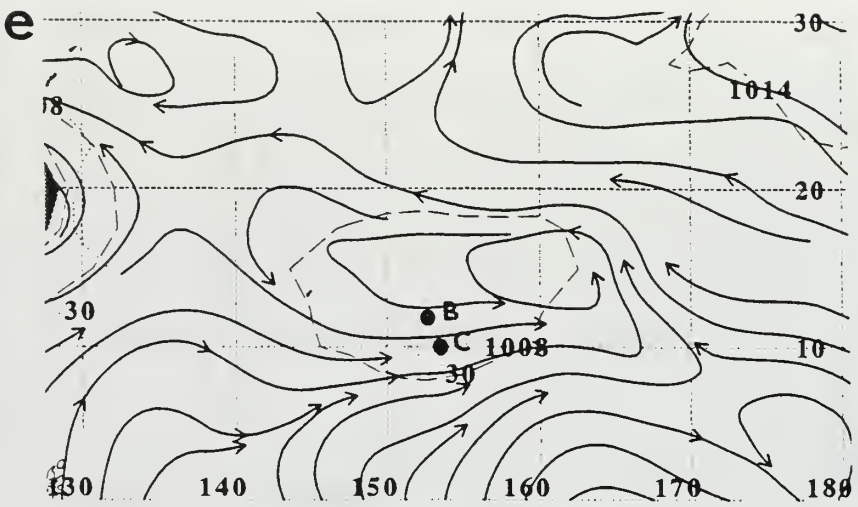

970827/0000V000 850 MB streamlines w/ mslp

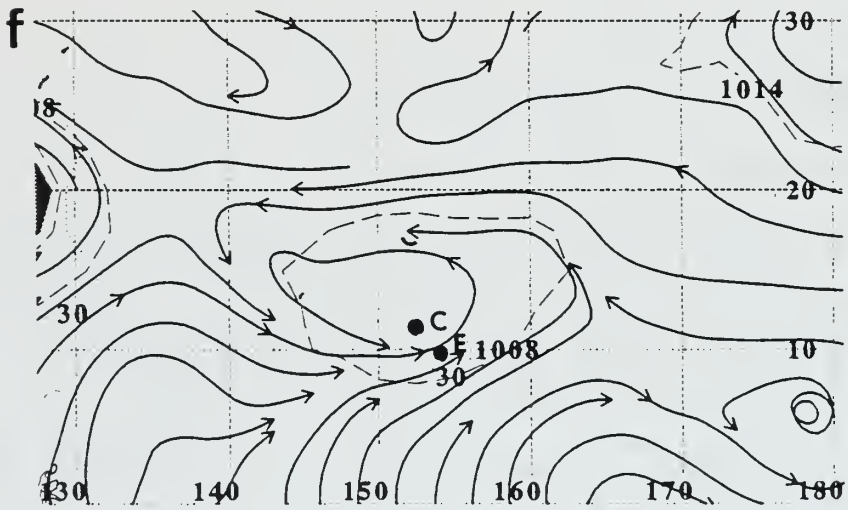

970827/1200V000 850 MB streamlines w/ mslp

Figure 3.12. (continued)

ST Bing can be classified as a combination-type TC formation, which is one pathway to TC genesis proposed by Finta (1997) that has significant contributions to TC development from both MCS and synoptic-scale dynamic forcing. At least three episodes of MCS life cycles and associated circulations occurred before a fourth MCS formed and the total circulation increased. The role of the synoptic scale was to provide conditions favorable for repeated MCS formation in the confluent southwesterly flow that defined the equatorward side of the monsoon trough. The initial MCS activity (MCS A) formed in an area where the synoptic dynamic forcing was weak. As MCS A moved westward toward the monsoon trough, the center moved into an area of favorable synoptic-scale forcing. However, upper-level shear seems to have been responsible for the decay of MCS A and the associated cyclonic circulation. The quick organization of MCS B and then MCS C seemed to consolidate the generally open environment of the monsoon trough. Even though these MCSs soon dissipated, the synoptic environment now was more favorable for the formation of MCS E.

In terms of the NOGAPS 850-mb analysis sequence (Figure 3.12 a-f), the small circulation near 9°N, 171°E by 0000 UTC 24 August 1997 moved into the eastern edge of the trough. However, the NOGAPS analysis indicates an organized circulation developed near 14°N, 149°E at 1200 UTC 26 August 1997, which appears to be 7° longitude west of the apparent circulation that is evident in Figure 3.6. Convection continued to be forced farther to the southeast in the low-level confluence, rather than being near the center of the synoptic-scale circulation. At 0000 UTC 27 August 1997, a

weak circulation center formed to the east at 5°N, 160°E, which reflected the formation of the new convection while the circulation at 14°N, 149°E weakened.

In summary, ST Bing is classified as a combination-type case because of the mutual interaction between the synoptic circulation (indicated by the NOGAPS 850-mb analysis sequence) and the MCS activity (indicated by the satellite imagery). Even though all the ingredients within the monsoon trough seemed to exist for imminent TC formation, repeated MCS activity was a vital ingredient that contributed to the overall system organization.

2. MCS Structure

As defined in Chapter II.C, the rain rates and cloud types are calculated for each tracked MCS. The rain rates and cloud types for MCS A, B, C, D, and E are defined within the areal extent of each MCS. A comparison between the stratiform and convective rain rates depicts the life cycles of each MCS during the formation period of ST Bing.

The time history of the hourly ellipse coverage for MCS A indicates the areal growth and shape evolution of the overall system (Figure 3.13). The area of each MCS is defined by a 95% coverage ellipse that is determined by the fit of a bivariate normal distribution to the contiguous pixels with satellite IR temperatures less than 235°K. The total area of the ellipse that is covered by convective and stratiform cloud types, along with the percent coverage of each ellipse, are then computed (Figures 3.14a,b). During the initial few hours, the amount of convective and stratiform cloud vary together. Near

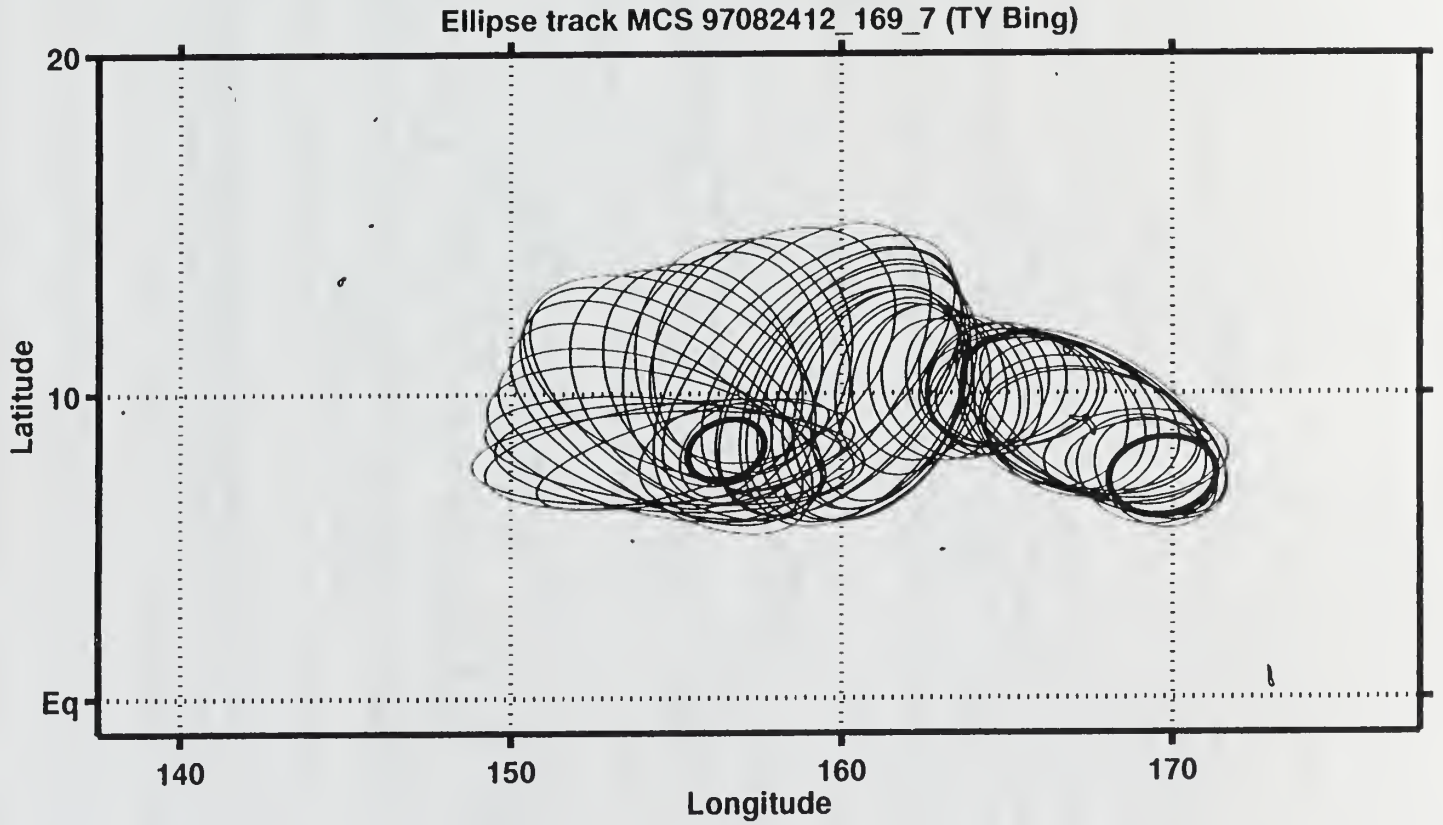

Figure 3.13. Sequence of ellipses centered along the track of MCS A from 1330 UTC 24 August 1997 through 1700 UTC 26 August 1997. The dark ellipse at 7°N, 170°E defines the beginning location and the dark ellipse at 8°N, 157°E defines the decay of MCS A.

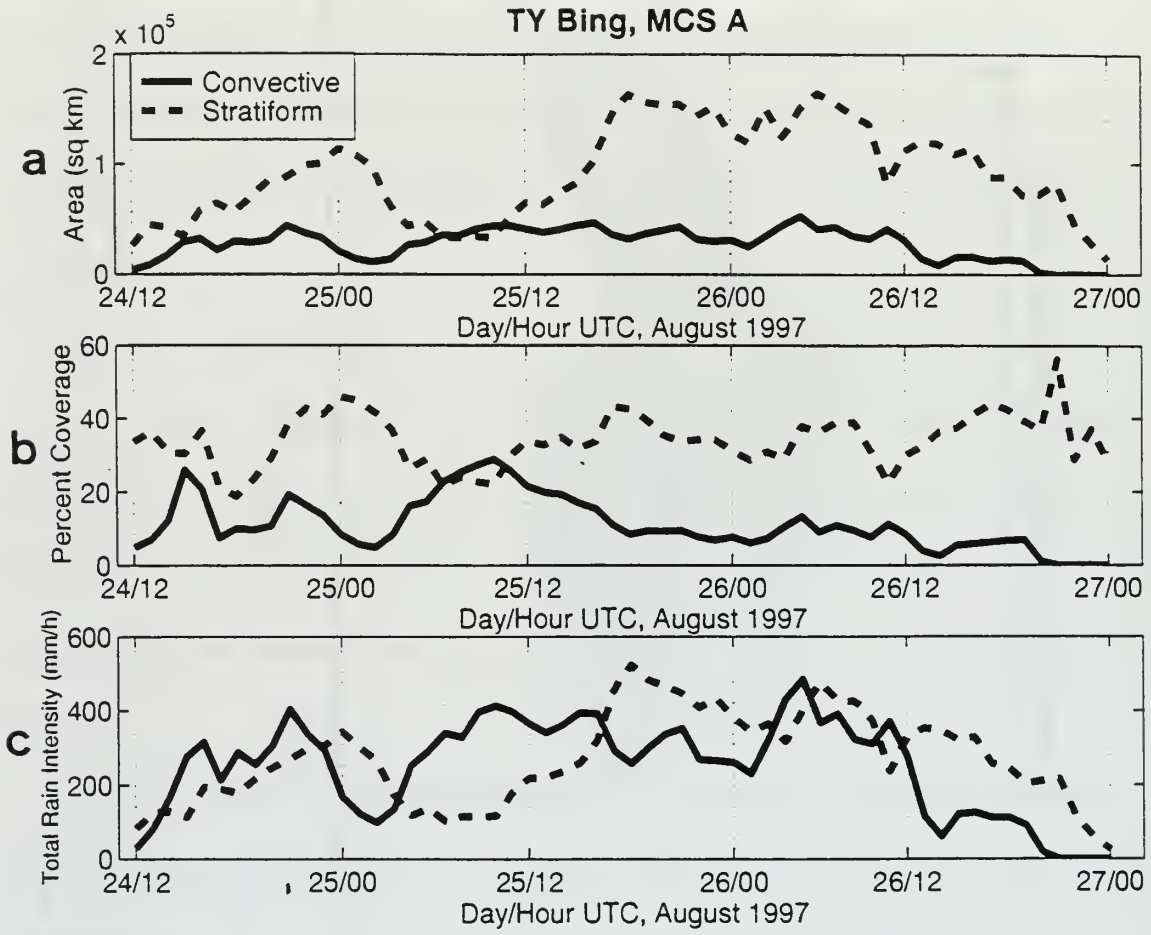

Figure 3.14.. (a) Area (sq km) and (b) coverage of convective and stratiform clouds for MCS A. (c) Total rain intensity (mm/h) averaged over the areas of convective and stratiform clouds for MCS A.

00 UTC 25 August 1997, a decrease in convective cloud coverage coincides with a large increase in stratiform cloud. A second convective increase peaks at 0900 UTC 25 August 1997 (Figure 3.14a), when the area of stratiform cloud is a minimum, an areal increase in convective clouds is then followed by a percent increase in stratiform cloud that then remains steady for nearly 24 h (Figure 3.14b). Also, the total areal coverage of stratiform cloud increases (Figure 3.14a) as the decaying MCS anvil spreads. This suggests a mature MCS structure that contains mesoscale ascent within the stratiform cloud over sinking motion within the unsaturated rain area (Houze 1992). These mechanisms coincide with mid-level convergence and vorticity production. It is during this period that rotation becomes evident in the curved cloud lines (Figure 3.5). During the decay stage (1200 UTC 26 August 1997), the convective and stratiform cloud areal coverages decrease rapidly (Figure 3.14a), while the percent coverage of stratiform cloud remains steady (Figure 3.14b).

The total rain intensities integrated over pixels containing each cloud type (Figure 3.14c) are consistent with the cloud-type history (Figures 3.14a,b). During the initial growth period, total convective rain intensity is larger than the stratiform amount. Afterwards, stratiform rain increases when convective rain decreases and vice versa until the decay stage in which both rain intensities decreased.

An east/west cross section (Figure 3.15) of the SSM/I PCT and 19 GHz temperature is constructed through MCS A at 2110 UTC 24 August 1997 (Figure 3.16), which corresponds to the time of the second convective increase in Figure 3.14. The cold

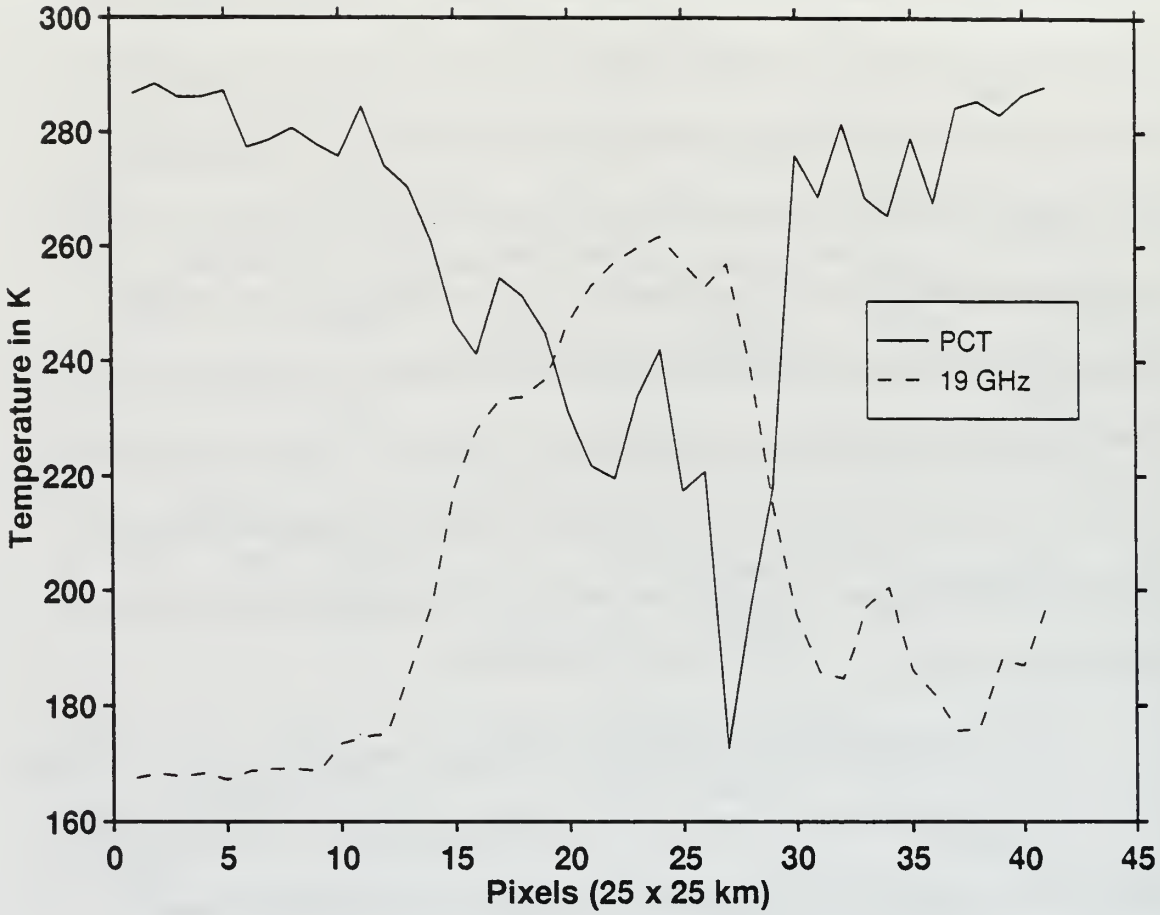

Figure 3.15. East/West cross section through MCS A at 2110 UTC 24 August 1997 along the line shown in Figure 3.16.

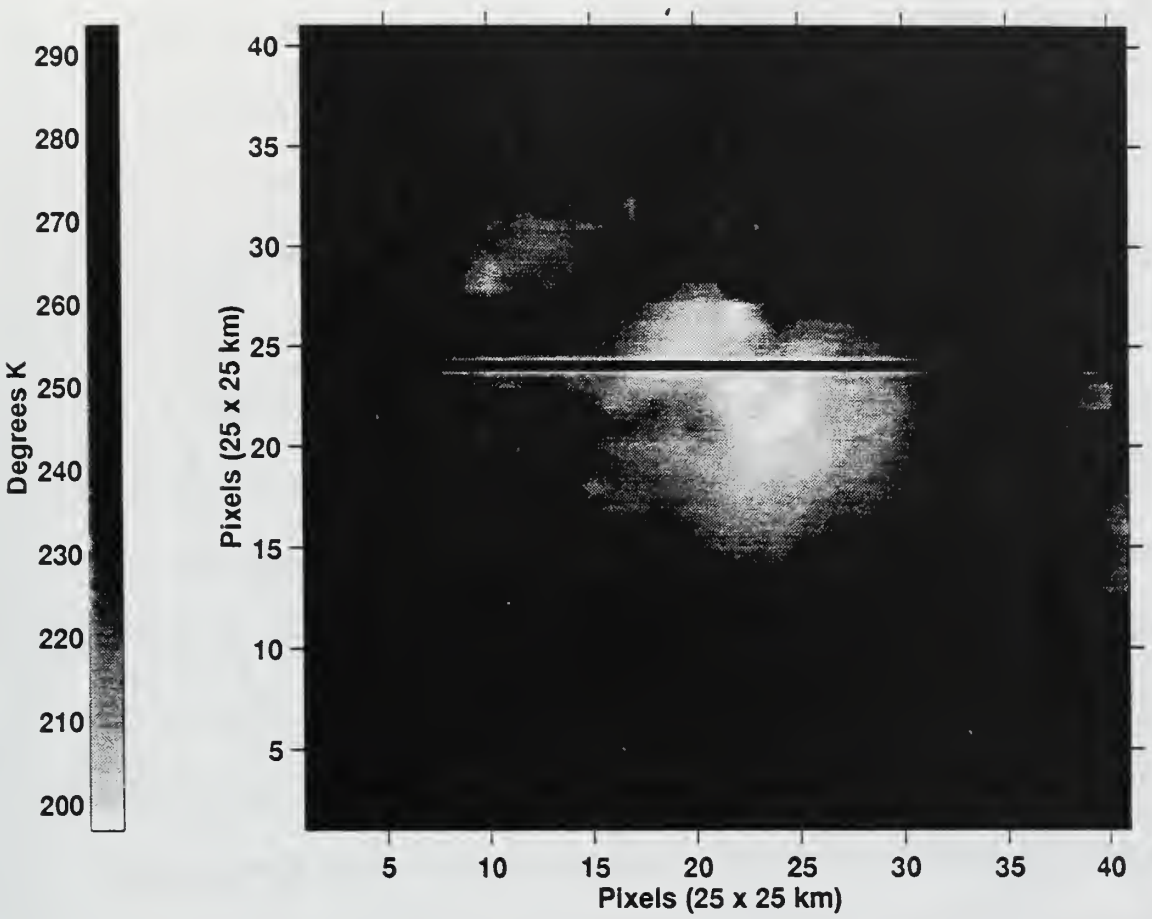

Figure 3.16. GMS IR image of MCS A at 2132 UTC 24 August 1997. The dark horizontal line is the cross section of MCS A for Figure 3.15.

(low) PCT values define the intense convective activity via scattering caused by ice particles suspended in the convective updraft. The high 19 GHz temperatures result from emission due to the low-level precipitation falling in the convective region. The cross section indicates the primary convective updraft (lowest PCT) is to the east of the low-level rainfall (warmest 19 GHz). This microwave signature has been found by McGaughey et al. (1996) to be indicative of a MCS that is beginning to decay.

The time history of hourly ellipse coverage for MCS B (Figure 3.17) indicates strong compact convection during the early life cycle stage that is quickly followed by a broadening of the total area as the MCS decayed rapidly. During the first 3 h, the area of convection is small (Figure 3.18a) with about 20% convective cloud (Figure 3.18b). Even though the convective cloud begins to decrease near 0000 UTC 27 August 1997, a large areal increase in stratiform cloud occurs (Figure 3.18a). This single convective-stratiform event over a short time interval resulted in a larger area with $\leq 235\,^{\circ}\mathrm{K}$ (Figure 3.18a) than did the multi-event, long-lasting MCS A in Figure 3.14. However, the maximum percentages of convective and stratiform clouds (Figure 3.18b) are about the same at 20% and 40%, respectively. During the decay period, stratiform coverage remains uniform, which may have contributed to the formation of a MCV that is revealed when the cirrus shield dissipates (Figure 3.9). At the time when the percent of convection decreases (0000 UTC 27 August 1997), the contribution to total rainfall intensity from the stratiform clouds becomes larger than the contribution from the convective clouds (Figure 3.18c).

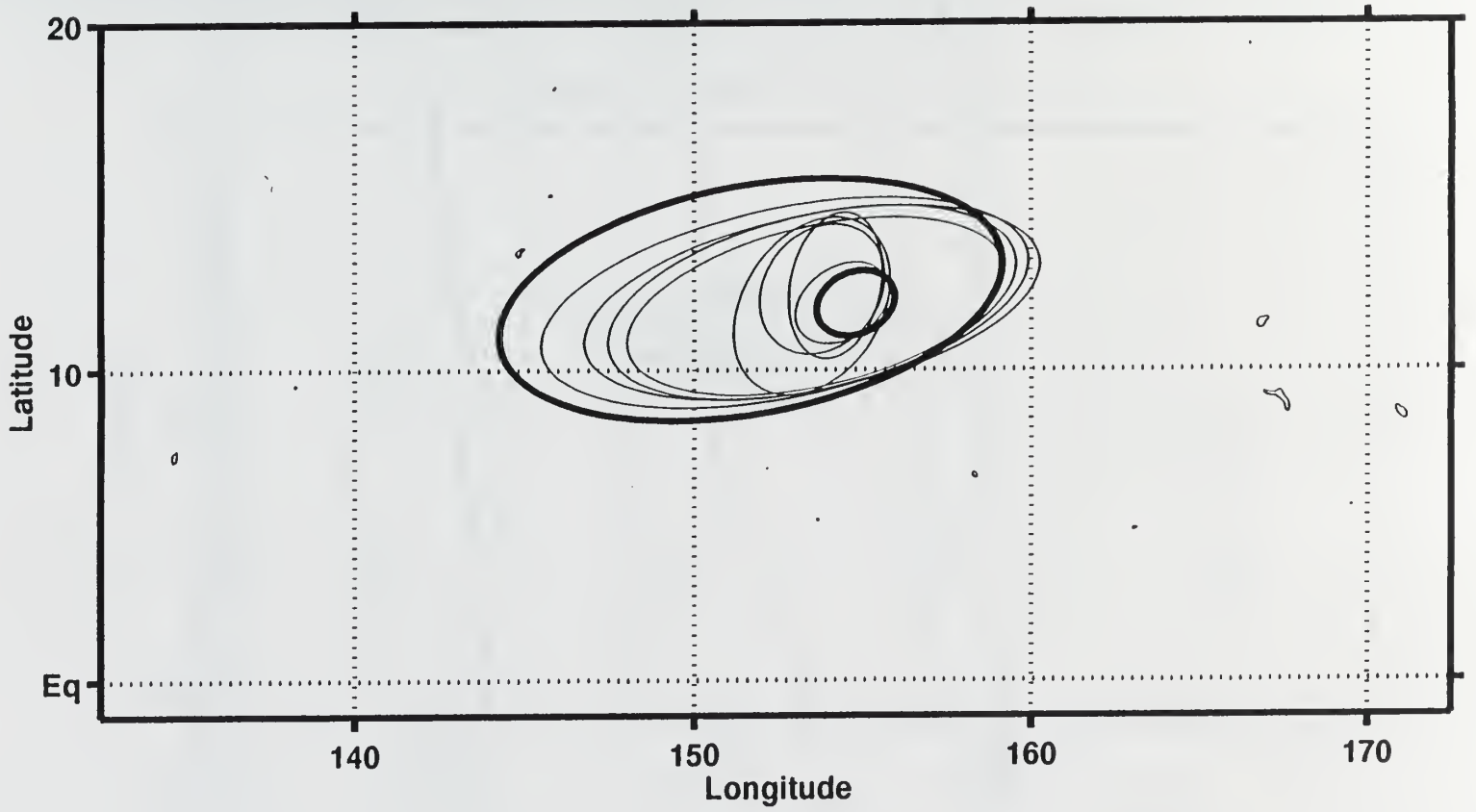

Figure 3.17. Sequence of ellipses centered along the track of MCS B from 2000 UTC 26 August 1997 through 0600 UTC 27 August 1997. The small and large dark ellipses are the start and finish of MCS B, respectively.

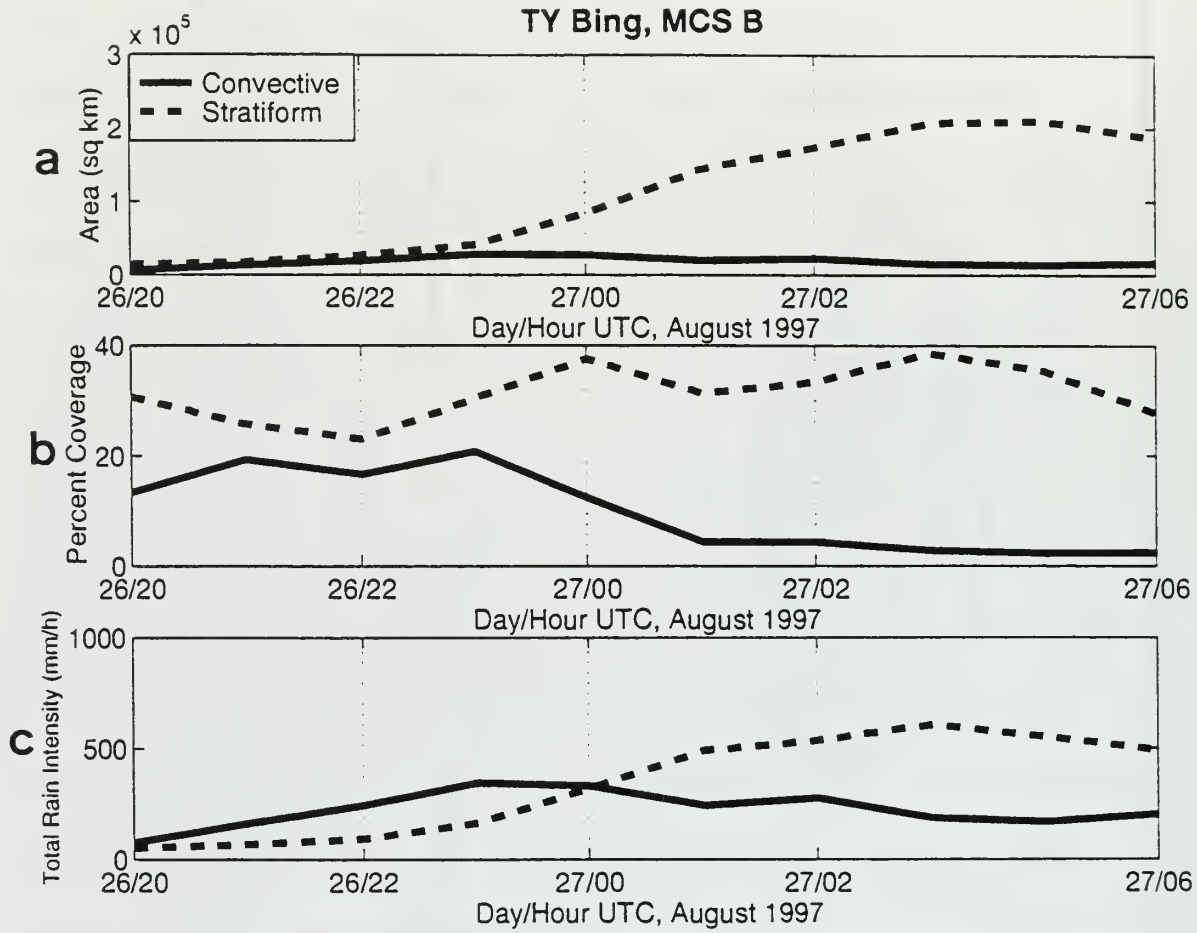

Figure 3.18. (a) Area (sq km) and (b) coverage of convective and stratiform clouds for MCS B. (c) Total rain intensity (mm/h) averaged over the areas of convective and stratiform clouds for MCS B.

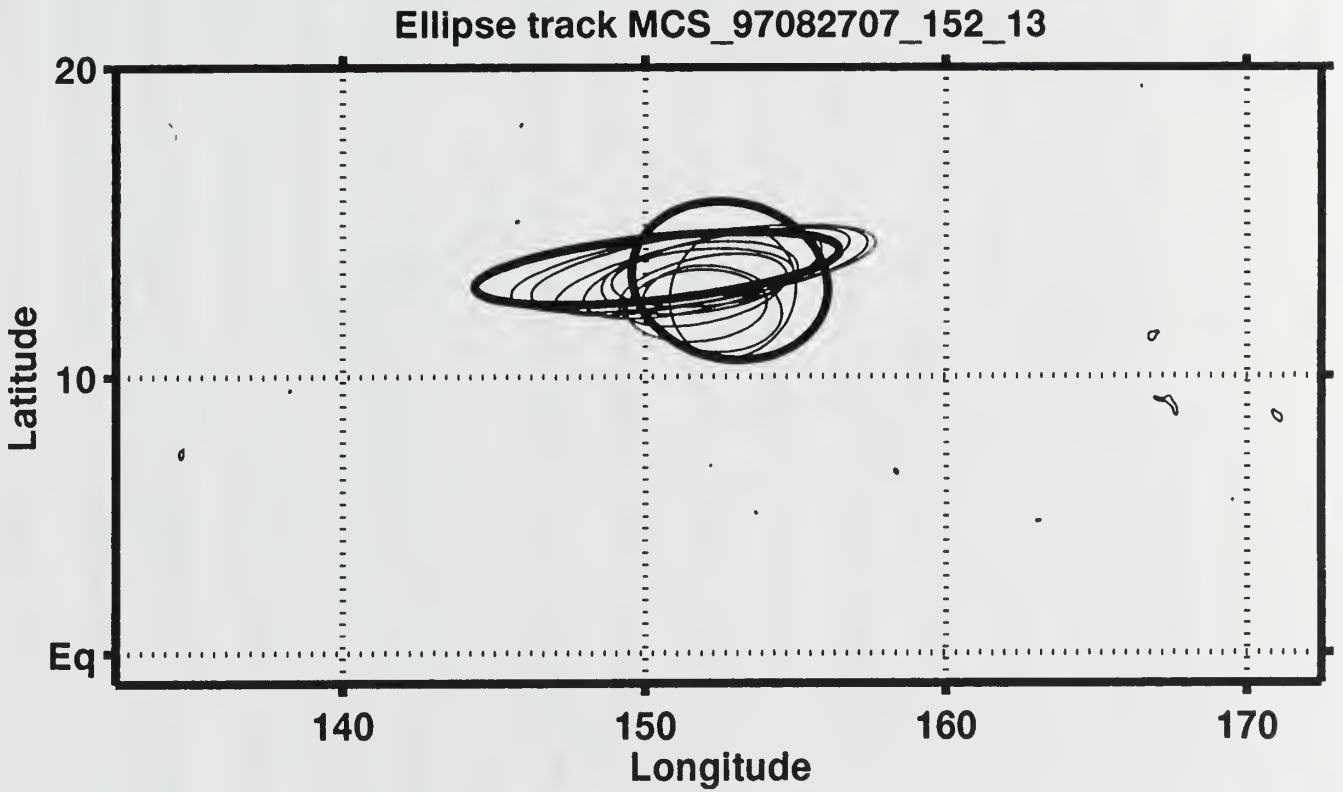

Figure 3.19. Sequence of ellipses centered along the track of MCS C from 0700 UTC 27 August 1997 through 1600 UTC 27 August 1997. The small and flat dark ellipses are the start and finish of MCS C, respectively.

At the same time the decay of MCS B occurs, MCS C begins to form. during the early life-cycle stage with an elongation as the MCS decayed. Notice that the maximum areal extent of this MCS is smaller than either MCS B or MCS A. After rapid growth in the first 3 h, a sharp decrease in convective cloud is followed by 8 h of moderate increase in area and percent coverage convective cloud (Figures 3.20a,b). Although the stratiform percent coverage did decrease when convection increased between 1100 UTC and 1600 UTC 27 August 1997, the stratiform cloud amount remained much larger than convective amount throughout MCS C life cycle. The sharp decrease in convective cloud amount following 0900 UTC 27 August 1997 coincides with a decrease in total convective precipitation (Figure 3.20c). Although the area coverage of convective cloud was less than stratiform cloud between 1200 UTC and 1700 UTC 27 August 1997, the total rain intensity from convective cloud is higher than the stratiform component. This is consistent with the compact intense character of MCS C as evident in the satellite image (Figure 3.10).

The east/west cross section (Figure 3.21) of the SSM/I data through MCS C at 0929 UTC 27 August 1997 (Figure 3.22), which is the minimum in the area and percent of convective coverage and rain intensity from convection, has one minimum PCT that is collocated with the warm low-level precipitation at 19 GHz (Figure 3.21). Compared to typical PCT values for intense tropical convection (McGaughey and Zipser 1996), the minimum PCT value of 225 °K is relatively high, which suggests that MCS C at the time of the SSM/I overpass is in the decay stage as shown in Figures 3.20a,b,c. However, the

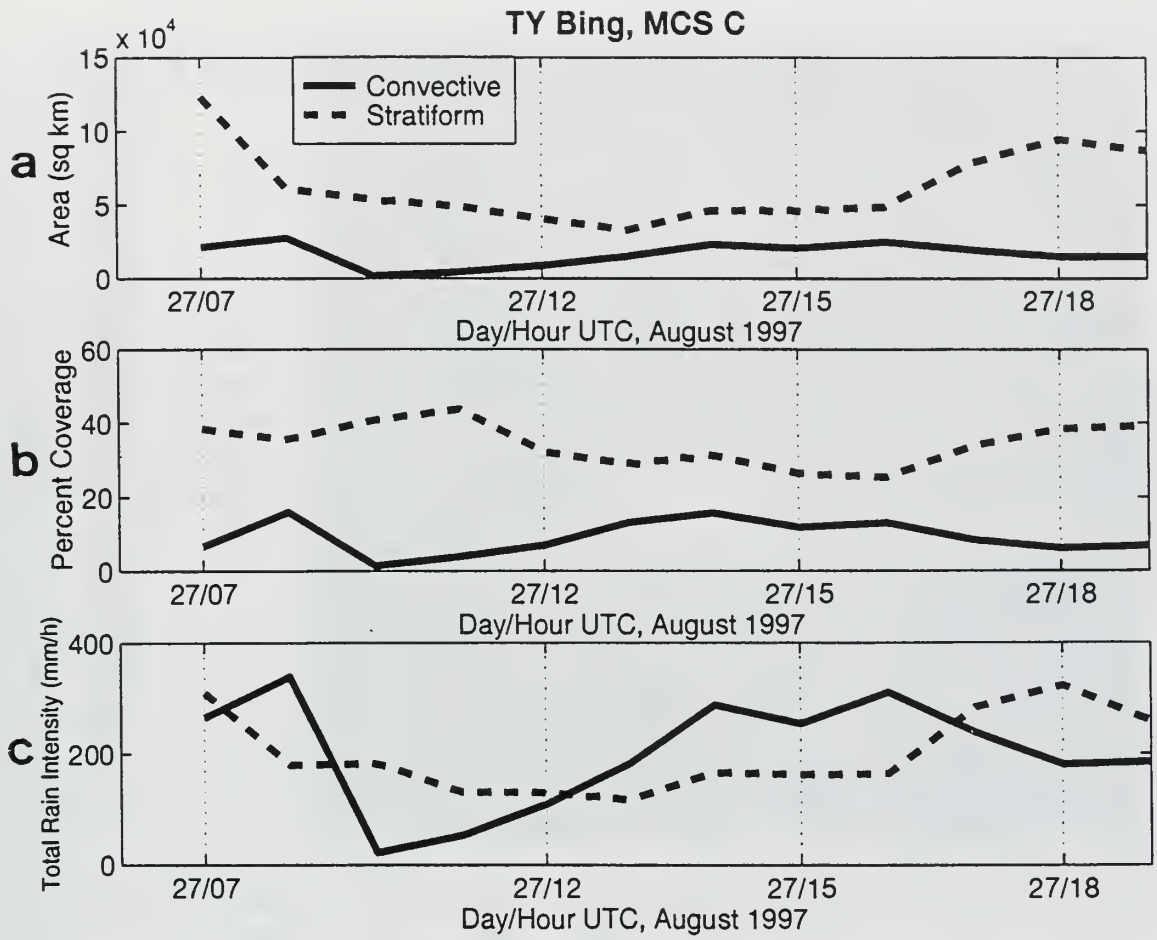

Figure 3.20. (a) Area (sq km) and (b) coverage of convective and stratiform clouds for MCS C. (c) Total rain intensity (mm/h) averaged over the areas of convective and stratiform clouds for MCS C.

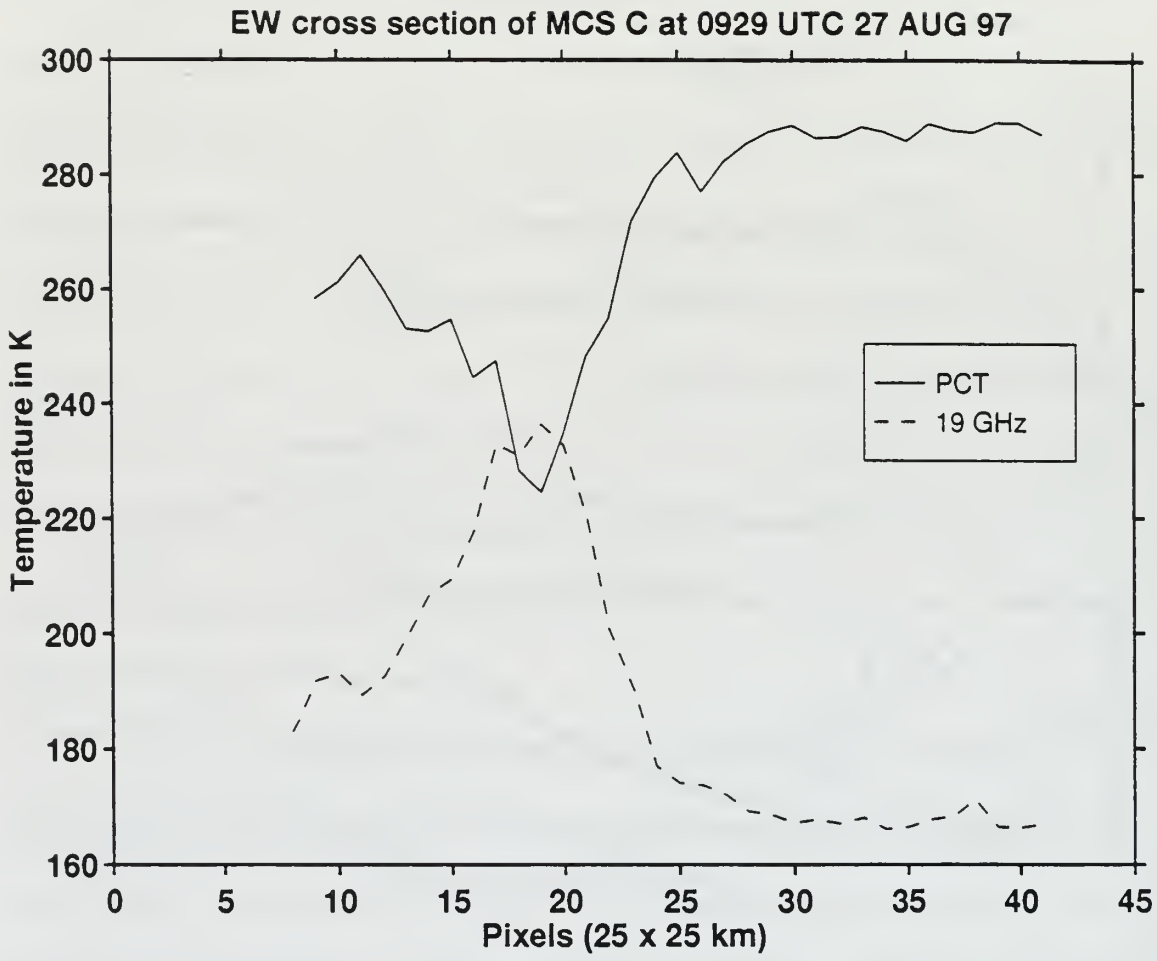

Figure 3.21. East/West cross section through MCS C at 0929 UTC 27 August 1997 along the line shown in Figure 3.22.

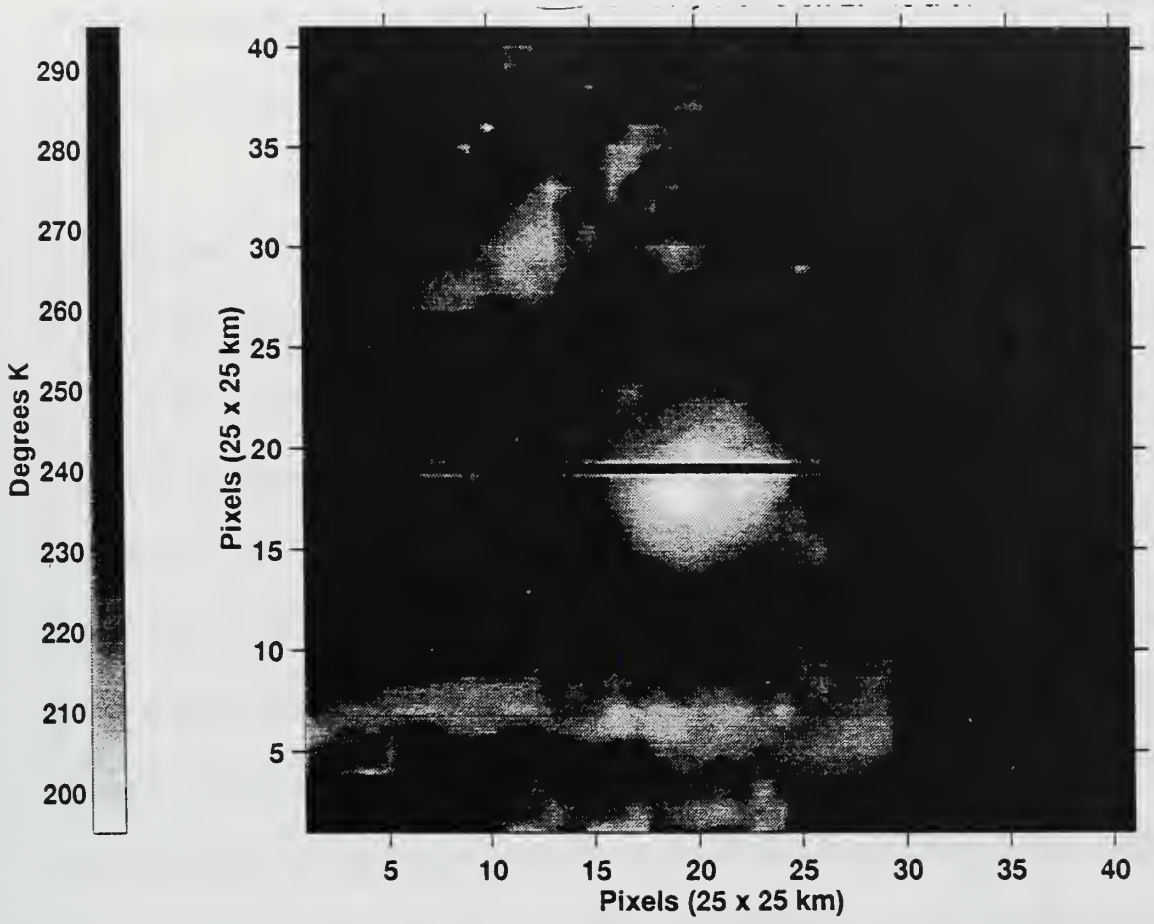

Figure 3.22. GMS IR image of MCS C at 0932 UTC 27 August 1997. The dark horizontal line is the cross section of MCS C for Figure 3.21.

convective components of the MCS increase after 0929 UTC 27 August 1997. After 1600 UTC 27 August 1997, the MCS begins to decay. Although the area of and percent coverage of convective (stratiform) cloud decreases (increases), the most important structural change is the increase in total rain intensity from stratiform cloud that is now larger than the amount from convective cloud. Therefore, the MCS structure during the decay period became dominated by stratiform characteristics that may act to contribute vorticity to the pre-Bing mid-tropospheric disturbance.

Although the convection along the southern portion of the broad pre-Bing disturbance does not meet the typical MCS criteria as defined by Houze (1992), it is tracked to compare with the characteristics of the convection occurring in the more central portion of the disturbance. The ellipse track of MCS D (Figure 3.23) has an elongated shape because it is oriented in the equatorial southwesterly flow. This is a region that is mostly stratiform cloud with very weak convection (Figure 3.24). Notice that the percent coverage of stratiform cloud (Figure 3.24b) within the ellipse is about 55% at 1600 UTC 27 August 1997. Most of the rain associated with MCS D is typical tropical stratiform rain in the confluent tropical flow that defined the southern portion of the disturbance in the monsoon trough. Although the peak stratiform integrated rain rates are around 400 mm/h at 1500 UTC 27 August 1997 (Figure 3.24), the rain rates are generally smaller than in the prior MCSs. Given the outer location and elongated stratiform rain areas, it is concluded that MCS D did not contribute to the mesoscale organization of the pre-Bing disturbance.

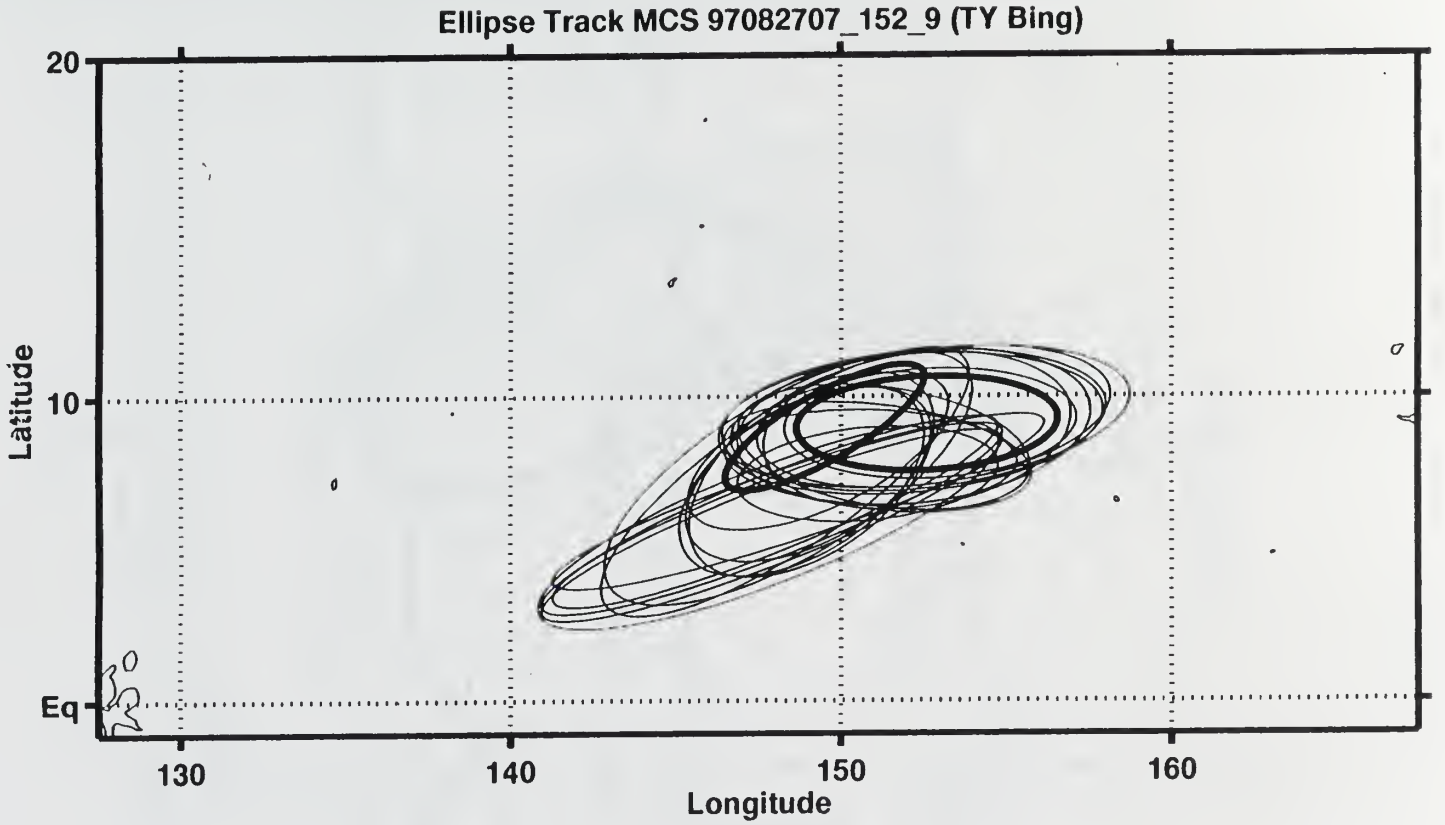

Figure 3.23. Sequence of ellipses centered along the track of MCS D from 0700 UTC 27 August 1997 through 0900 UTC 28 August 1997. The small and large dark ellipses are the start and finish of MCS D, respectively.

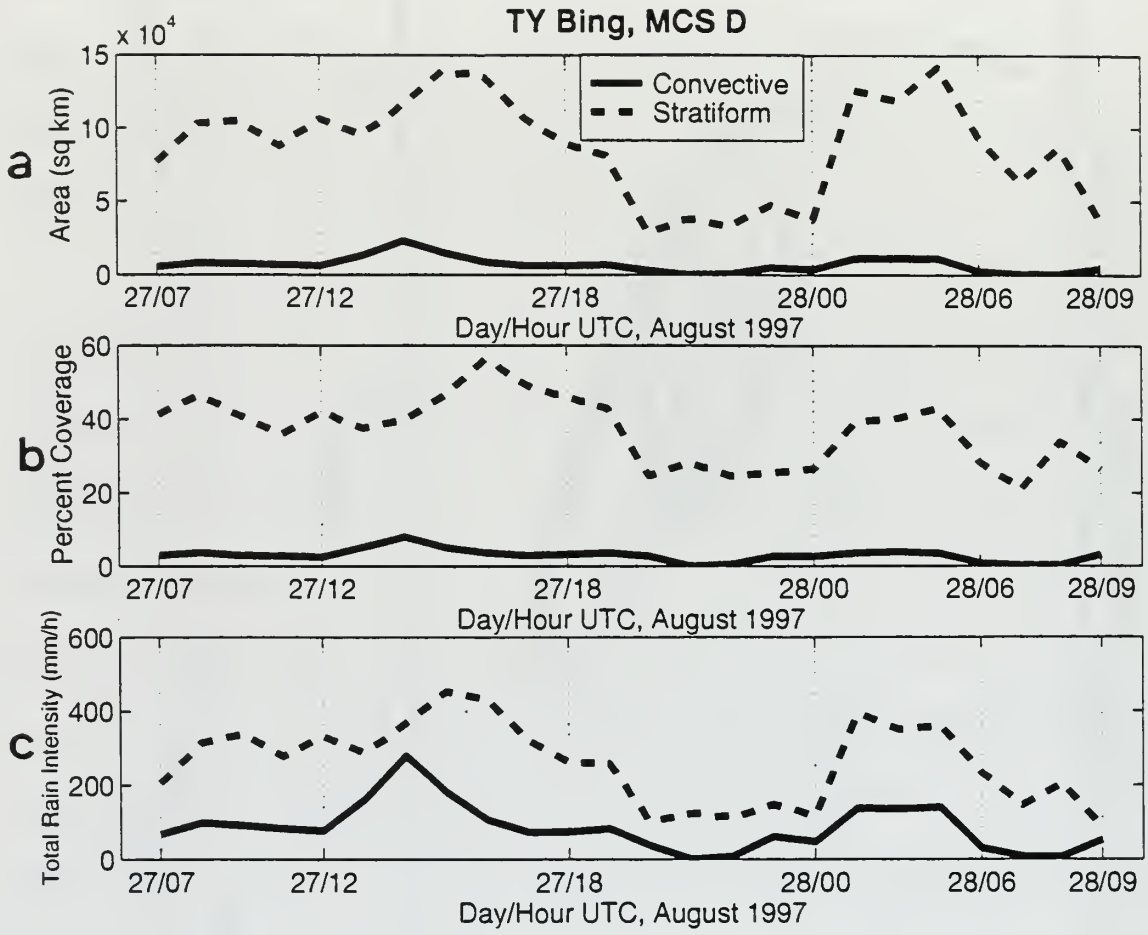

Figure 3.24. (a) Area (sq km) and (b) coverage of convective and stratiform clouds for MCS D. (c) Total rain intensity (mm/h) averaged over the areas of convective and stratiform clouds for MCS D.

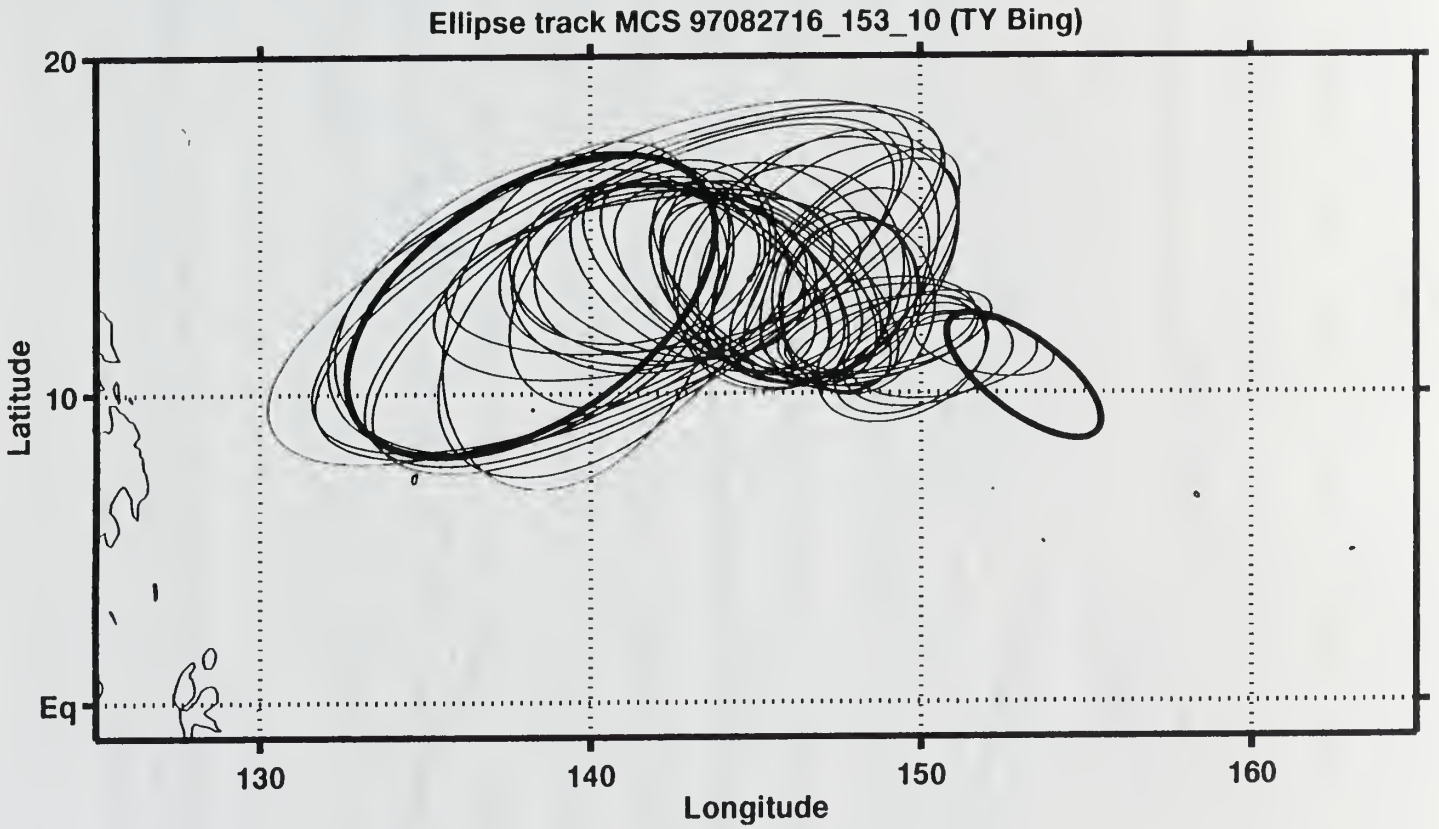

Figure 3.25. Sequence of ellipses centered along the track of MCS E from 1600 UTC 27 August 1997 through 2300 UTC 29 August 1997. The small and large dark ellipses are the start and finish of MCS E, respectively.

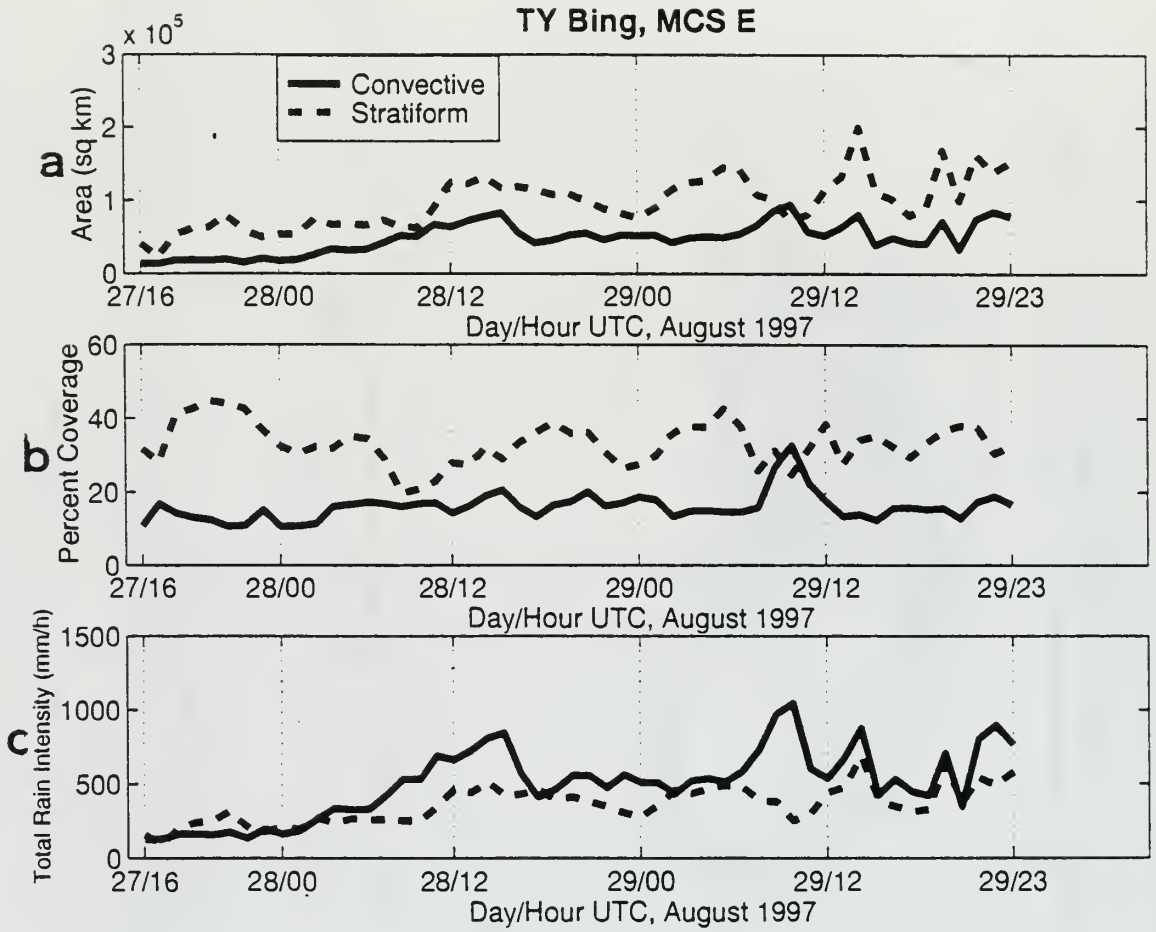

Figure 3.26. (a) Area (sq·km) and (b) coverage of convective and stratiform clouds for MCS E. (c) Total rain intensity (mm/h) averaged over the areas of convective and stratiform clouds for MCS E.

The shape of MCS E (Figure 3.25) is elongated initially, then grows rapidly and becomes more circular. During the initial 20 h, the convective and stratiform coverage amounts increase (Figure 3.26a,b). Whereas the convective area of MCS E becomes slightly larger than for MCS A (Figure 3.14a), the stratiform area is generally smaller. The percent coverage of convective and stratiform clouds are fairly constant throughout the entire MCS E period. The characteristic that distinguishes MCS E from the previous MCSs is that the total rain rate for convective clouds is larger than the stratiform total through almost all of the period (Figure 3.25c). This is indicative of the continued intensity of the convective portion of the MCS, which does not seem to be entering a decay stage at any time during the period it was tracked. The entire system became Tropical Storm Bing by 1800 UTC 28 August 1997. The peak total convective rain rate becomes almost 1000 mm/h, which is double any value during MCS A (Figure 3.14c), and peak values of about 800 mm/h continue through the end of the period, even though the percent convective coverage is nearly constant. This type of pattern appears to be consistent with developing TCs and suggests that MCS E developed within a vorticity-rich area that has evolved in the presence of the previous MCSs.

Two major factors to the combination-type of tropical cyclone evolution are exhibited during the formation of ST Bing. First, the synoptic-scale equatorial southwesterly flow within the monsoon trough created the favorable conditions for repeated MCS formation. Second, vigorous convective activity resulted in formation of large stratiform regions that contributed to vorticity production. These two roles are

proposed to be critical for ST Bing to develop over a four-day period.

B. SUPER TYPHOON IVAN

1. Overall Evolution

ST Ivan was a large TC in the western North Pacific during October 1997 (Figure 3.27). Prior to the formation of Ivan, convection began to increase in the eastern portion of the monsoon trough and MCS A (Figure 3.28) formed near 6°N, 168°E at 1500 UTC 10 October 1997. Although MCS A did not contribute to the initial circulation of the pre-Ivan disturbance, it was the start of convection in the region. It dissipated near 5°N, 164°E at 0400 UTC 11 October 1997.

A new MCS (labeled MCS B in Figure 3.28) formed 4 h later at 0800 UTC 11 October 1997 as a cloud cluster at approximately 7°N, 163°E and grew rapidly (Figure 3.29). MCS B moved westward as it progressed through its life cycle and eventually dissipated at approximately 0600 UTC 12 October 1997 near 8°N, 158°E. As MCS B was decaying, MCS C (Figure 3.28) formed as a line of convection on the northern boundary of MCS B (Figure 3.30). It is possible that the convection associated with MCS C formed along a low-level outflow boundary from MCS B. MCS C was short-lived as it dissipated approximately 8 h later. As MCS C entered its mature stage by 1232 UTC 12 October 1997, the convection formed an arc to the north with the stratiform region in the middle of the arc (Figure 3.31).

By 1500 UTC 12 October 1997, MCS D formed to the southeast of MCS C near 10°N, 158°E (Figure 3.28). MCS D formed near the dissipation location of MCS B,

Super Typhoon Ivan (27W)

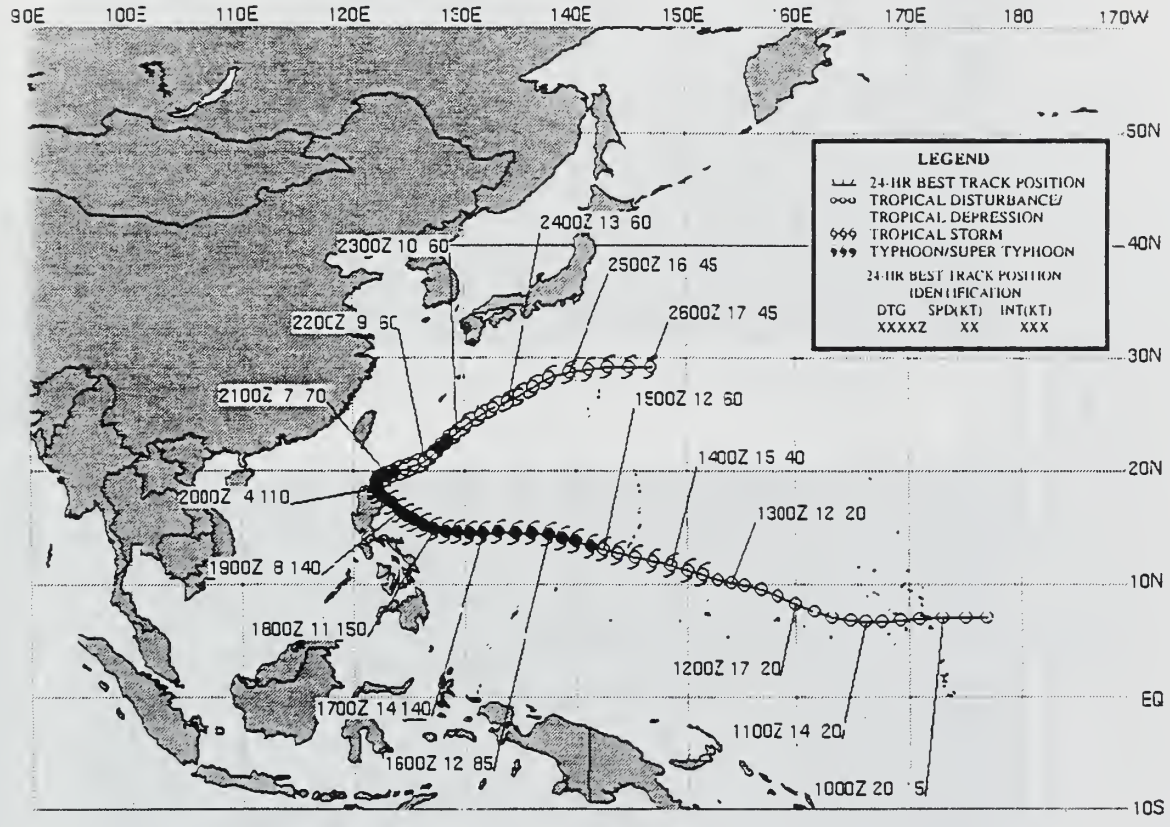

Figure 3.27. Super Typhoon Ivan (27W) best track from JTWC each 6 h from 9 October to 26 October 1997. The minimum sea-level pressure (not shown) was 872 mb and the maximum intensity was 160 kt.

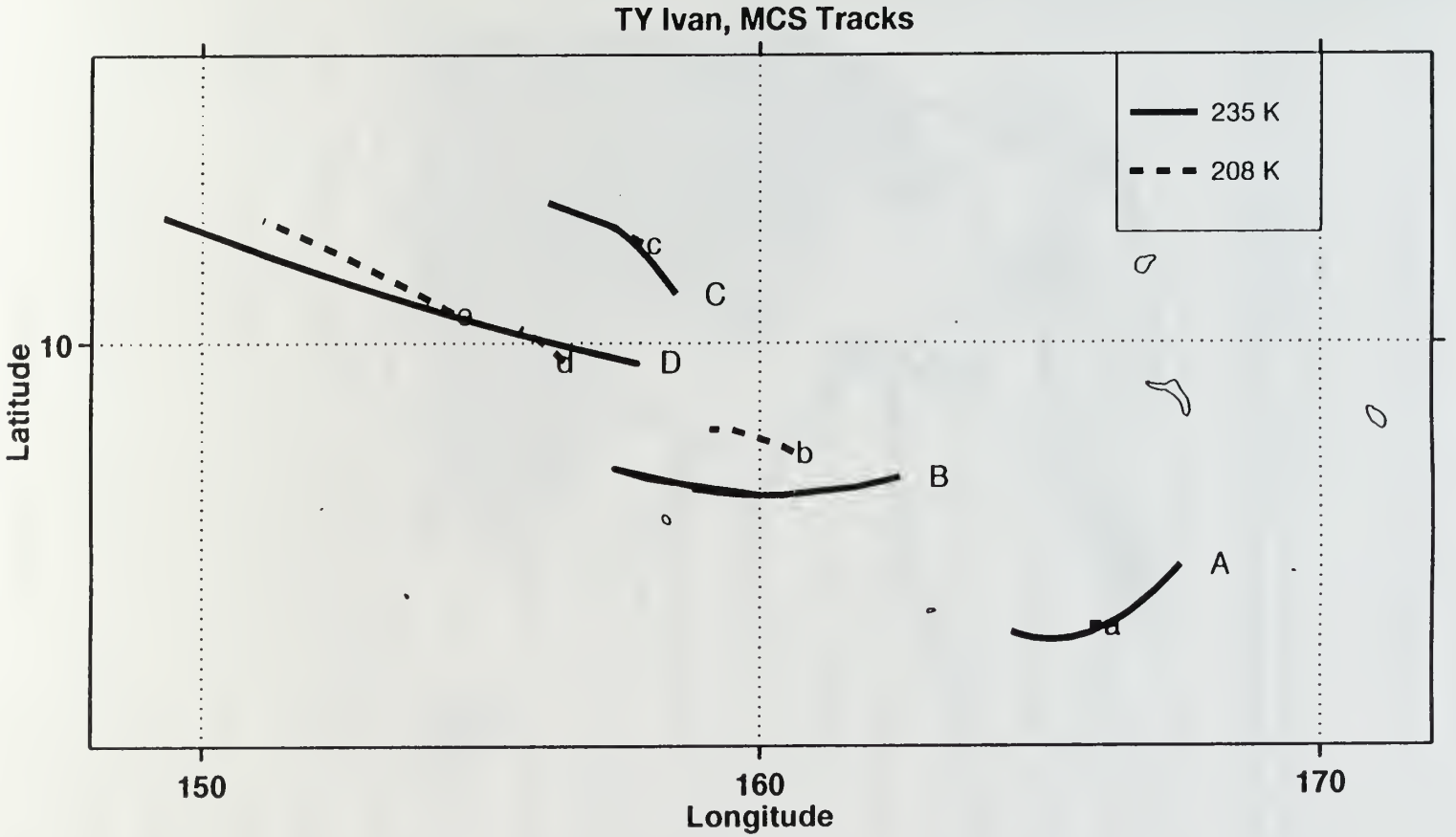

Figure 3.28. Tracks of MCSs associated with the development of Super Typhoon Ivan from 1500 UTC 10 October 1997 through 1300 UTC 13 October 1997. The solid lines with upper case letters are the track of the 235°K temperature core of the MCS, and the dashed lines with lower case letters are the track of the 208°K temperature core of the MCS.

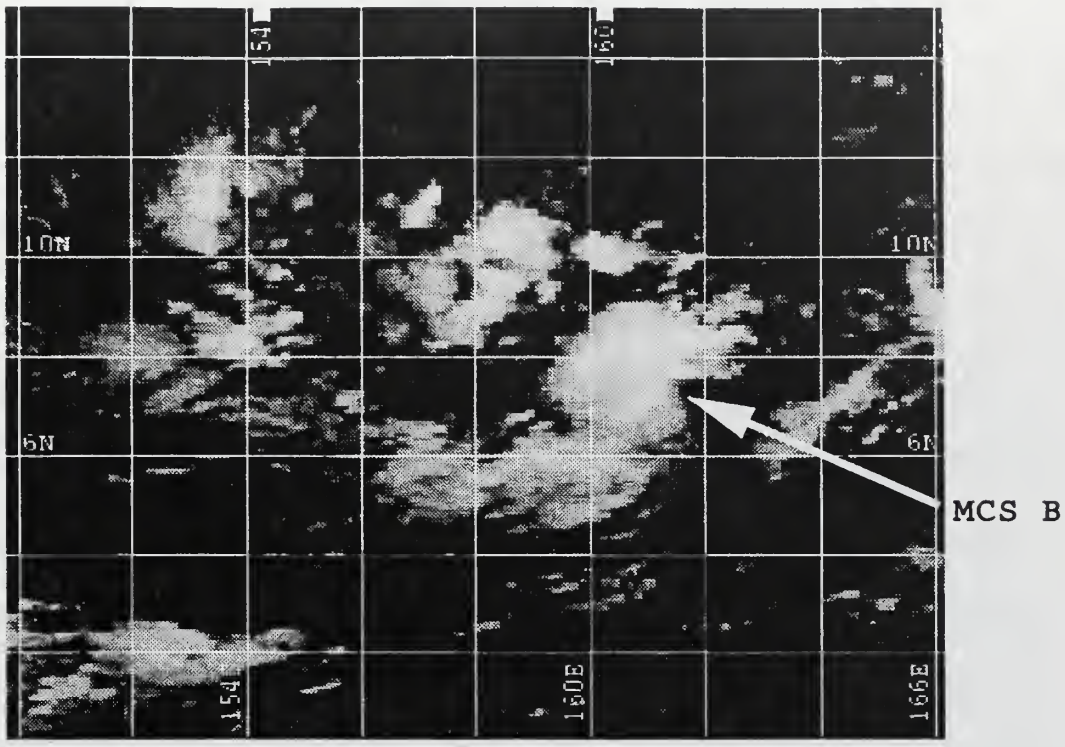

Figure 3.29. GMS IR image of MCS B at 2332 UTC 11 OCT 97.

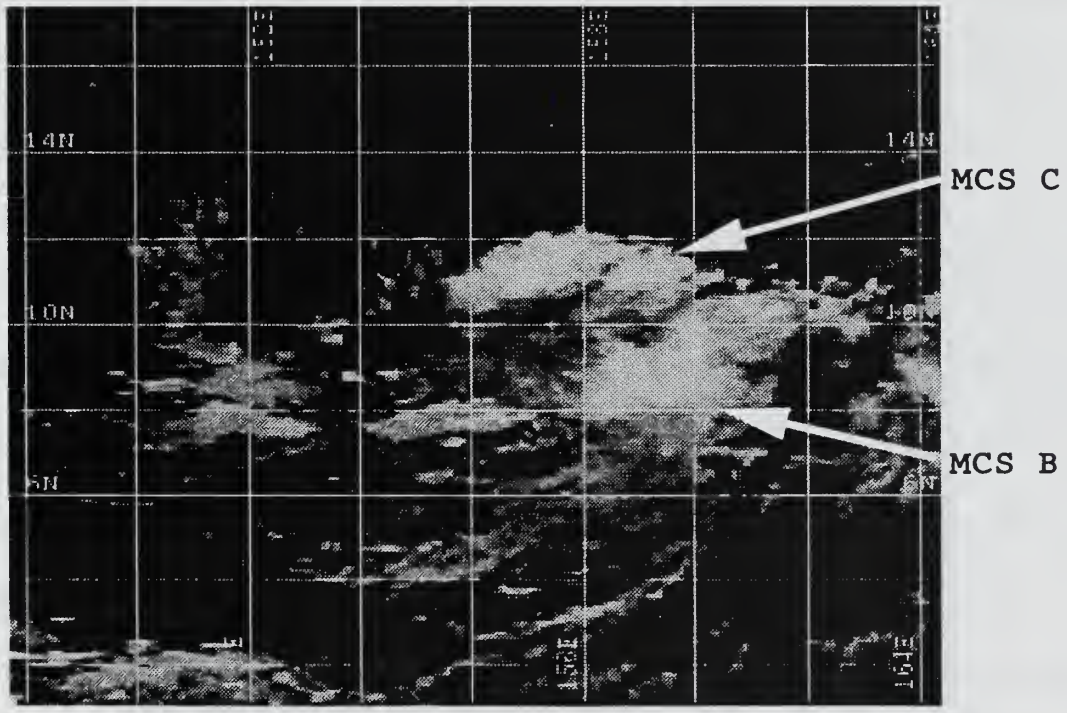

Figure 3.30. GMS IR image of decaying MCS B and developing MCS C at 0425 UTC 12 OCT 97.

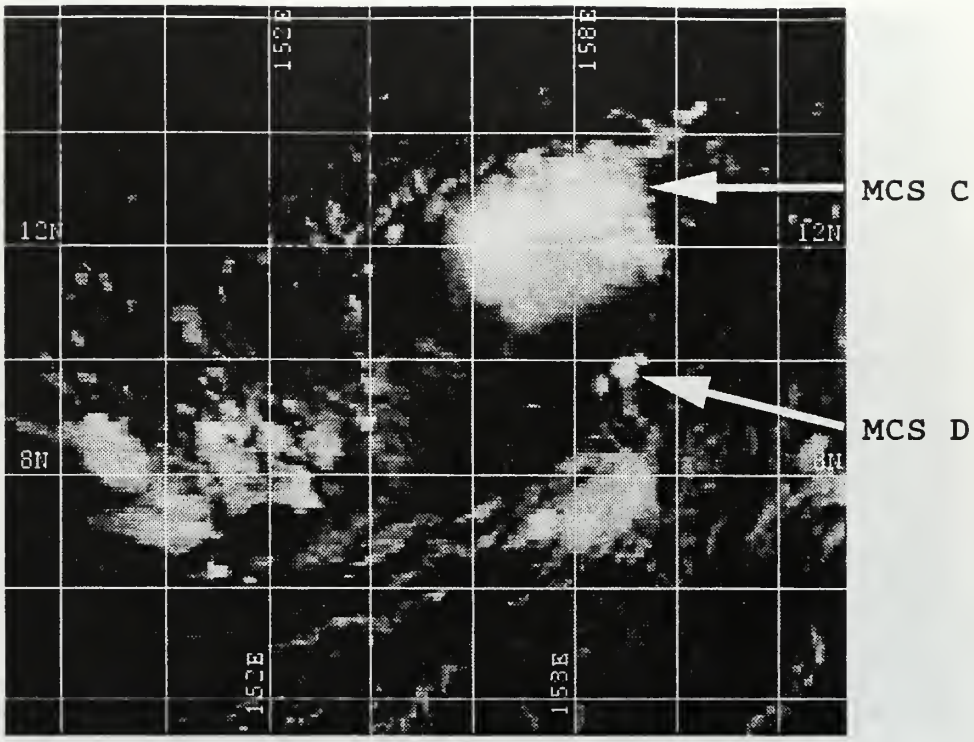

Figure 3.31. GMS IR image at 1232 UTC 12 OCT 97.

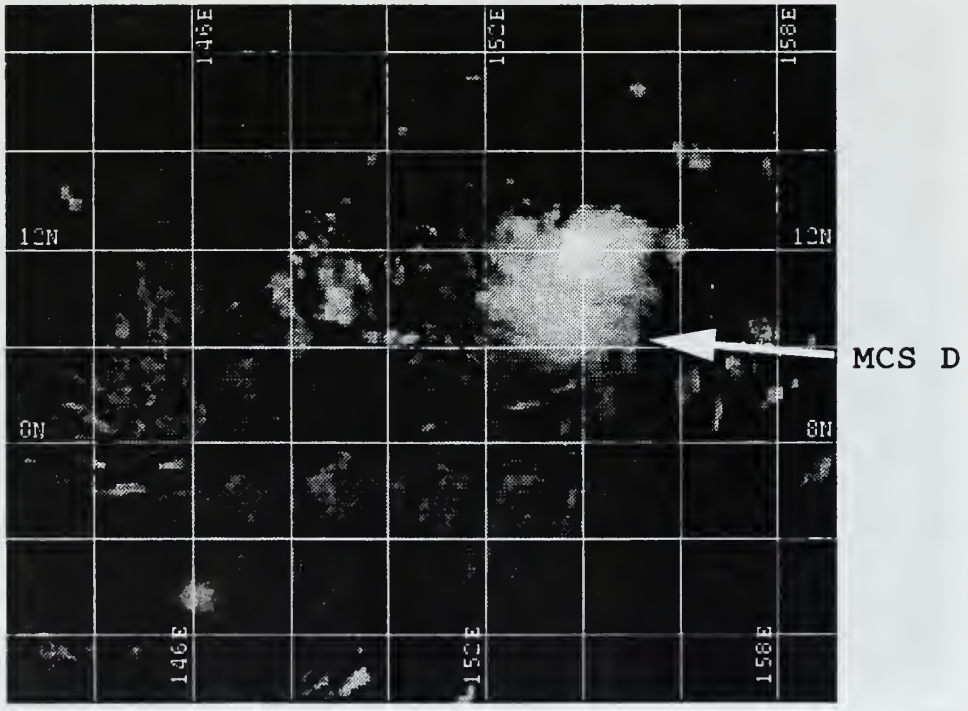

Figure 3.32. GMS IR image at 0632 UTC 13 OCT 97.

which had decayed approximately 9 h earlier. This MCS formed rapidly and became the center of convection for the developing pre-Ivan disturbance. By 0630 UTC 13 October 1997, convection was well established and rotation was evident in the curved cloud lines (Figure 3.32). This was the time that JTWC issued the first warning as Tropical Depression 27W with a wind speed of 25 kt, three days after the first MCS had formed about 5° latitude to the south and 13° longitude to the east. The JTWC tropical depression position (10°N, 153°E) was consistent with the satellite imagery. By the next warning at 1200 UTC 13 October 1997, Tropical Depression 27W became Tropical Storm Ivan (Figure 3.33). Although this system had been developing for three days before the first warning was issued, its intensification from TD to TS stage was accomplished in about 6 h, once a central MCS formed.

The general increase in convection in the eastern portion of the monsoon trough and formation of MCS A is associated with a broad, east-west, 850-mb trough (Figure 3.34a). In addition to being close to the Equator (small Coriolis parameter), the NOGAPS 200-mb analysis (not shown) suggests that MCS A did not develop due to moderate easterly upper-level wind shear. The NOGAPS 850-mb analysis at 0000 UTC 12 October 1997 (Figure 3.34b) depicts a cyclonic circulation near 9°N, 162°E in which the MCS activity associated with the pre-Ivan disturbance is embedded in the northern portion. MCS C forms in the northern portion of the monsoon trough about 1 h after MCS B dissipates. Although MCS C is in an area of cyclonic vorticity, it does not develop due to moderate easterly upper-level shear (not shown). Although the NOGAPS

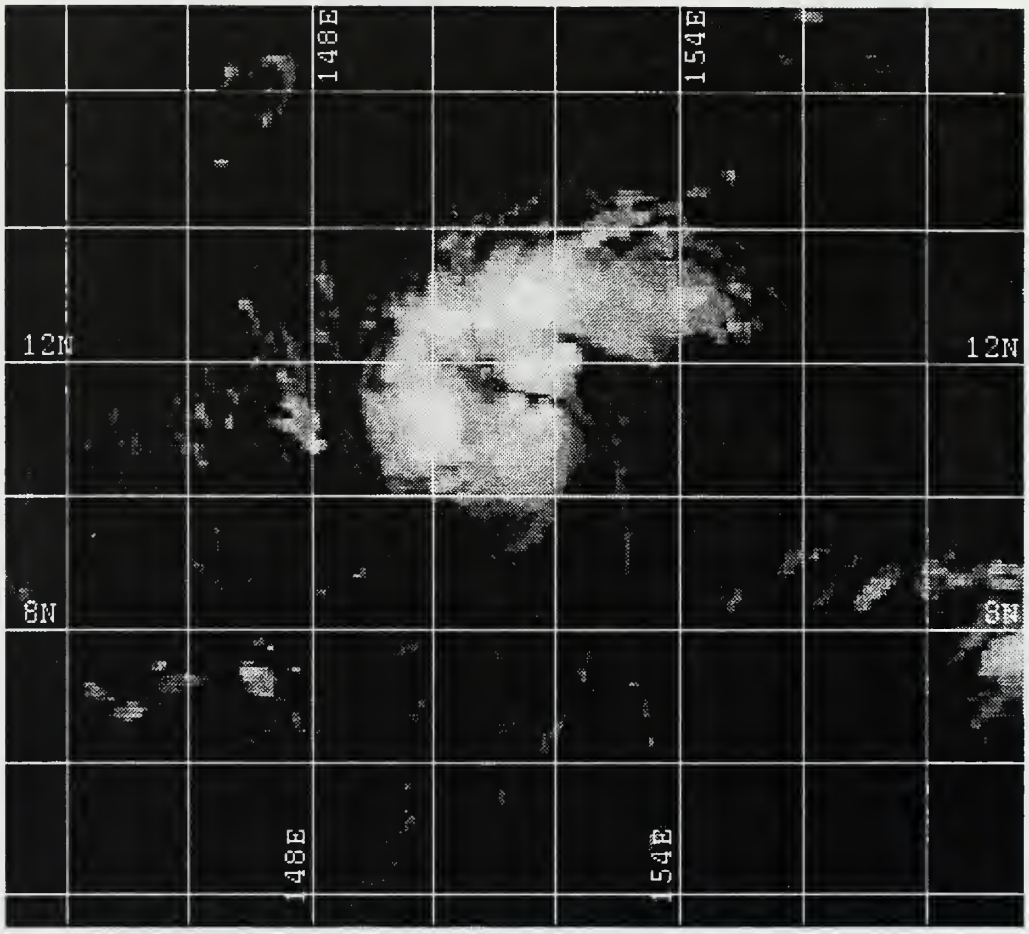

Figure 3.33. GMS IR image of Tropical Storm Ivan at 1232 UTC 13 OCT 97.

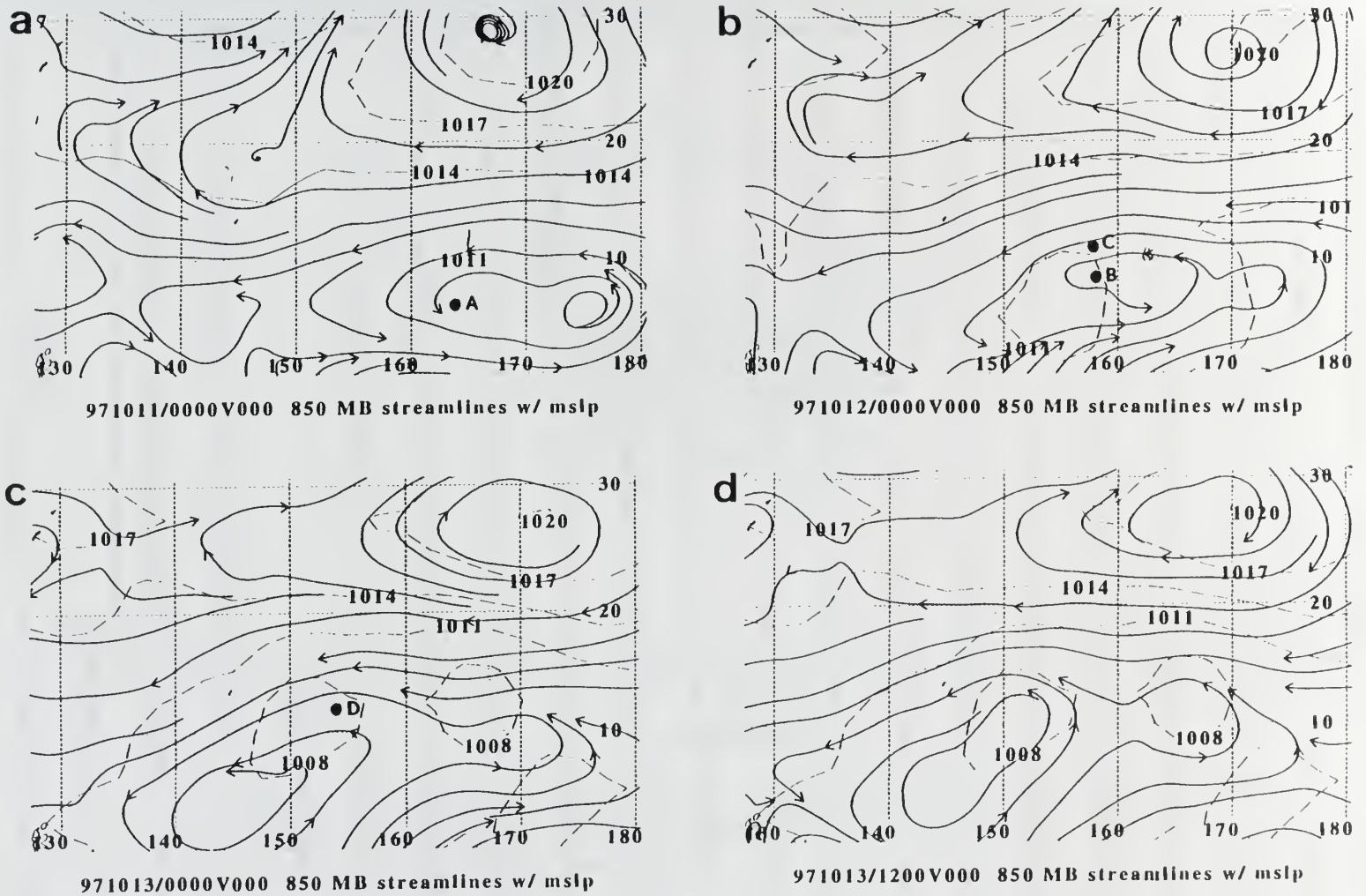

Figure 3.34. NOGAPS 850-mb streamline (solid with arrows), 850-mb 30 kt isotach (dotted), and mean sea-level pressure analyses (dashed, interval 4 mb) for 0000 UTC on (a) 11, (b) 12, and (c) 13 October, and (d) 1200 UTC 13 October 1997. Locations of the MCSs in Figure 3.28 at the times of these analyses are shown by dots.

analysis at 0000 UTC 13 October 1997 (Figure 3.34c) has a southwestward tilt in the 850-mb circulation, MCS C and MCS D formed in the cyclonic curved flow to the north near 10°N, 158°E. By 1200 UTC 13 October 1997 (Figure 3.34d), the northern portion of the 850-mb circulation reflects the intensifying pre-Ivan disturbance. Whereas the synoptic analyses depict the monsoon circulation has shifted southwestward, the MCS activity may have concentrated a smaller region of vorticity that contributes to the intensification of the pre-Ivan disturbance to the northeast of the synoptic-scale center.

Because of the contributions from both the synoptic and mesoscale components, ST Ivan is also be classified as a combination-type case. The synoptic environment was favorable for enhanced convective activity and the MCS activity helped to concentrate the vorticity. In contrast to the case of ST Bing in which the synoptic system seemed to get more organized as the multitude of MCSs appeared to contribute, this case seems to have weaker synoptic forcing. The formation of MCS B is related to the favorable condition of a low-level southwesterly confluent flow. Because MCS D forms near the decay position of MCS B (although about 9 h later), the mesoscale circulation remnants from MCS B may have been a significant contribution to the eventual formation of ST Ivan.

2. MCS Structure

Because MCS A represented a transient increase in the overall convective activity within the monsoon trough and not the pre-Ivan disturbance, a detailed analysis of the structure of MCS A is not presented.

The time history of the ellipse coverage for MCS B (Figure 3.35) indicates major

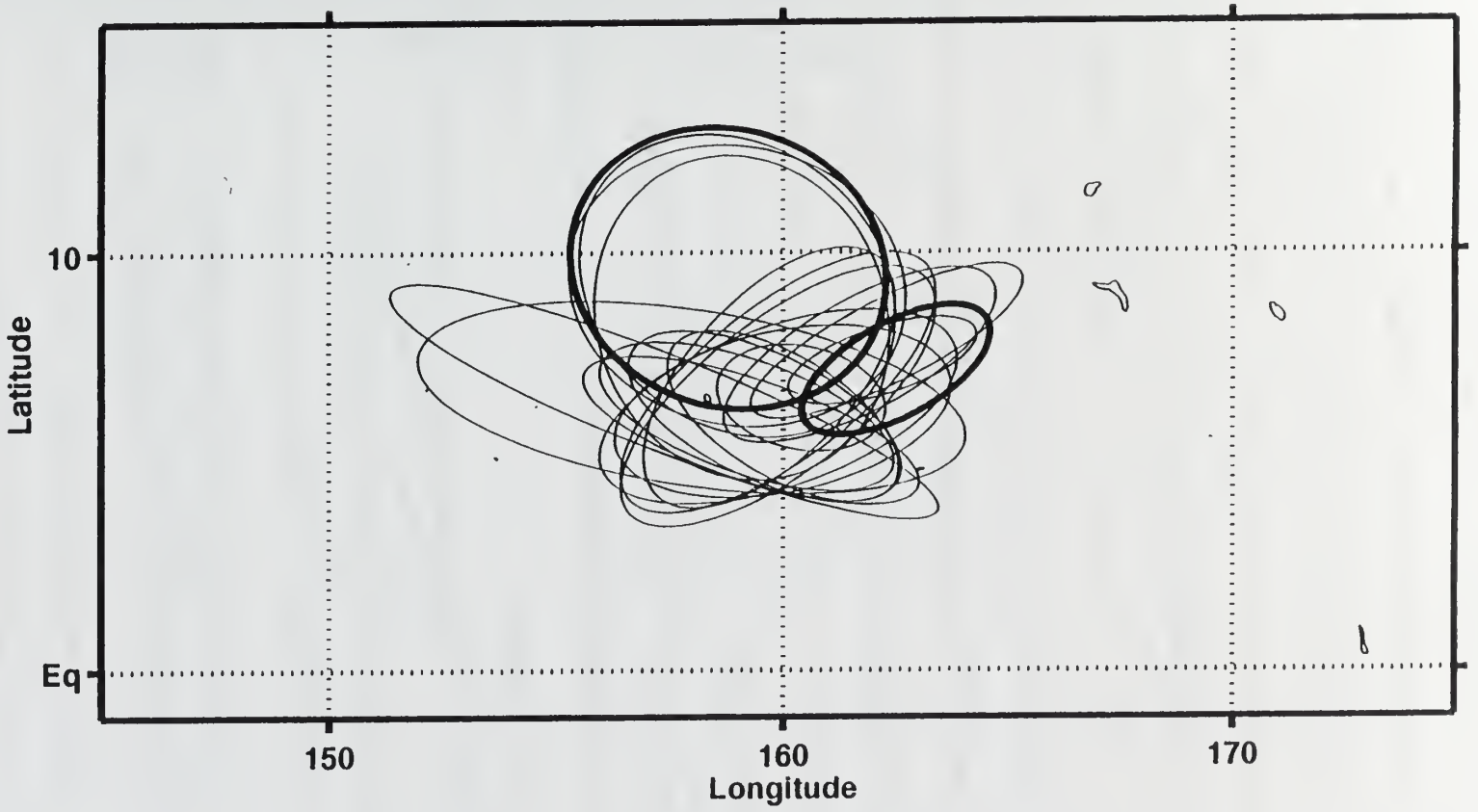

Figure 3.35. Sequence of ellipses centered along the track of MCS B from 0800 UTC 11 October 1997 through 0600 UTC 12 October 1997. The small and large dark ellipses are the start and finish of MCS B, respectively.

shape changes as the MCS moved through the southwesterly flow and cirrus clouds spread appreciably. This is also reflected by the steadily increasing amount of stratiform areal coverage (Figure 3.36a). Overall, the percent coverage of stratiform cloud is consistently much higher than the percent coverage of convective cloud (Figure 3.36b). An increase in stratiform coverage follows each increase in convective coverage at 1200 UTC and 2100 UTC on 11 October 1997 and 0200 UTC 12 October 1997. Conversely, sharp decreases in both stratiform and convective coverage occur at 1900 UTC 11 October 1997. During the increase in convection after 1900 UTC 11 October 1997 and at 0200 UTC 12 October 1997, the total convective rain intensity (Figure 3.36c) is larger than the stratiform rain intensity. The slow increase in convective cloud coverage, and the fact that total stratiform rain intensity is larger than convective rain intensity except for specific short-lived convective increases, suggest that MCS B is more related to the synoptic forcing present in the southwesterly flow of the monsoon trough rather than the central portion of the pre-Ivan disturbance.

Unfortunately, there were no SSM/I passes over MCS C during its short life cycle. Therefore, detailed analysis of the structure of the MCS was not possible.

The ellipse track of MCS D (Figure 3.37) indicates that the MCS has a nearly circular shape throughout its lifetime as it expands, shrinks, and expands again. During the formation time, the total area (Figure 3.38a) and percent area (Figure 3.38b) covered by convective clouds are larger than the stratiform coverages. Also, the total rain rate associated with convection is larger than the stratiform values during the formative stage

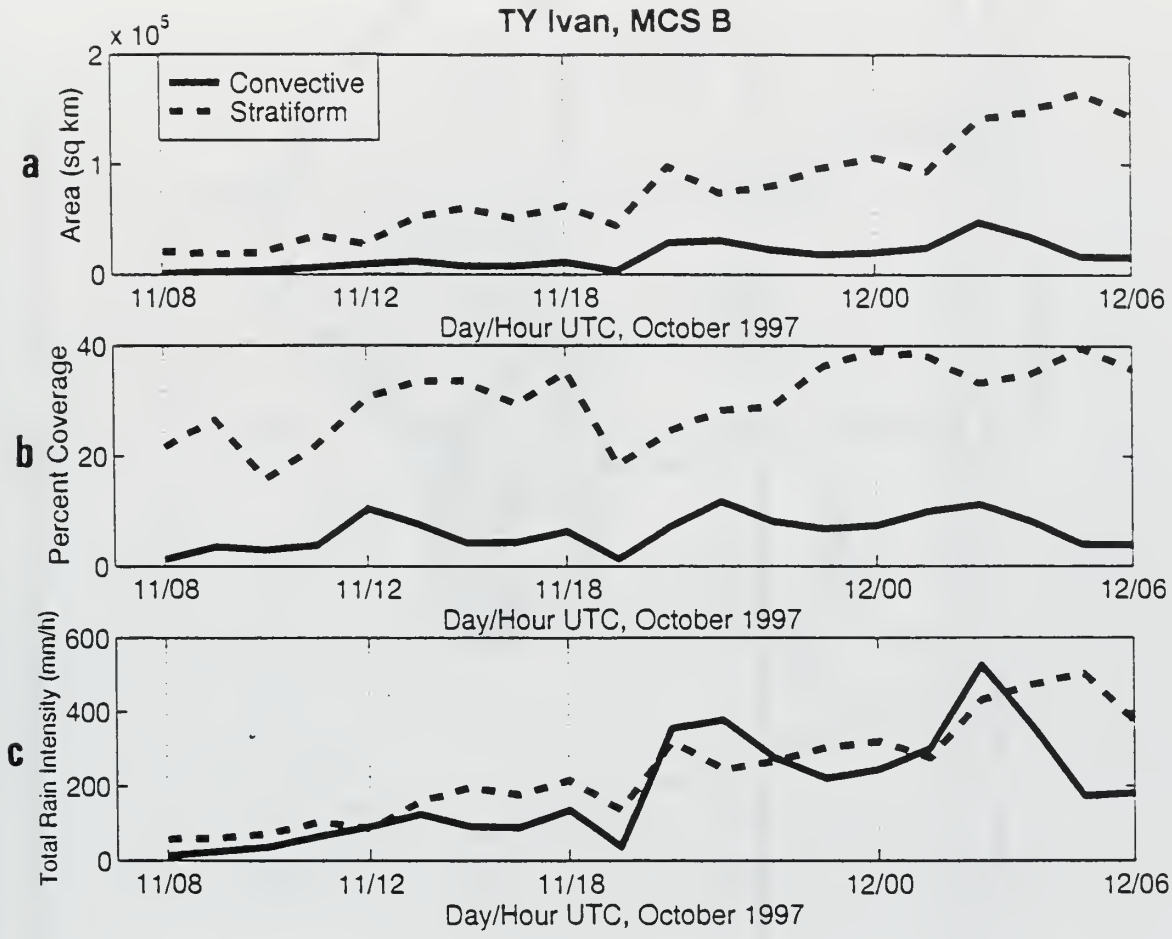

Figure 3.36. (a) Area (sq km) and (b) coverage of convective and stratiform clouds for MCS B. (c) Total rain intensity (mm/h) averaged over the areas of convective and stratiform clouds for MCS B.

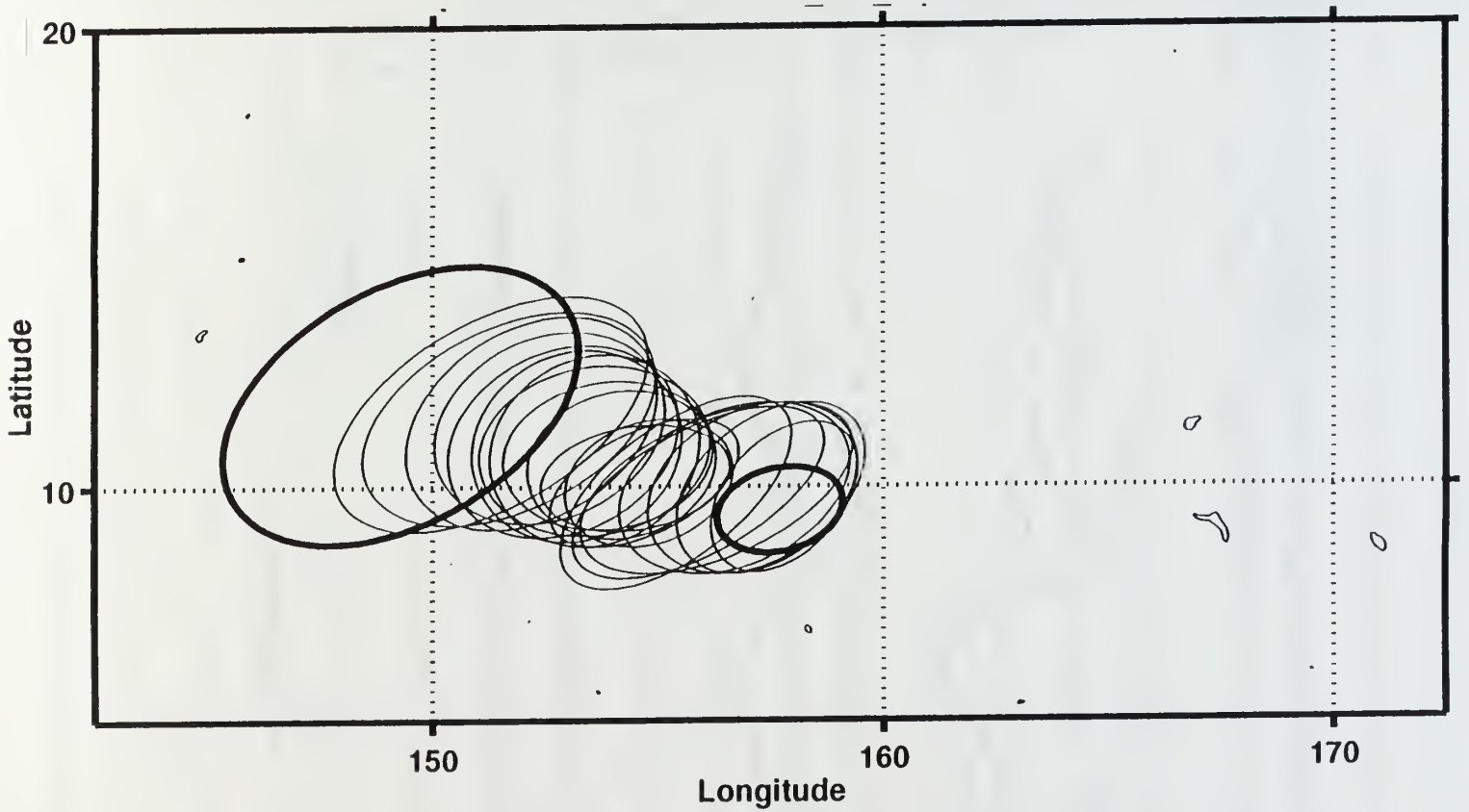

Figure 3.37. Sequence of ellipses centered along the track of MCS D from 1500 UTC 12 October 1997 through 1300 UTC 13 October 1997. The small and large dark ellipses are the start and finish of MCS D, respectively.

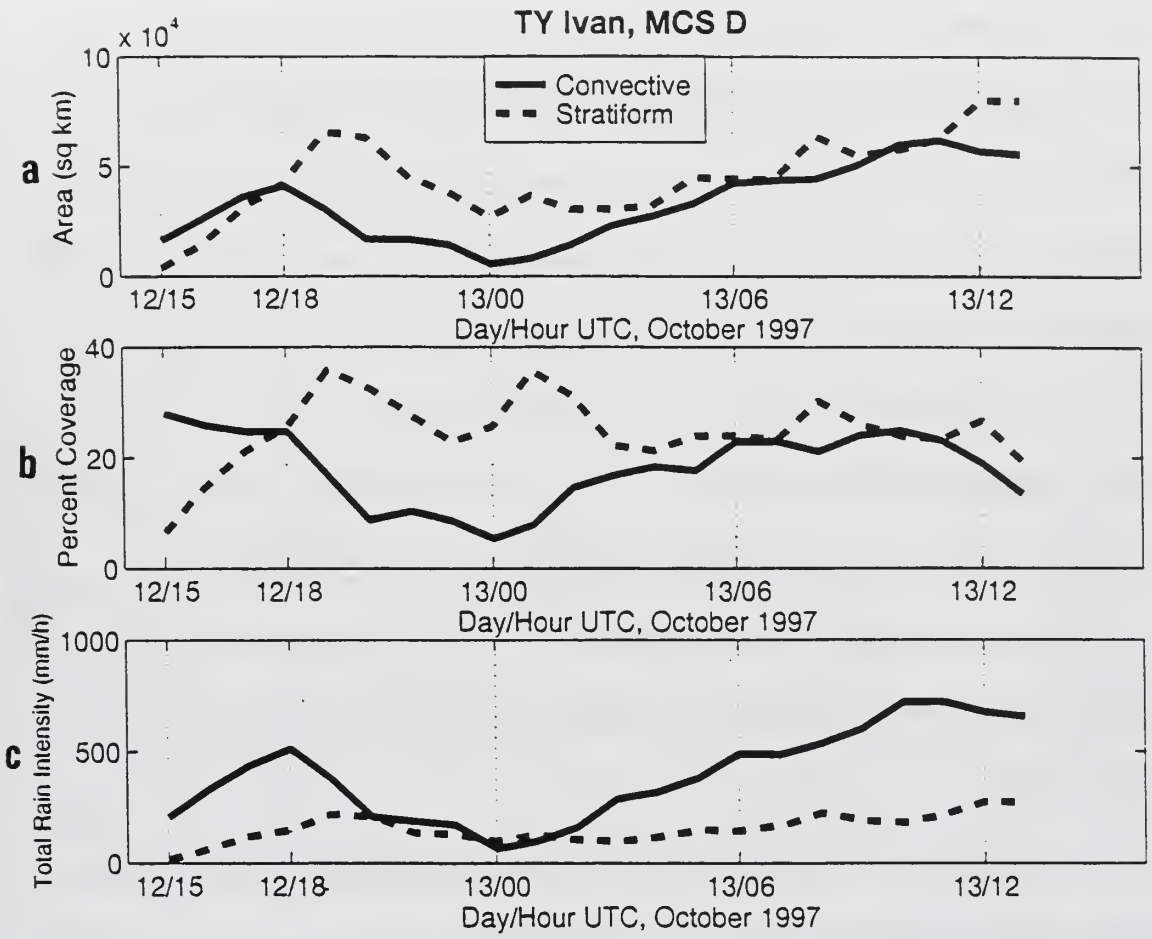

Figure 3.38. (a) Area (sq km) and (b) coverage of convective and stratiform clouds for MCS D. (c) Total rain intensity (mm/h) averaged over the areas of convective and stratiform clouds for MCS D.

(Figure 3.38c). Shortly after 1800 UTC 12 October 1997, convective coverage reaches its minimum and stratiform coverage reaches its maximum. Convective activity then increases rapidly from 0000 UTC to 0632 UTC 13 October 1997, during which a circular MCS forms (Figure 3.32). Although the first peak of convection at 1800 UTC (0400 local) is consistent with a diurnal convective maximum, the subsequent growth to the second peak at 1000 UTC (2000 local) is not related to the diurnal cycle; rather it is more synoptic-related forcing. From this time on, the total rainrate from convective clouds increases regularly in association with the organization of the pre-Ivan disturbance. By contrast, the total rain intensity in the expanding stratiform area remains constant.

An east/west cross section (Figure 3.39) of the SSM/I PCT and 19 GHz data is constructed through MCS D at 0649 UTC 13 October 1997 (Figure 3.40). The very low PCT of about 170°K defines the intense convective activity at the peak of the intensification stage that is evident in Figure 3.32, and this corresponds nicely with the amount of convective coverage and total rainrate at 0700 UTC 13 October 1997 in Figures 3.38b,c.

In summary, ST Ivan develops rapidly from a small disturbance into a tropical cyclone. Although the initial MCS A does not contribute directly to increasing the circulation of the disturbance, it did provide the initial concentrated convection within the monsoon trough. Formation of MCS B appears to be associated with the synoptic flow while MCS C appears to begin intensification of the pre-Ivan disturbance. Although microwave observations of MCS C are not available, the formation of MCS C appears to

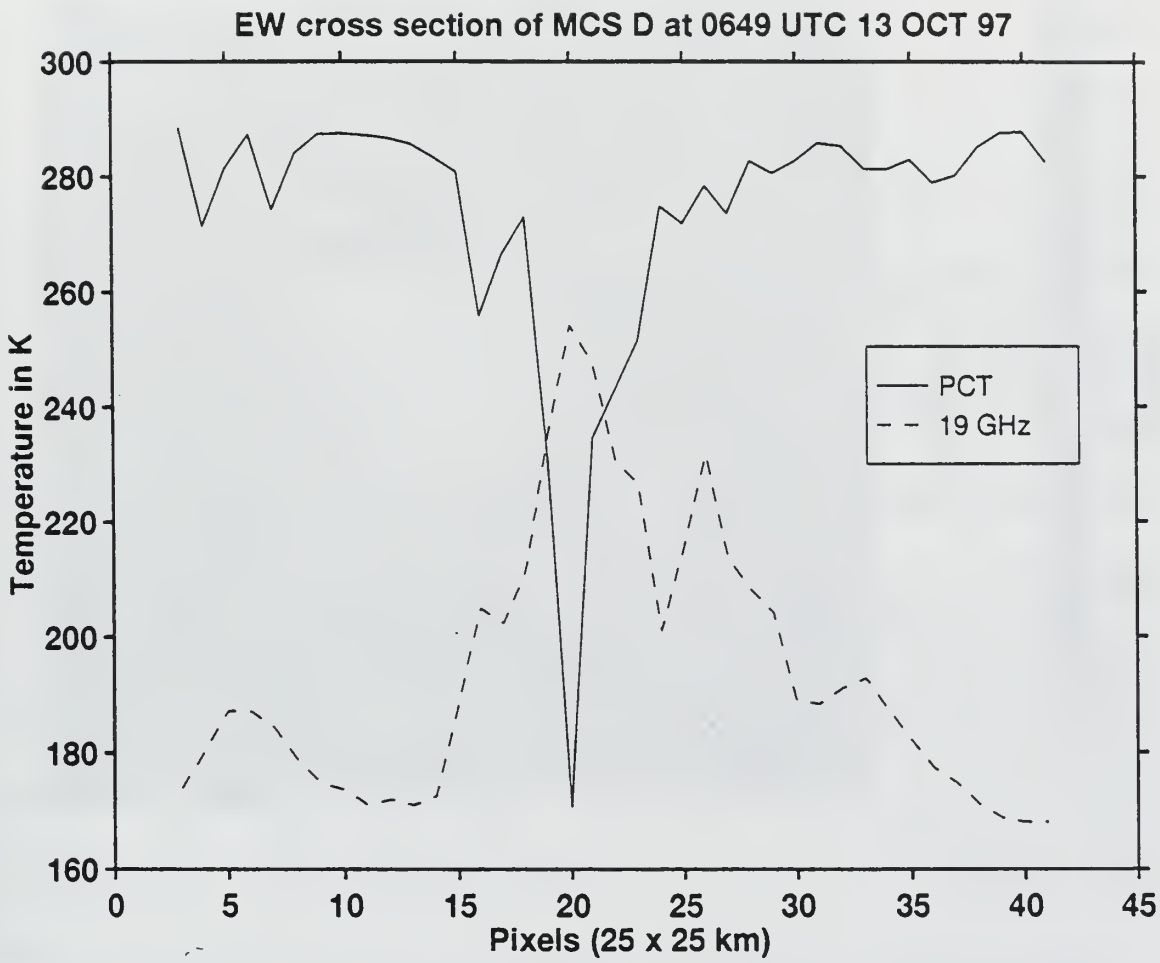

Figure 3.39. East/West cross section through MCS D at 0649 UTC 13 October 1997 along the line shown in Figure 3.40.

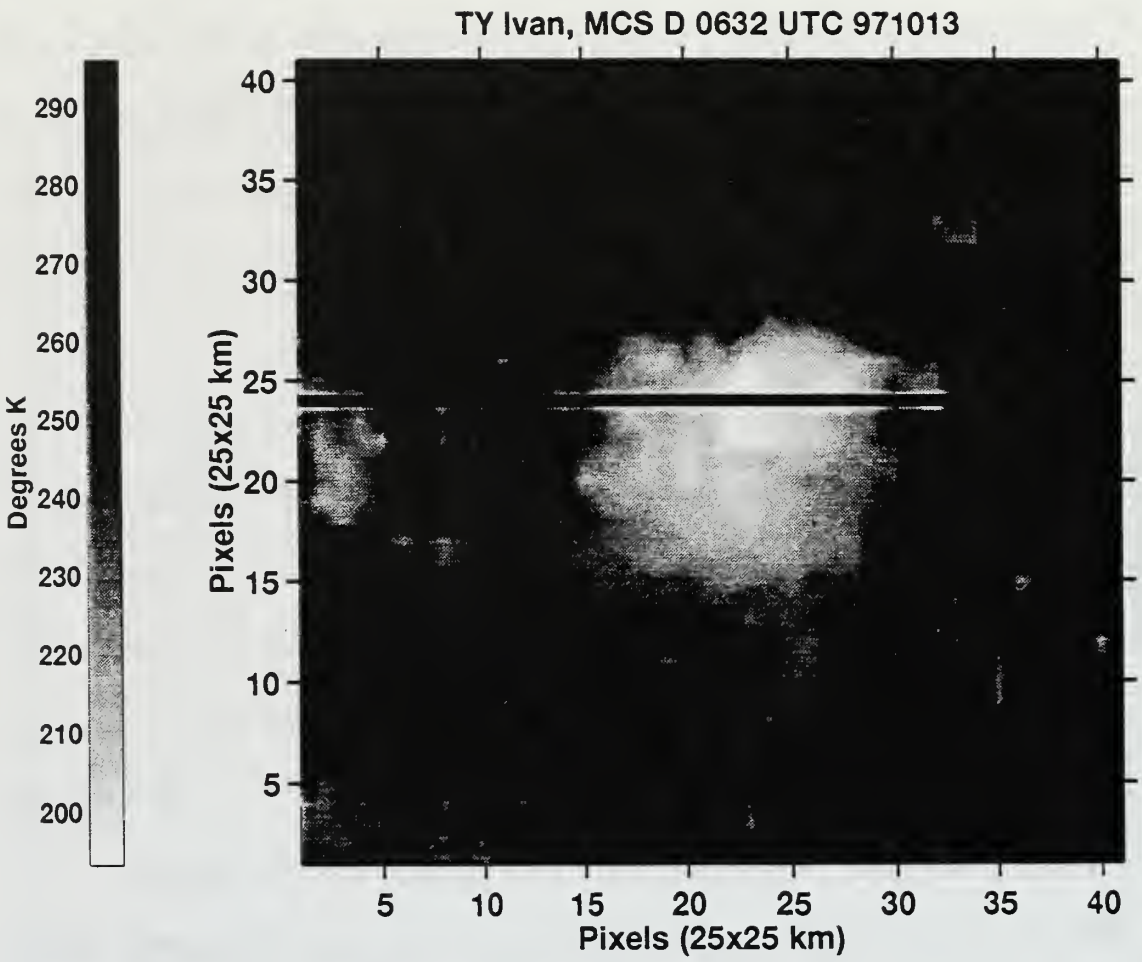

Figure 3.40. GMS IR image of MCS D at 0632 UTC 13 October 1997. The dark horizontal line is the cross section of MCS D for Figure 3.39.

be related to the northern outflow boundary for MCS B. The formation of MCS D also occurs just north of the position where MCS B decayed approximately 9 h earlier. Therefore, it is possible that MCS B may have contributed to the formation of MCS D, which had the best chance for further development because the intense convection developed in the region of a pre-existing circulation center.

C. NON-DEVELOPING MCS

1. Overall Evolution

A convective area around at 13°N, 164°E was the center of a TCFA issued by JTWC at 0030 UTC 23 August 1997 based on the outlook for continued convective activity. Over a 6-h period, two MCSs formed that are labeled MCS A and MCS B in Figure 3.41. Between 2000 UTC (Figure 3.42) and 2300 UTC 22 August 1997 (Figure 3.43), MCS A began to weaken while MCS B increased in size. Both MCSs had dissipated by 0500 UTC 23 August 1997 (Figure 3.44).

At 0000 UTC 23 August 1997, uniform upper-level outflow (Figure 3.45a) was analyzed over a low-level circulation (Figure 3.45b). These circulation characteristics persisted over the next 24 h even though MCS A and MCS B had decayed by 0500 UTC 23 August 1997. Although a small circulation became evident at 13°N, 157°E in satellite imagery at 1132 UTC 23 August 1997 (Figure 3.46) that seems to correspond with the 850-mb circulation in the NOGAPS analyses (Figure 3.45d) and the dissipating upper-level outflow (Figure 3.45c), convection did not re-develop and the total circulation eventually dissipated over the next 24 h. This could be an indication that the circulation

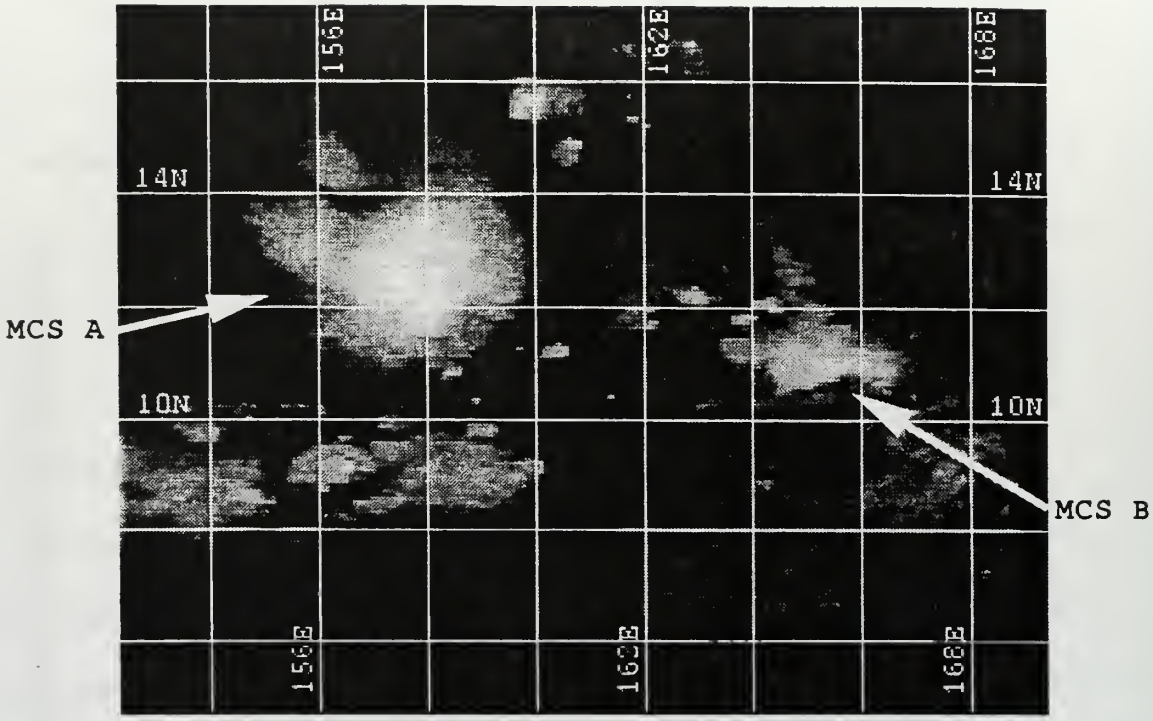

Figure 3.41. GMS IR image at 1625 UTC 22 August 1997.

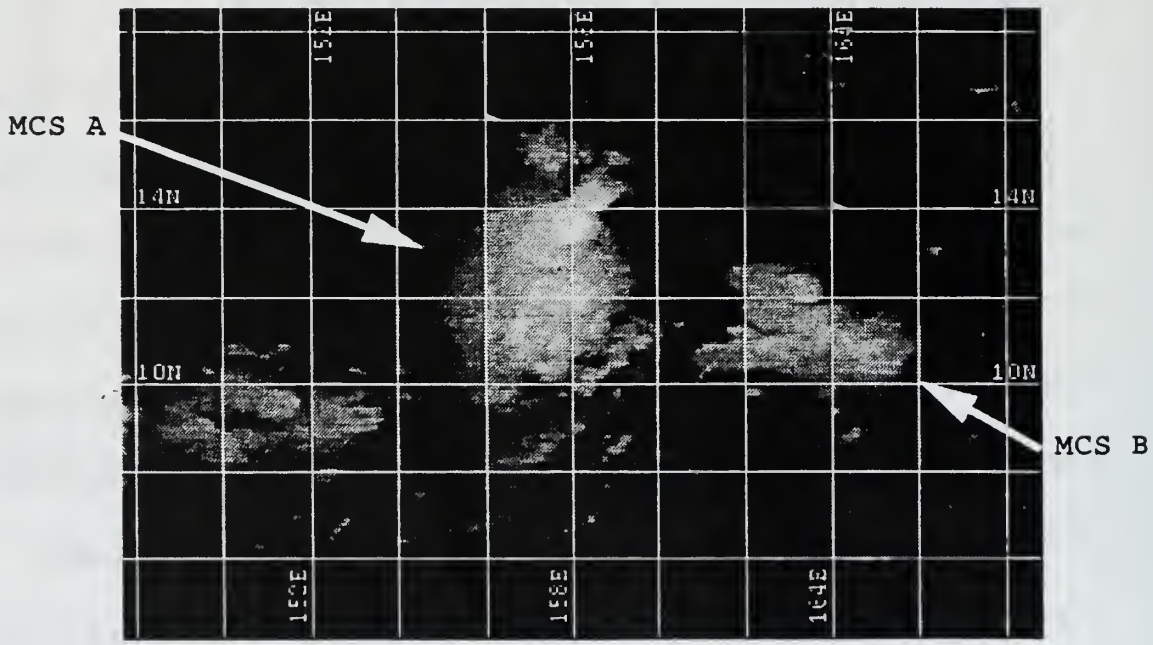

Figure 3.42. GMS IR image at 2032 UTC 22 August 1997.

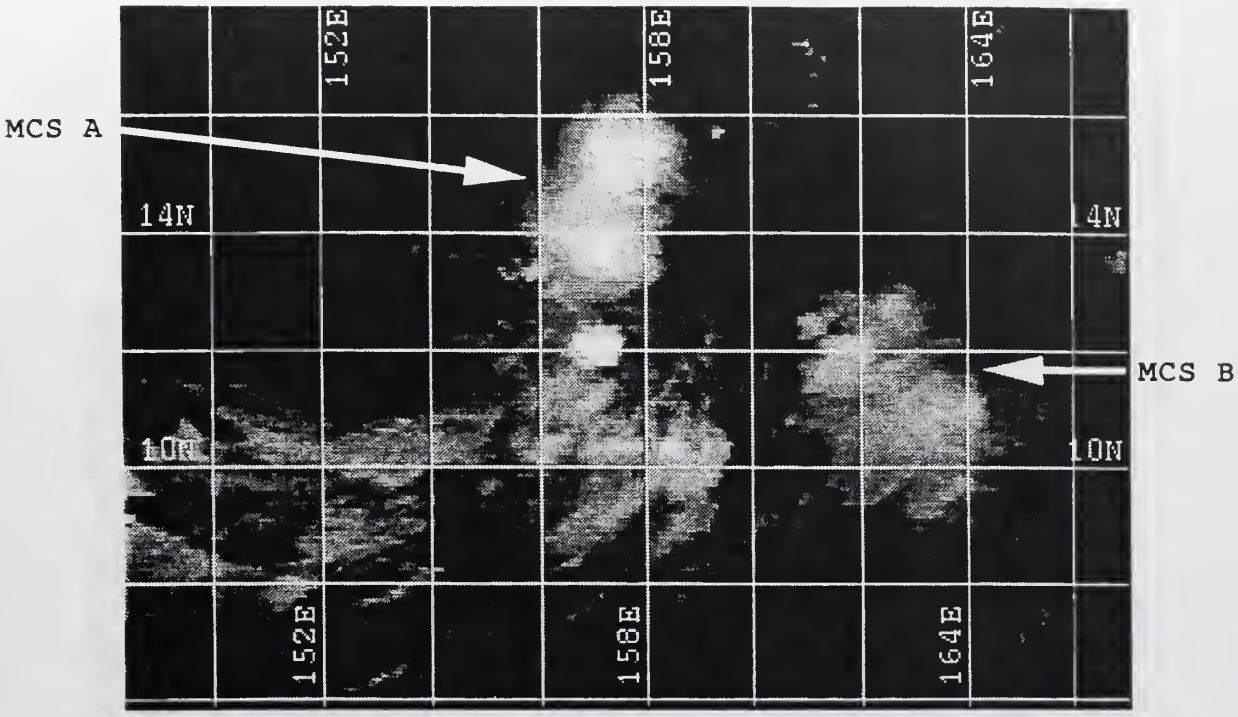

Figure 3.43. GMS IR image at 2332 UTC 22 August 1997.

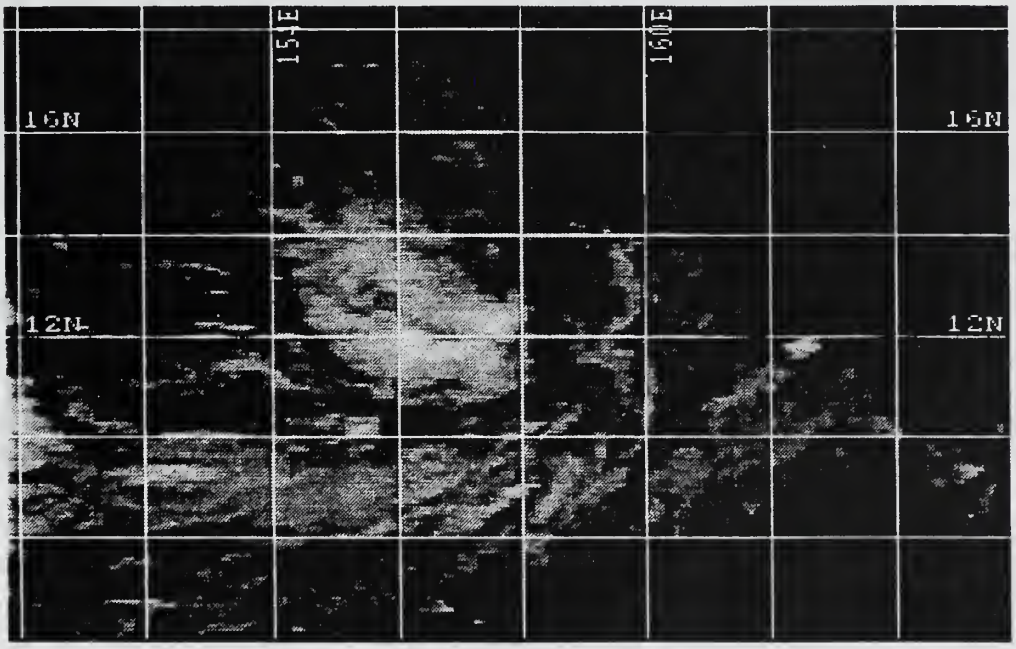

Figure 3.44. GMS IR image of decayed MCS A and B at 0532 UTC 23 August 1997.

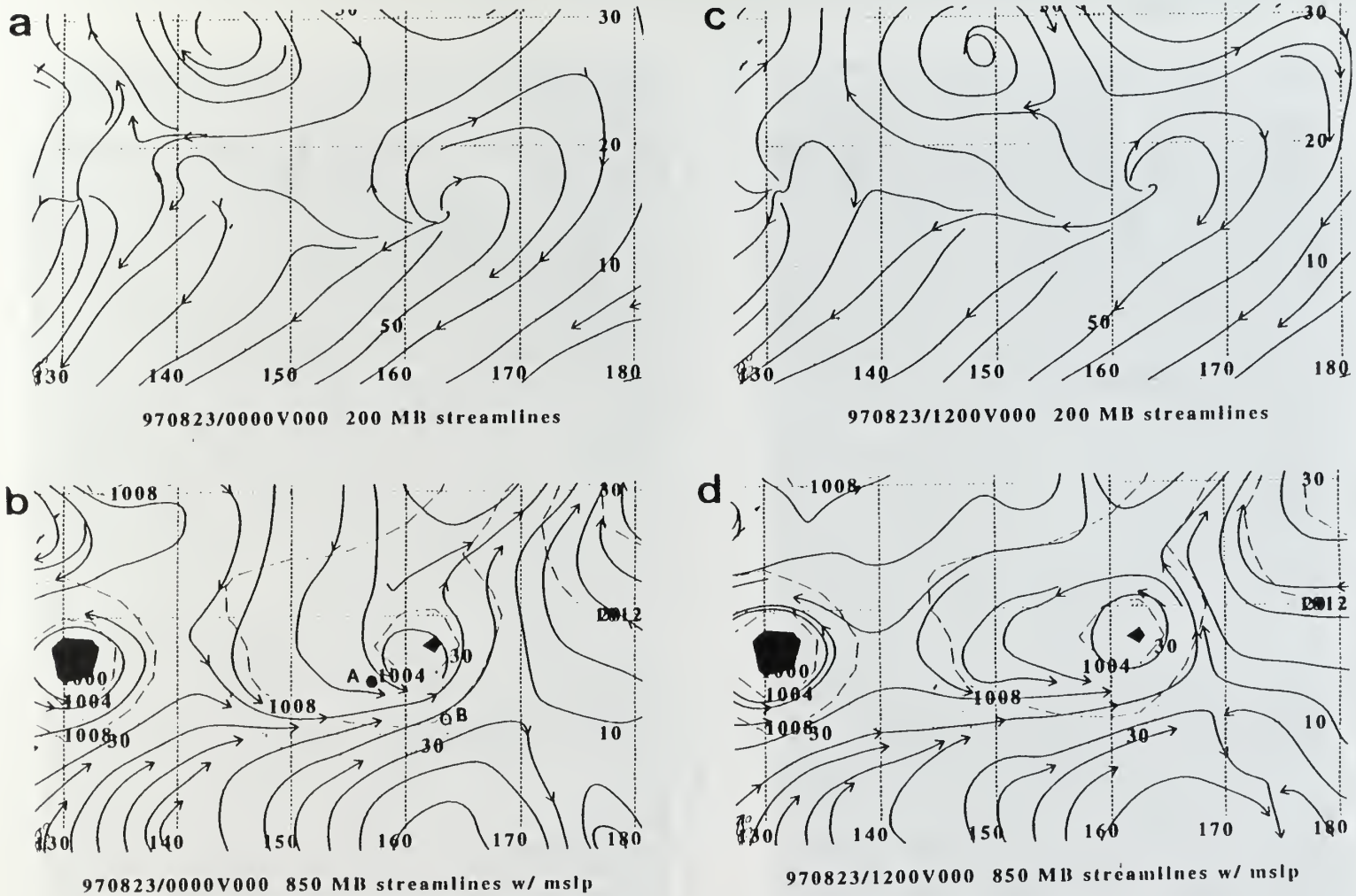

Figure 3.45. NOGAPS 200-mb streamline (solid with arrows) and 200-mb 50 kt isotach (dotted) for (a) 0000 UTC and (c) 1200 UTC 23 August 1997 and 850-mb streamline (solid with arrows), 850-mb 30 kt isotach (dotted), and mean sea-level pressure analyses (dashed, interval 4 mb) for (b) 0000 UTC and (d) 1200 UTC 23 August 1997. Location of MCS A at the times of these analyses is shown by dot.

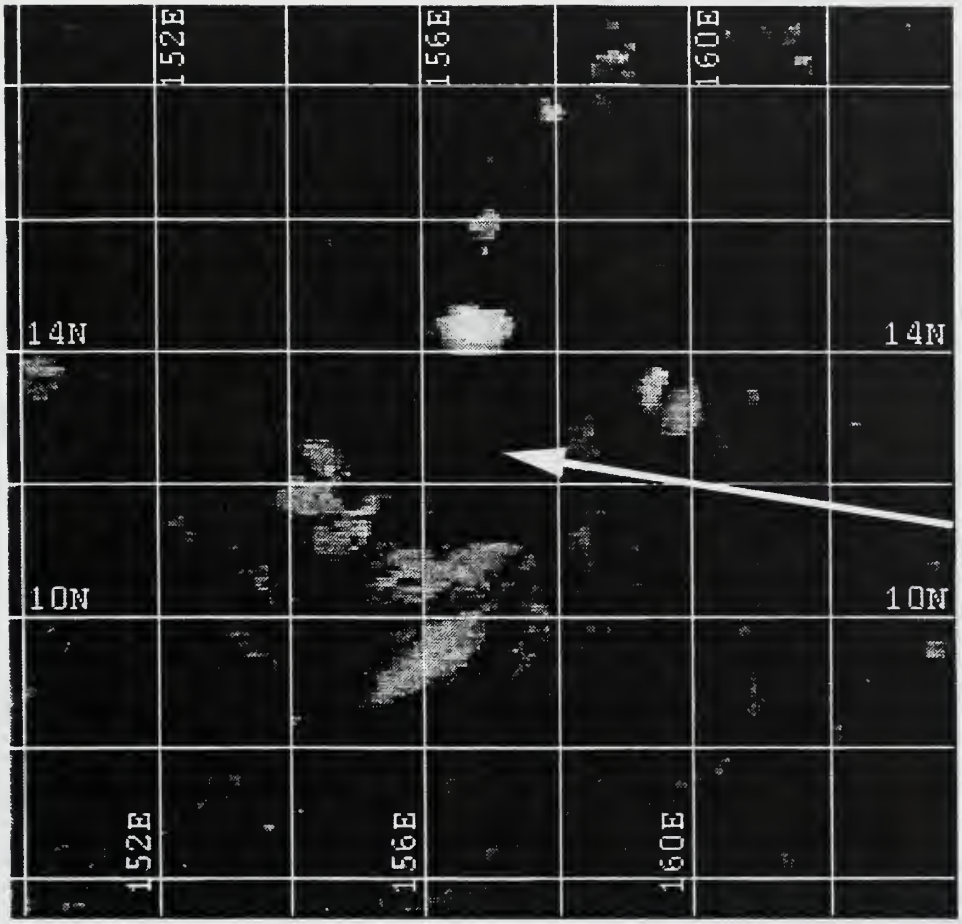

Figure 3.46. GMS IR image at 1132 UTC 23 August 1997. Arrow indicates small circulation.

evident in satellite imagery may have been confined to mid-levels and never descended to tap into surface energy sources. JTWC canceled the TCFA at 1600 UTC 24 August 1997.

2. MCS Structure

As mentioned above, two MCSs formed in the TCFA area. The first, labeled MCS A, formed near 12°N, 156°E at 1100 UTC 22 August 1997. The ellipse track (Figure 3.47) shows that MCS A did not move very far during its lifespan. During the first 8 h of development, the MCS began as a compact feature, the ellipse area expanded as the cirrus shield spread, and then became more compact and circular as it dissipated. The areal extent of convective cloud increased steadily (Figure 3.48a) and the total rain intensity increased due to convection (Figure 3.48c). Moreover, the percent coverage of convective cloud remained consistently near 45%. However, MCS A began to decay steadily after 2200 UTC 22 August 1997 and completely dissipated by 0500 UTC 23 August 1997 (Figure 3.44). After 2000 UTC 22 August 1997, both the total areal coverage and percent coverage of stratiform cloud remained greater than the convective cloud amount. The total rain intensity for both the stratiform and convective clouds decreased steadily between 2200 UTC 22 August 1997 and 0500 UTC 23 August 1997 (Figure 3.48c). This is an important distinction from the MCS characteristics associated with TC formation where total rain intensity for stratiform cloud increased for a time when the total MCS was decaying. In this case, stratiform rain intensity decreased as rapidly as the convective intensity declined. This may indicate that the structural

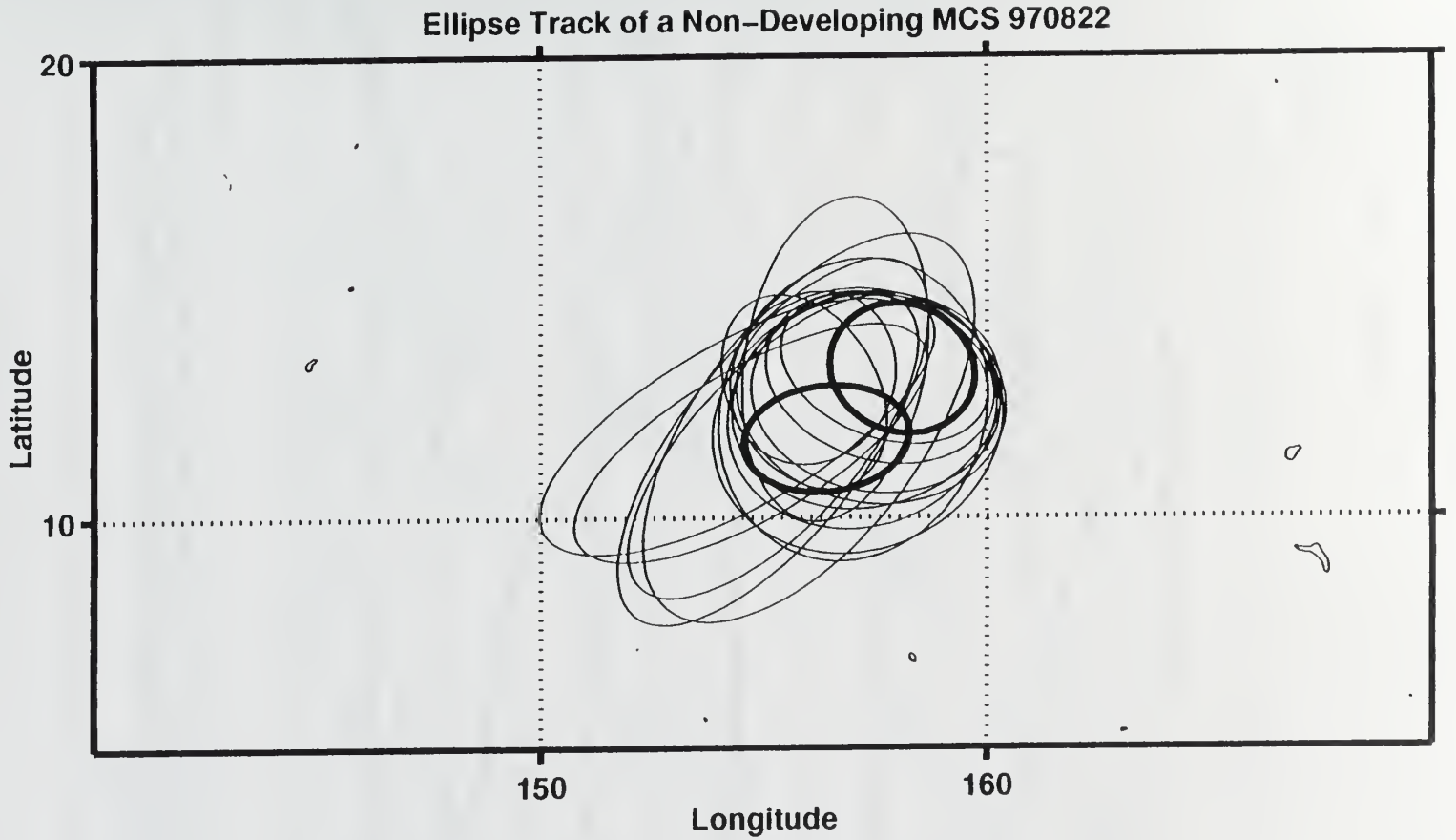

Figure 3.47. Sequence of ellipses centered along the track of MCS A from 1100 UTC 22 August 1997 through 0500 UTC 23 August 1997. The small and large dark ellipses are the start and finish of MCS A, respectively.

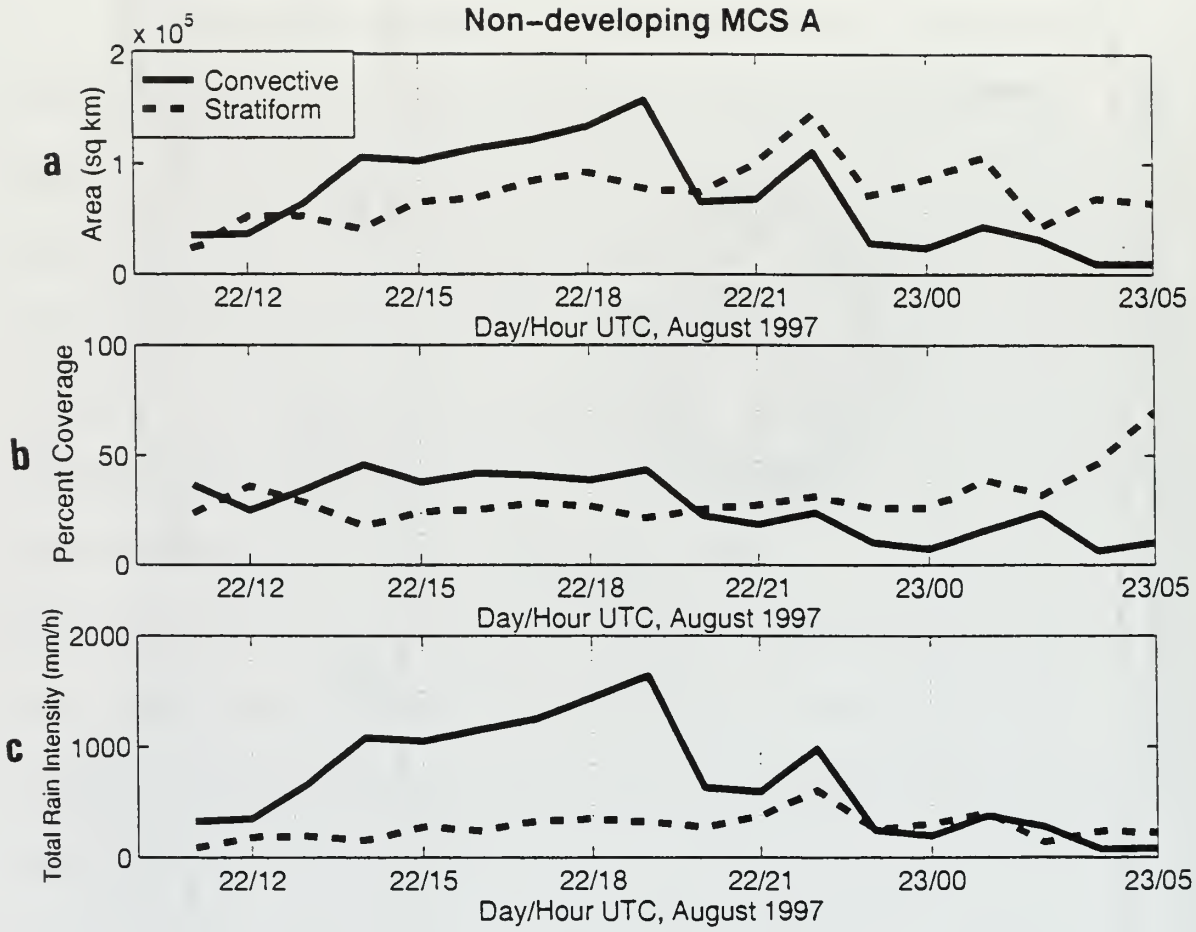

Figure 3.48. (a) Area (sq km) and (b) coverage of convective and stratiform clouds for MCS A. (c) Total rain intensity (mm/h) averaged over the areas of convective and stratiform clouds for MCS A.

characteristics of the mature to decaying MCS may not have been inclusive for production of sufficient vorticity to organize a vortex that could facilitate continued development.

The second MCS B formed near 10°N, 163°E at 1600 UTC 22 August 1997. The ellipse track (Figure 3.49) also shows that MCS B did not move very far during its lifespan and was comparable in size to MCS A. The structural evolution of MCS B is similar to MCS A. That is, the amount of convective coverage and total intensity increase while the percent coverage is nearly constant (Figure 3.50). During the first 4 h of development, intense convection is present. By 2000 UTC 22 August 1997, convection has reached its maximum and MCS B begins to decay over the next 8 h, and finally dissipates by 0400 UTC 23 August 1997. During the first 8 h, the convective cloud is larger in area and percent coverages (Figure 3.50a,b) than the stratiform cloud amounts. Only at 2200 UTC 22 August 1997 midway through the decay stage did the stratiform percent become greater than the convective percent. As with MCS A, the total rain intensity of the convective cloud was much greater than the stratiform cloud (Figure 3.50c). Although the stratiform rain intensity became larger than the convective intensity during the decay stage at about 0000 UTC 23 August 1997, the rain intensity was still rather small.

The low total rain intensities associated with the stratiform cloud of both MCS A and B, and the short life cycles, suggest that insufficient vorticity production occurred for a MCV to form. Even though the disturbance seemingly had good synoptic support for

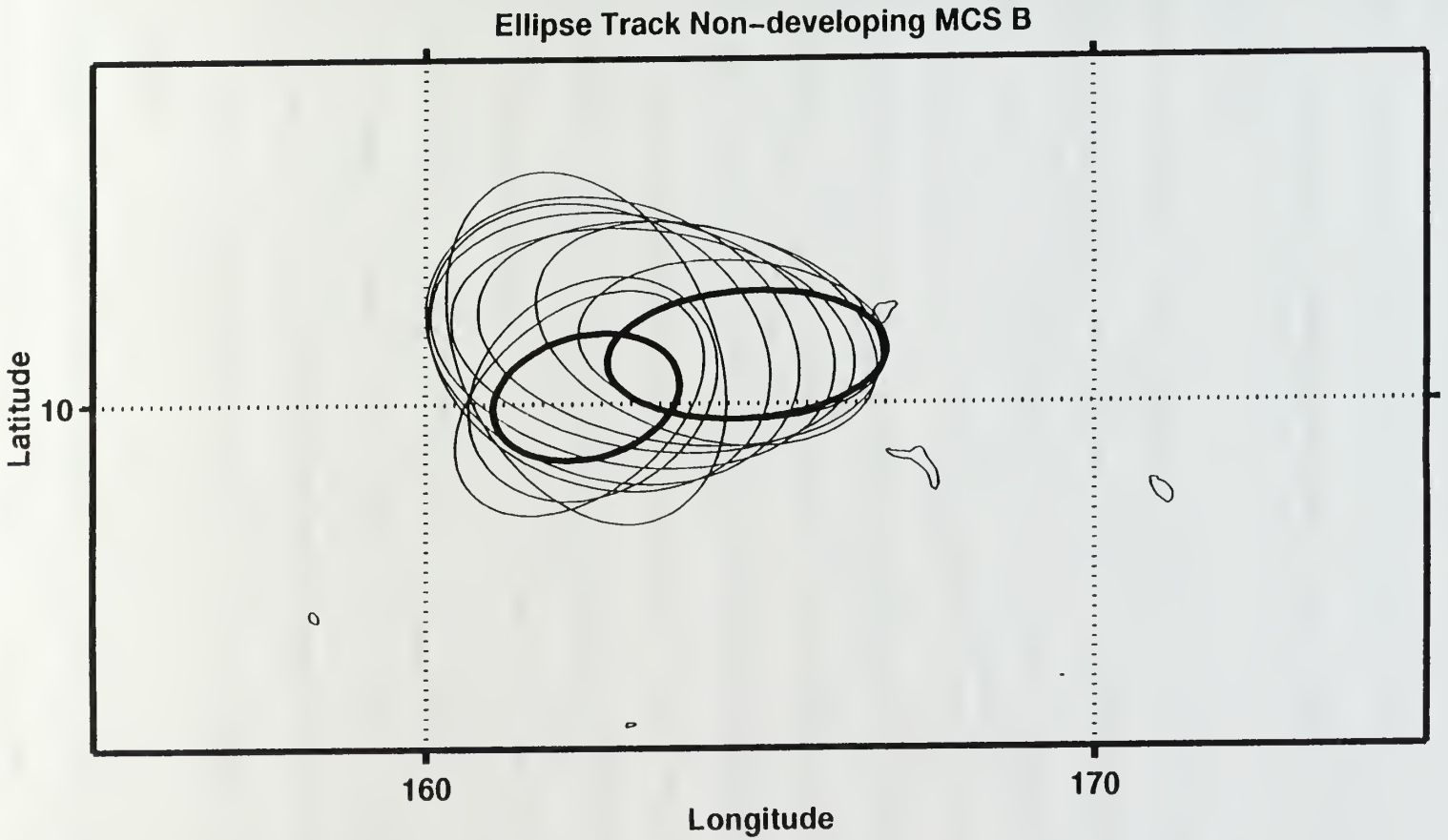

Figure 3.49. Sequence of ellipses centered along the track of MCS B from 1600 UTC 22 August 1997 through 0400 UTC 23 August 1997. The small and large dark ellipses are the start and finish of MCS B, respectively.

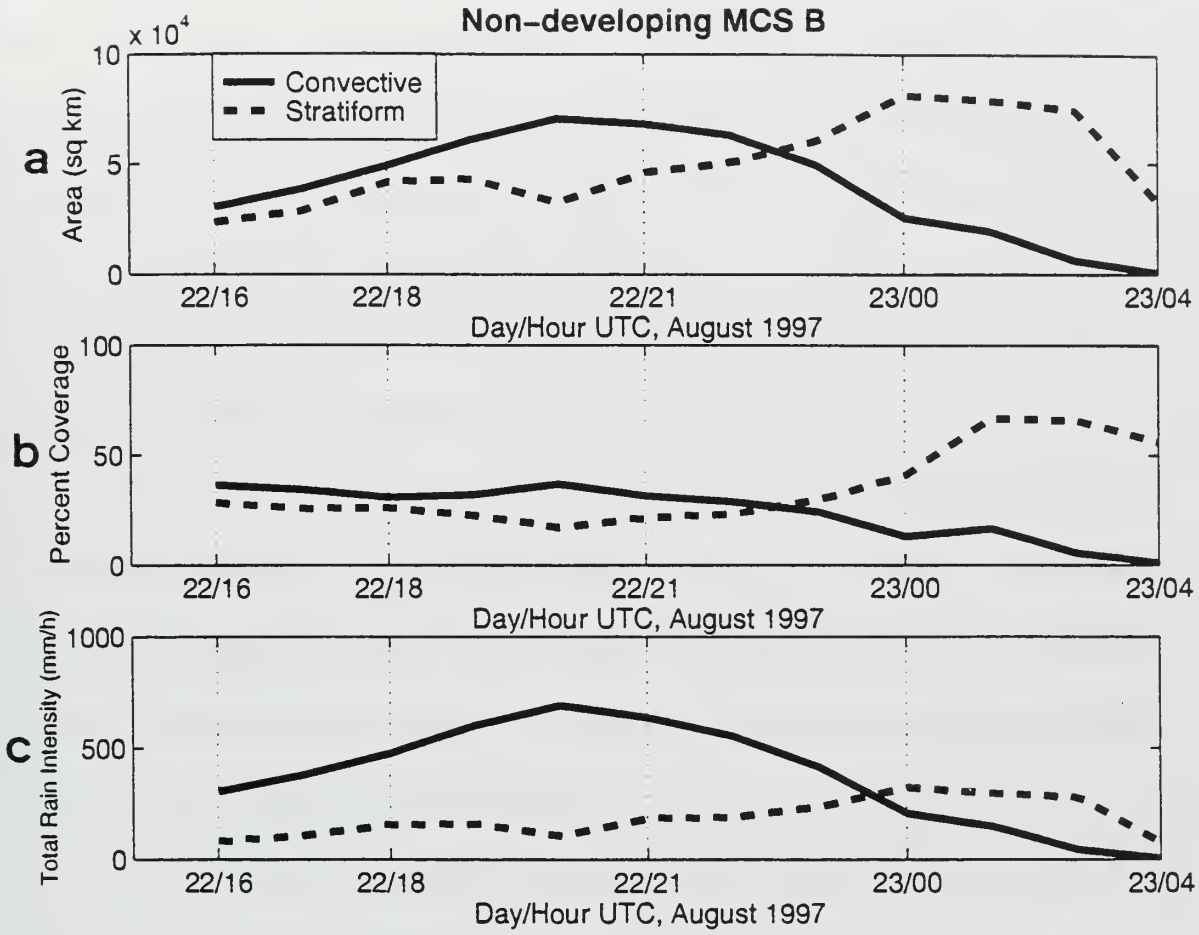

Figure 3.50. (a) Area (sq km) and (b) coverage of convective and stratiform clouds for MCS B. (c) Total rain intensity (mm/h) averaged over the areas of convective and stratiform clouds for MCS B.

development at all levels, the stratiform activity was not sufficient to form a mesoscale circulation about which to concentrate further development.

IV. SUMMARY AND CONCLUSIONS

A. SUMMARY

The formation of ST Bing involved the interaction of a synoptic-scale circulation and five MCSs over a period of several days. The formation of ST Ivan involved four MCSs over a three-day period. However, the interaction of the synoptic-scale and mesoscale components did not seem as strong in association with the formation of ST Ivan. Two MCSs that were not related to the formation of a tropical cyclone were also examined. The combination of microwave and infrared imagery was used to examine the rain rate and cloud type evolutions of each MCS.

The individual MCS structures can be examined with respect to characteristics that have been associated with mid-level vorticity production and potential extension of the midlevel vortex to low-levels, which is required for intensification. Also, variability in MCS characteristics can be examined between MCSs that seem to be directly related, or not related, to tropical cyclone formation.

The variation in MCS structure is manifest via the amount of heating and the vertical location of the heating over the area containing the MCS. This relationship is important because it is through the release of heat that the MCS influences the environment. Typically, convective heating is maximum in the lower troposphere, and stratiform (anvil) heating is maximized at upper levels with cooling due to unsaturated downdrafts at lower layers. Studies of MCS structure based on various field programs

have associated the amount of stratiform rain with the magnitude and level of maximum heating in the upper troposphere (e.g., Johnson 1984, Frank and McBride 1989, Tao et al. 1993). Furthermore, the upper-level heating is associated with maximum vertical motion. In addition, an association is implied between the amount of stratiform coverage and the potential for midlevel vorticity production due to convergence. These relationships can be examined for the MCSs analyzed in connection to ST Bing, ST Ivan, and the non-developers by comparing the total (time integrated over the area) coverage and rain rates for each cloud type for each MCS.

For all five MCSs associated with the formation of ST Bing, the time-integrated areal coverage of stratiform cloud is larger than the coverage of convective cloud (Figure 4.1). However, important differences among these MCSs are found by examining the time-integrated rain intensities (Figure 4.2) and time evolutions of cloud coverage (Chapter III.). The time-integrated rain intensities are comparable for both stratiform and convective cloud for MCSs A, B, and C. In conjunction with the larger stratiform areal coverage, this suggests that the stratiform region probably exhibited structural characteristics conducive to mid-tropospheric vortex production because rather large (compared to the convective clouds) total rain intensities were produced. That is, persistent ascent in long-lived stratiform cloud with descent associated with evaporation in unsaturated downdrafts below promotes vertical stretching and horizontal convergence and mid-tropospheric vorticity. Furthermore, the time evolutions of cloud coverage for MCS A (Figure 3.14a), MCS B (Figure 3.18a), and MCS C (Figure 3.20a) indicate that

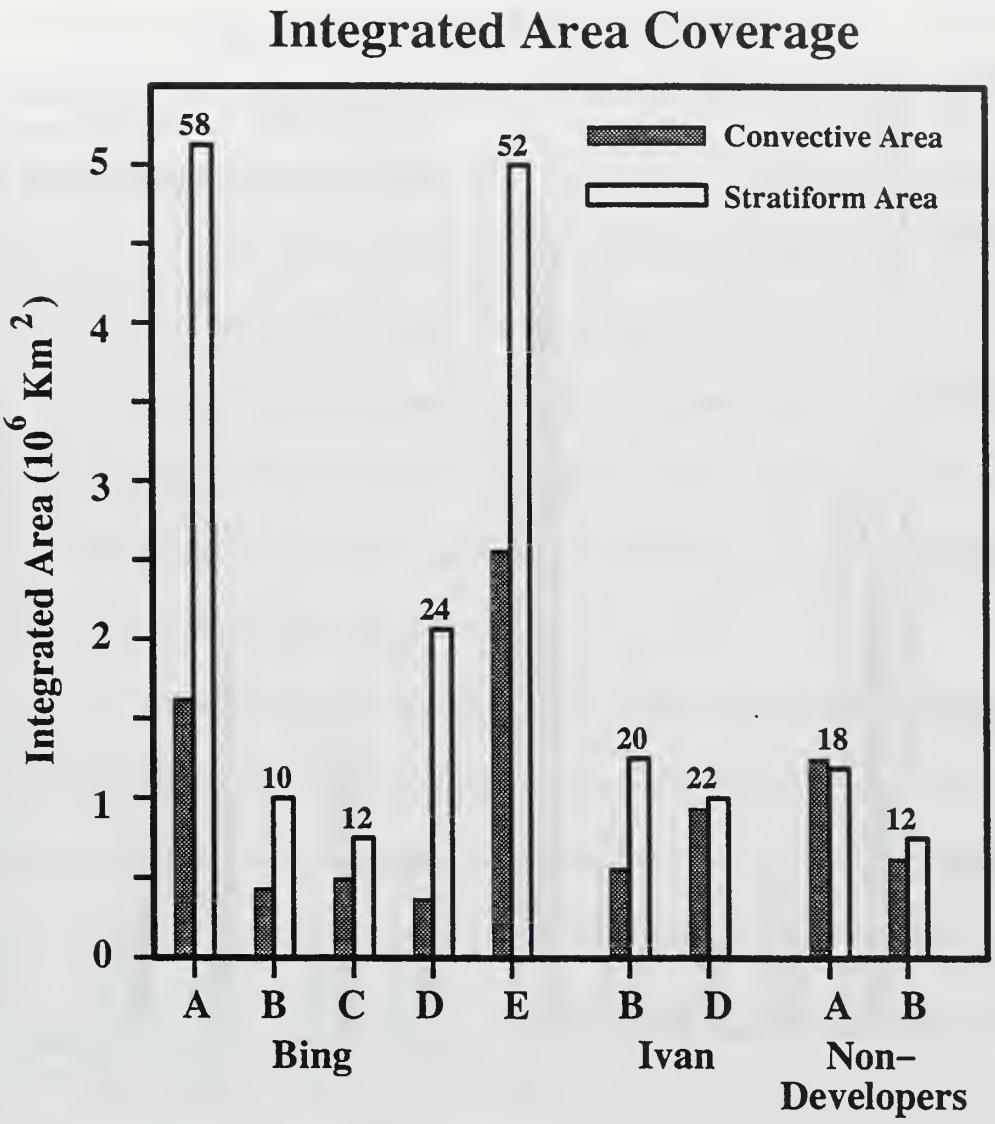

Figure 4.1. Total integrated area coverage for all MCSs associated with ST Bing, ST Ivan, and the non-developers. The number of hours the MCS existed is given above the bars.

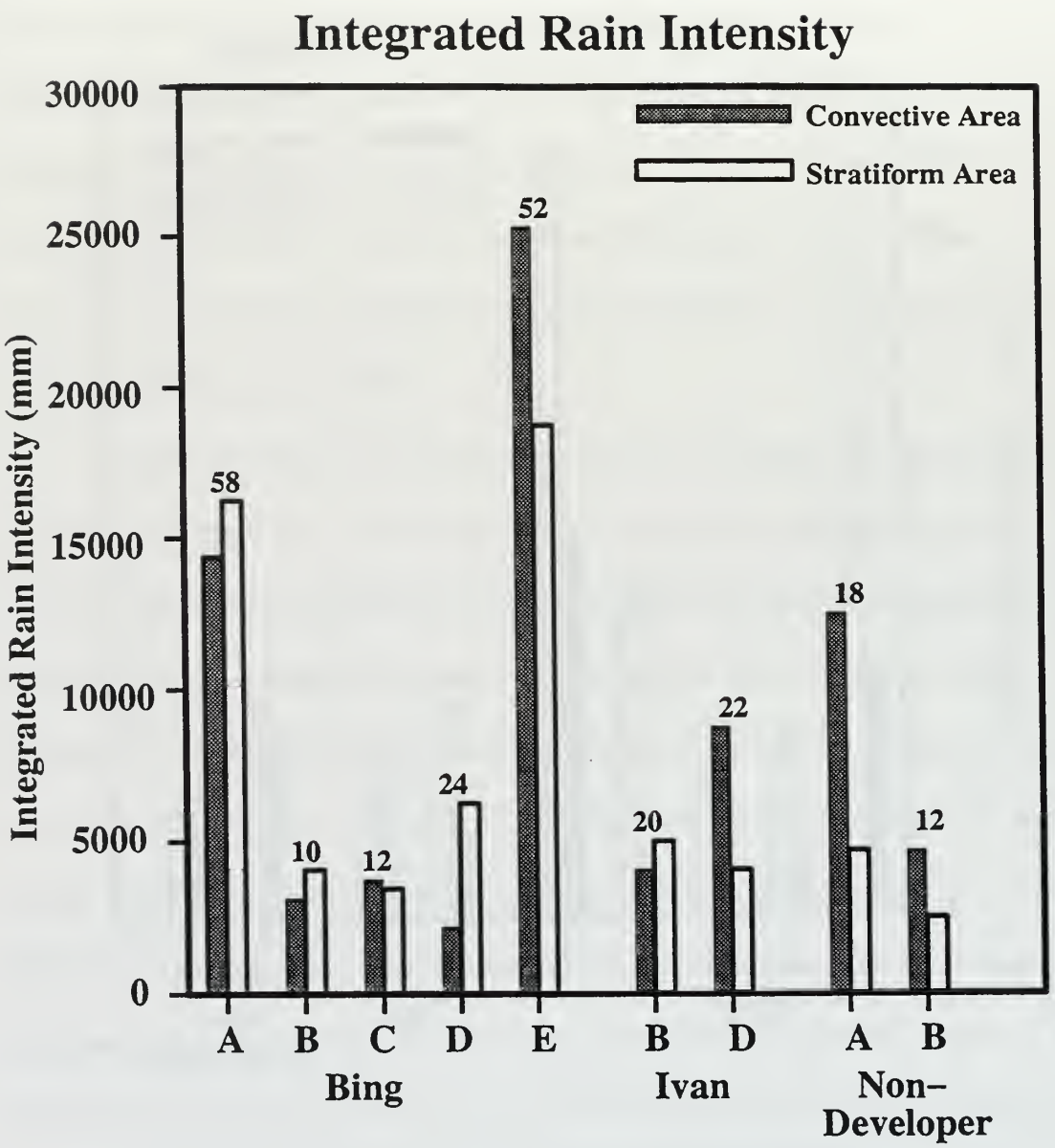

Figure 4.2. Total integrated rain intensities for all MCSs associated with ST Bing, ST Ivan, and the non-developers. The number of hours the MCS existed is given above the bars.

the stratiform cloud coverage remains large during the time that the convective cloud began to decay. An important difference associated with the structure of MCS E in pre-Bing is that the total integrated amount of rain intensity due to convective cloud is larger than the stratiform cloud even though the time-integrated area of stratiform cloud is much larger than the convective cloud (Figure 4.1). Therefore, MCS E has a large stratiform area plus the convective rain area is concentrated, intense, and long-lasting. This implies that the dominant heating profile over the MCS area has become convective in nature, which is conducive to a low-level vortex structure representative of a warm-core tropical disturbance. Although the magnitudes of integrated cloud coverage and rain intensities are smaller, similar characteristics are associated with MCS B and MCS D during the formation of ST Ivan (Figures 4.1 and 4.2).

The MCSs not associated with a developing tropical disturbance exhibit some basic structural differences with the MCSs associated with ST Bing and ST Ivan. Although the total time-integrated areas of stratiform and convective cloud coverage (Figure 4.1) are nearly equal for both of the non-developer MCSs, the total integrated rain intensity (Figure 4.2) for convective clouds is much larger than the stratiform amount, which is a characteristic of the MCS E in pre-Bing and MCS D in pre-Ivan. Thus, the time evolution of the non-developer MCSs is further analyzed by comparing the convective and stratiform areal coverage with respect to the average coverage computed for all nine MCSs analyzed (Figure 4.3). For each non-developer MCS, the areal coverage of convective cloud increases rapidly and is larger than the stratiform coverage.

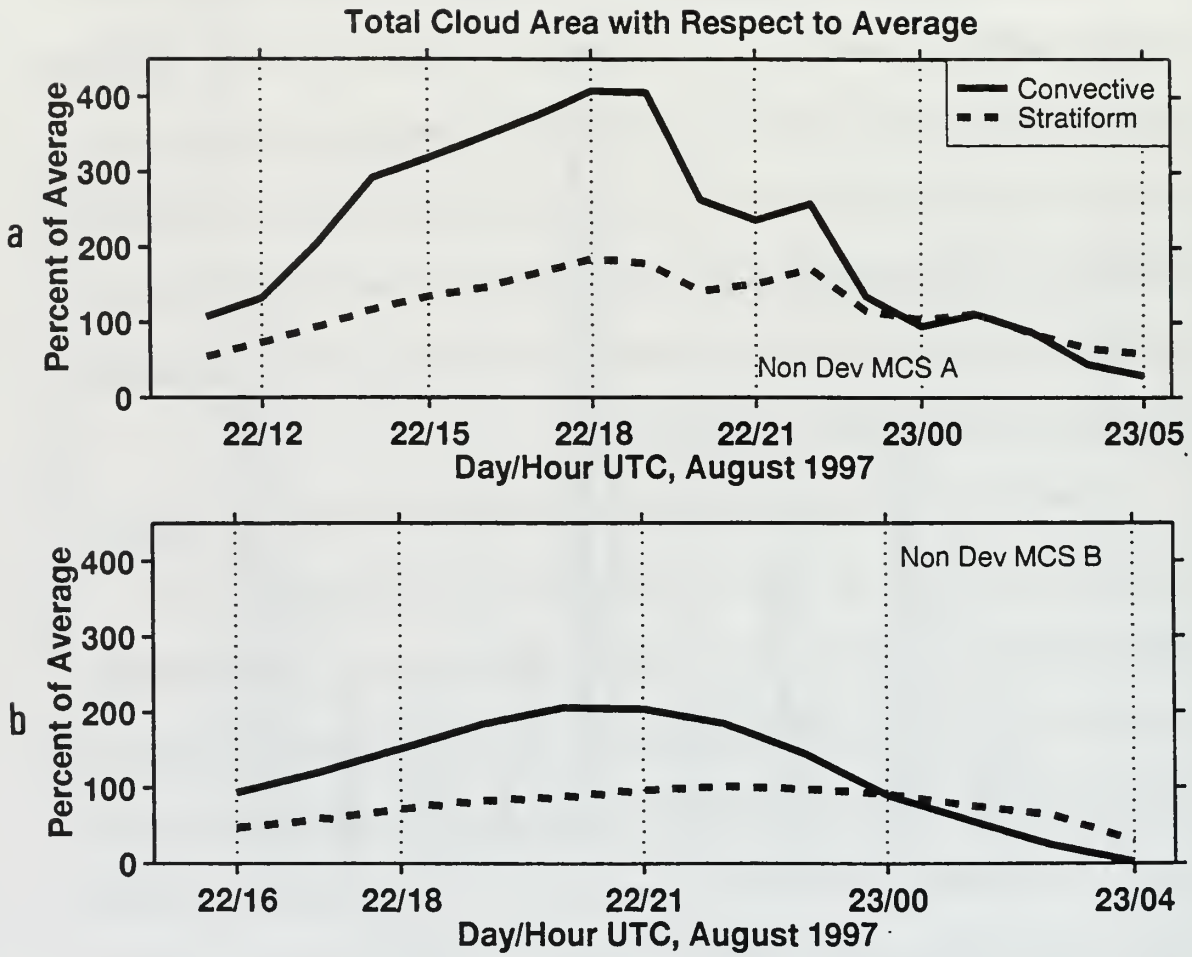

Figure 4.3. Total cloud area with respect to the nine-MCS average for (a) MCS A, and (b) MCS B in the non-developing TC.

Notice that the amount of convective coverage is nearly 400% of the average for MCS A, and 200% of the average for MCS B. The most important difference for the MCSs associated with the non-developing TC versus the two developing tropical cyclones occurs during the decay of each MCS where the coverage of stratiform cloud decays nearly as rapidly as the convective cloud. This feature, together with the large convective rain intensities, suggests that an extensive stratiform rain region never developed fully. Therefore, mid-level vortex production may not have been favored, even though vigorous convective rain exists.

B. CONCLUSIONS

The combination of geostationary infrared and polar-orbiting microwave imagery allows identification of distinct MCS structure characteristics. As summarized in section A, this study identified MCS characteristics that defined the relative roles of MCS activity associated with two TC formations. Although based on a small sample, this study also proposes certain differences may be found between MCSs associated with developing tropical disturbances and those not associated with tropical disturbances.

C. RECOMMENDATIONS

The use of high-resolution microwave satellite imagery is a valuable tool for studying the physical structure of MCSs and how they affect TC genesis. The implementation of the following items would further increase the utility and add greatly to the understanding of TC genesis.

1. *Additional case studies.* This thesis describes only two case studies of the 17

TC formations during the portion of the 1997 TC season analyzed. The case studies were restricted to MCS shape (elliptical only) and sizes as defined in Chapter II.B. No examples of over-land MCSs that drifted over the ocean were represented. Additionally, all selected case studies were taken from the western North Pacific basin. This small, potentially basin-biased sample size limits the applicability of the conclusions that may be drawn from the study. Clearly, these analyses need to be extended to a larger data base.

2. *Methodology for JTWC watchstanders.* The infrequent SSM/I passes from the DMSP satellites make each pass over tropical disturbances even more valuable, so that procedures need to be developed to provide the watchstander microwave data from each pass. Computer algorithms that combine the polar-orbiter microwave and geostationary infrared information with time as shown in this thesis can help the watchstander make necessary decisions on how and when the TC may form in conjunction with the MCSs in the tropical disturbance.

3. *Improved representation of the environment.* This study should be expanded to take into account other important factors in the environment that are contributors to TC formation such as vertical wind shear, background or environmental vorticity, disturbances in the monsoon trough, etc.

4. *Mesoscale convective vorticies.* At least four theories have been suggested to describe how a mid-level vortex may extend downward to become a low-level vortex. Further case studies of MCS structure via microwave imagery may help to isolate the

factors that may contribute to evolution from a mid-level vortex to a low-level vortex, and thus advance understanding of how these dangerous tropical cyclones form.

LIST OF REFERENCES

Bister, M., and K. A. Emanuel, 1997: The genesis of Hurricane Guillermo: TEXMEX analyses and a modeling study. *Mon. Wea. Rev.*, **125,** 2662-2682.

Chen, L. S., and W. M. Frank, 1993: A numerical study of the genesis of extra-tropical convective meso-vorticies. Part I: Evolution and dynamics. *J. Atmos. Sci.*, **50,** 2401-2426.

_____, R. A. Houze, and B. E. Mapes, 1996: Multiscale variability of deep convection in relation to large-scale circulation in TOGA COARE. *J. Atmos. Sci.*, **53,** 1380-1409.

Elsberry, R. L., G. Foley, H. Willoughby, J. McBride, I. Ginis, and L. Chen, 1995: *Global Perspectives on Tropical Cyclones.* Tech. Doc. No. 693, World Meteor. Organiz., Geneva, Switzerland, 289 pp.

Finta, C. A., 1997: Observations of mesoscale convective systems during tropical cyclone genesis. M.S. Thesis, Naval Postgraduate School, Monterey, CA 93943, 80 pp.

Frank, W. M., and J. L. McBride, 1989: The vertical distribution of heating in AMEX and GATE cloud clusters. *J. Atmos. Sci.*, **46,** 3464-3478.

Harr, P. A., R. L. Elsberry, and J. C. L. Chan, 1996: Transformation of a large monsoon depression to a tropical storm during TCM-93. *Mon. Wea. Rev.*, **124,** 2625-2643.

Houze, R. A., Jr., 1993: *Cloud Dynamics*. Academic Press, 573 pp.

_____, 1997: Stratiform precipitation in regions of convection: A meteorological paradox? *Bull. Amer. Meteor. Soc.*, **78,** 2179-2196.

Johnson, R. H., 1984: Partitioning tropical heat and moisture budgets into cumulus and mesoscale components: Implications for cumulus parameterization. *Mon. Wea. Rev.*, **112,** 1656-1665.

Liu, G., and J. A. Curry, 1992: Retrieval of precipitation from satellite microwave measurement using both emission and scattering. *J. Geophys. Res.*, **97,** 9959-9974.

_____, J. A. Curry, and R. S. Sheu, 1995: Classification of clouds over the western equatorial Pacific Ocean using combined infrared and microwave satellite data. *J. Geophys. Res.*, **100,** 13811-13826.

McBride, J. L., 1995: Tropical cyclone formation. Chap. 3, Tech. Doc. No. 693, *Global Perspectives on Tropical Cyclones* (R. L. Elsberry, ed.), World Meteor. Organiz., Geneva, Switzerland, 63-105.

McGaughey, G. R., and E. J. Zipser, 1996: Passive microwave observations of the stratiform regions of two tropical oceanic mesoscale convective systems. *J. Appl. Meteor.*, **35,** 1949-1962.

_____, G. R., E. J. Zipser, R. W. Spencer, and R. E. Hood, 1996: High-resolution passive microwave observations of convective systems over the tropical Pacific Ocean. *J. Appl. Meteor.*, **35,** 1921-1947.

Mohr, K. I., and E. J. Zipser, 1996: Mesoscale convective systems defined by their 85-Ghz ice scattering signature: Size and intensity comparison over tropical oceans and continents. *Mon. Wea. Rev.*, **124,** 2417-2437.

Ritchie, L. A., and G. J. Holland, 1997: Scale interactions during the formation of Typhoon Irving. *Mon. Wea. Rev.*, **125,** 1377-1396.

Rossow, W. B., and R. A. Schiffer, 1991: ISCCP cloud data products. *Bull. Amer. Meteor. Soc.*, **72,** 2-20.

Savage, R. C., 1976: The transfer of thermal microwaves through hydrometeors. Ph.D. thesis, University of Wisconsin, 147 pp.

Spencer, R. W., H. M. Goodman, and R. E. Hood, 1989: Precipitation retrieval over land and ocean with the SSM/I: Identification and characteristics of the scattering signal. *J. Atmos. Oceanic Technol.*, **6,** 254-273.

Tao, W. -K., S. Lang, J. Simpson, and R. Adler, 1993: Retreival algorithms for estimating the vertical profiles of latent heat release: Their applications for TRMM. *J. Meteor. Soc. Japan*, **71,** 685-700.

Wilheit, T. T., A. T. C. Chang, M. S. V. Rao, E. B. Rodgers and J. S. Theon, 1977: A satellite technique for quantitatively mapping rainfall rates over the oceans. *J. Appl. Meteor.*, **16,** 551-560.

Zehr, R. M., 1992: Tropical cyclogenesis in the western North Pacific. Tech. Rep. 61 NESDIS, NOAA, Washington D. C., 20233, 181 pp.

INITIAL DISTRIBUTION LIST

No. Copies

1. Defense Technical Information Center 2
   8725 John J. Kingman Rd., STE 0944
   Ft. Belvoir, VA 22060-6218

2. Dudley Knox Library 2
   Naval Postgraduate School
   411 Dyer Rd.
   Monterey, CA 93943-5101

3. Meteorology Department 1
   Code MR/Wx
   Naval Postgraduate School
   589 Dyer Rd Rm 252
   Monterey, CA 93943-5114

4. Dr. R. L. Elsberry 2
   Code MR/Es
   Naval Postgraduate School
   589 Dyer Rd Rm 252
   Monterey, CA 93943-5114

5. Dr. P. A. Harr 2
   Code MR/Hr
   Naval Postgraduate School
   589 Dyer Rd Rm 252
   Monterey, CA 93943-5114

6. LT David Milot 2
   OIC, NAVTRAMETOC DET
   651 Bataan St. STE 116
   Corpus Christi, TX 78419-5250

7. Chief of Naval Research 1
   800 N Quincy Street
   Arlington, VA 22217

8. Superintendent, Naval Research Laboratory 1
   7 Grace Hopper Ave Stop 2
   Monterey, CA 93943-5502

9. Commanding Officer 1
   Naval Pacific Meteorology and Oceanography Center West
   PSC 489, Box 12
   FPO AP 96540-0051

10. Dr. Mark Lander 1
    c/o: 36 OSS/OSJ
    PSC 489, Box 20
    FPO AP 96536-0051

3 483NPG TH 2643
10/99 22527-200

DUDLEY KNOX LIBRARY
3 2768 00350138 8